

A NUMERICAL STUDY OF BOREHOLE HEAT
EXCHANGERS

A NUMERICAL STUDY OF THE SHORT- AND LONG-TERM
HEAT TRANSFER PHENOMENA OF BOREHOLE HEAT
EXCHANGERS

By BRIANNA HARRIS, MSc

A Thesis Submitted to the School of Graduate Studies in Partial
Fulfilment of the Requirements for
the Degree Doctor of Philosophy

McMaster University © Copyright by Brianna Harris, April 2024

McMaster University

DOCTOR OF PHILOSOPHY (2024)

Hamilton, Ontario, Canada (Mechanical Engineering)

TITLE: A numerical study of the short- and long-term heat transfer phenomena of borehole heat exchangers

AUTHOR: Brianna Harris
MAsc (Mechanical Engineering),
McMaster University, Hamilton, Canada

SUPERVISORS: Marilyn Lightstone
James Cotton

NUMBER OF PAGES: xix, 160

Lay Abstract

This thesis provides an in-depth comparative study of two different designs of borehole heat exchanger, the u-tube and coaxial, which are used in geothermal applications to transfer heat to and from the ground. While many researchers anticipated that the coaxial design would perform better, several studies comparing the heat exchangers were not able to provide a clear answer about which heat exchanger performed best. This study addressed this gap by using detailed numerical simulations which showed that there was a marginal difference in performance between the two heat exchangers when operated for periods longer than a few hours, but that larger differences occurred early in operation (under 15 minutes). The results also showed that operating intermittently resulted in improvements in performance of the heat exchanger, particularly when operated for periods less than the time it takes fluid to travel the length of the piping.

Abstract

This thesis contributes an in-depth comparative study of u-tube and coaxial borehole heat exchangers. While it is widely accepted that the lower resistance of the coaxial heat exchanger should result in a performance advantage, the findings of several studies comparing the heat exchanger configurations did not definitively establish the mechanisms causing differences in performance. This study employs numerical modelling to consider heat exchangers over a broad range of time scales and under carefully controlled geometry and flow conditions, resulting in the identification of the key parameters influencing borehole heat exchanger performance.

The first part of this study consists of a comparison of u-tube and coaxial heat exchangers under continuous loading. A detailed conjugate heat transfer numerical model was developed in OpenFOAM, designed to capture both short and long time scales of heat exchange, necessary to understand the nuanced differences between designs. A novel transient resistance analysis was employed to understand the dominant factors influencing performance. This study established that marginal differences exist between u-tube and coaxial borehole heat exchangers (BHEs) when operated continuously long term but that greater differences occur early in operation.

The second phase of this investigation provided a framework for analysing borehole heat exchanger performance during intermittent operation, while also comparing

u-tube and coaxial designs. During this study, it was found that reducing operating time, improving the the rate of the ground's recovery to its original temperature, and lowering the duty cycle improved BHE performance. Transit time was identified as a influential time scale, below which heating at the outlet was limited. Further, the benefits of operating below the transit time were mitigated by design-specific interaction between inlet and outlet flows. Finally, this study found that non-dimensionalizing operating time by transit time causes the differences between u-tube and coaxial performance to vanish, leading to the conclusion that differences in BHE performance are caused by variations in flow rather than thermal mass.

Acknowledgements

This thesis would not have been possible without the support of the community surrounding me. I am deeply grateful to everyone who helped me through this process.

I would like to thank my supervisors, Marilyn Lightstone and Jim Cotton, for their wisdom and guidance throughout my PhD. I would also like to thank Stanley Reitsma for his invaluable insight into practical geothermal systems. I am grateful to the members of my committee, Stephen Tullis and Tom Adams, for their thoughtful feedback on my work.

I am thankful for the support my family, who have stood by my side through the most difficult parts of this process and celebrated every accomplishment along the way. They have always encouraged me to take my education as far as I could. As my grandmother, Joan, always says, you can never have too much education. (Though I feel I may have nearly proven her wrong).

Most of all, I am forever grateful to my partner, Salim, for his patience and unwavering support. There are simply not enough words to express how thankful I am for all the ways he helped me through this PhD. Every part of this process was made better having shared it with him.

Table of Contents

Nomenclature	xvi
1 Introduction	1
1.1 Background	1
1.2 Objectives	9
1.3 Thesis Outline	10
2 Literature Review	11
2.1 Modelling Borehole Heat Exchanger Systems	11
2.2 Improvements to Borehole Heat Exchanger Design	27
2.3 Intermittent Operation of Borehole Heat Exchangers	31
2.4 Summary	33
3 Methodology	36
3.1 Geometry and Mesh	36
3.2 Numerical Modelling	49
4 Results and Discussion	61
4.1 Experimental Validation	61

4.2	Strategies for comparing borehole heat exchanger designs	65
4.3	Comparative Study of U-tube and Coaxial Heat Exchangers Under Continuous Loading	69
4.4	Intermittent Operation of U-tube and Coaxial Heat Exchangers . . .	100
4.5	Design Considerations for U-tube and Coaxial Heat Exchangers . . .	124
4.6	Assessment of Models for Multiple Thermally Interacting Boreholes .	131
5	Summary and Conclusions	139
5.1	Summary	139
5.2	Conclusions	142
5.3	Original Contributions	147
5.4	Future Work	148
A	Input data file used for test case set up	161
A.1	Input file for a u-tube type heat exchanger	161
A.2	Input file for a coaxial type heat exchanger	164

List of Figures

1.1	Vertical and horizontal ground heat exchanger arrangements [6] . . .	2
1.2	Pit and aquifer thermal storage systems	4
1.3	Aerial view of the Drake Landing borehole thermal energy storage field [14]	5
1.4	Axial and lateral cross-sections of the u-tube and coaxial heat ex- changer designs, with the grout shaded in grey, not to scale	8
2.1	g-functions for a 10 by 10 borehole field with variable borehole spacing, digitized from Eskilson [9], where B is the borehole spacing and H is the borehole depth	16
2.2	Borehole heat exchanger models	18
2.3	A high-resolution finite element model developed by Chen et al. [48] .	24
3.1	Model domains and boundary conditions for the u-tube and coaxial heat exchangers	37
3.2	Mesh of the u-tube domain	38
3.3	1D semi-circular mesh development	41
3.4	Mesh of the coaxial domain	42
3.5	Multiple borehole domain	44

3.6	Results from Beier et al. demonstrating the effect of coaxial inlet location [61]	46
3.7	Diagram of the borehole heat exchanger system for unsteady Bernoulli analysis	53
3.8	Relationship between Nusselt number and Reynolds number for circular cross section	58
4.1	Experimental validation of the u-tube model, with a fixed flow rate of 0.56 kg/s, a ground conductivity of 3.77 W/mK, and inlet temperatures taken from experimental data. Experimental results provided by GeoSource Energy	63
4.2	Experimental validation of the coaxial model using data published by Beier et al. [61]. Modelling uses a fixed flow rate of 0.58 kg/s, a ground conductivity of 3.8 W/mK, and inlet data from the experiment.	64
4.3	U-tube and coaxial inlet and outlet temperatures during a thermal response test, for a case with a constant heat injection rate of 50 W/m	72
4.4	U-tube temperatures over time, for a case with a constant heat injection rate of 50 W/m. Top view and side view taken at the top of the domain, near the ground surface	73
4.5	Coaxial temperatures over time, for a case with a constant heat injection rate of 50 W/m. Top view and side view taken at the top of the domain, near the ground surface	74
4.6	U-tube and coaxial inlet and outlet temperatures during the first three hours of a thermal response test, for a case with a constant heat injection rate of 50 W/m	76

4.7	Cross-sections of the u-tube and coaxial heat exchangers over the first 30 minutes of operation during a thermal response test with a heat injection rate of 50 W/m. Cross-sections taken at the top surface of the domain	77
4.8	Effectiveness and percentage difference of effectiveness for u-tube and coaxial heat exchangers during a thermal response test with a constant heat injection rate of 50 W/m	78
4.9	Heat transfer rate and percentage difference of heat transfer rate for u-tube and coaxial heat exchangers subject to an inlet temperature of 25°C	80
4.10	Effectiveness and percentage difference of effectiveness for u-tube and coaxial heat exchangers subject to a constant inlet temperature of 25°C	82
4.11	U-tube and coaxial radial borehole temperatures are taken along the x -axis at a depth of $H/2$	83
4.12	U-tube radial borehole temperatures and axial fluid temperatures for a case with a constant heat injection rate of 50 W/m, $\tau_{transit}=381$ s .	84
4.13	Coaxial radial borehole temperatures and axial fluid temperatures for a case with a constant heat injection rate of 50 W/m, $\tau_{transit}=883$ s .	87
4.14	Net heat transfer rate delivered by the inlet and outlet fluids and lateral heat transfer into the outlet fluid of a u-tube heat exchanger, for a case with a constant heat injection rate of 50 W/m	90
4.15	Percentage of heat transfer and surface area in outlet pipe due to lateral heat transfer	92

4.16	Net heat transfer rate delivered by the inlet and outlet fluids and lateral heat transfer into the outer annulus of a coaxial heat exchanger, for a case with a constant input heat transfer rate of 50 W/m	93
4.17	U-tube and coaxial system resistances during a thermal response test for a case with a constant heat injection rate of 50 W/m	96
4.18	Percentage difference between u-tube and coaxial total and borehole resistances for a thermal response test with a constant heat injection rate of 50 W/m	99
4.19	Fluid velocity for a case where flow is on for one out of every six hours. The plot shows the ramp up and down of velocity during the intermittent cycles	102
4.20	Outlet temperatures and average outlet temperatures during operation for a u-tube and coaxial heat exchanger operated intermittently with an inlet temperature of 25°C for one out of 11 hours	103
4.21	Outlet temperatures and average outlet temperatures during the last operating period of the intermittent operation test with an inlet temperature of 25°C for one out of 11 hours	104
4.22	Heat transfer rates per unit length and cycle averages during operation for a u-tube and coaxial heat exchanger operated intermittently with an inlet temperature of 25°C for one out of 11 hours	105
4.23	Heat transfer rates per unit length and cycle averages during the last operating period of the intermittent operation test with a inlet temperature of 25°C for one out of 11 hours	107

4.24	Heat transfer per unit length averaged over operating duration for 1/2 hour, 1 hour, and 2 hour durations compared with q' for continuously operated u-tube and coaxial heat exchangers. All cases are operated with a constant inlet temperature of 25°C	108
4.25	Heat transfer per unit length averaged over operating duration for 5, 10, and 20 minute durations, where the u-tube transit time is 6.35 minutes and the coaxial transit time is 14.7 minutes. All cases are operated with a constant inlet temperature of 25°C	111
4.26	Outlet temperatures during the first cycle of a two-hour recovery time test, where the undisturbed ground temperature is 11°C. Both heat exchangers are operated at a constant inlet temperature of 25°C, with the u-tube heat exchanger operated for 1 hour and the coaxial heat exchanger operated for 1.17 hours	114
4.27	The minimum, average, and maximum operating outlet temperatures of the u-tube and coaxial heat exchangers over 35 cycles with a two-hour recovery period, where the u-tube operated for 1 hour and the coaxial operated for 1.17 hours, each with a constant inlet temperature of 25°C	116
4.28	Heat transfer rate per unit length for u-tube and coaxial heat exchangers operating intermittently with a 2-hour recovery period, with heat transfer rates averaged over each operating period. The u-tube operated for 1 hour and the coaxial operated for 1.17 hours, each with a constant inlet temperature of 25°C	117

4.29	Average operating heat transfer rate per unit length for recovery times of 20 minutes, 1, 2, 4, and 8 hours, where the u-tube was operated for 1 hour and the coaxial was operated for 1.17 hours, each with a constant inlet temperature of 25°C	118
4.30	Outlet temperature after 24 hours of operation vs. operating durations for the u-tube and coaxial heat exchangers for duty cycles of 25%, 50%, and 75%. Heat exchangers are operated intermittently with an inlet temperature of 25°C	121
4.31	Outlet temperature after 24 hours of operation vs. operating durations for the u-tube and coaxial heat exchangers for duty cycles of 25%, 50%, and 75%, for durations below 0.5 hours. Heat exchangers are operated intermittently with an inlet temperature of 25°C	122
4.32	Non-dimensionalized outlet temperature after 24 hours of operation vs. operating duration for the u-tube and coaxial heat exchangers for duty cycles of 25%, 50%, and 75%. Heat exchangers are operated intermittently with an inlet temperature of 25°C	123
4.33	Effectiveness after 24 hours of operation vs. normalized operating duration for the u-tube and coaxial heat exchangers for duty cycles of 25%, 50%, and 75%. Heat exchangers are operated intermittently with an inlet temperature of 25°C	125
4.34	Resistances for u-tube and coaxial heat exchangers (not to scale) . . .	127
4.35	Effectiveness of u-tube heat exchanger with enhanced grout and coaxial heat exchanger with steel outer tube compared with base cases for each heat exchanger	129

4.36	Constant heat transfer at the wall: comparison between a 2x2 borehole field modelled in OpenFOAM vs. FLS model of 2x2 boreholes using superposition for a case with a constant heat transfer rate at the borehole wall of 50 W/m	133
4.37	Constant heat transfer at the wall: comparison between boreholes modelled in OpenFOAM vs. FLS model for a single borehole, 2x2, 3x3, and 4x4 borehole fields, for cases with a constant heat transfer rate at the borehole wall of 50 W/m	135
4.38	Radial g-functions of a single borehole and a 2x2 borehole field at depths of $z = H/2, H,$ and $3H/2$ for a case with a constant heat transfer rate of 50 W/m, modelled in OpenFOAM	137
4.39	g-functions for constant surface temperature and zero surface heat flux boundaries, 2x2 borehole field, $r_b/H = 0.0005,$ $B/H = 0.05,$ each with a heat transfer rate at the borehole wall of 50 W/m	138

List of Tables

3.1	U-tube dimensions	39
3.2	Coaxial dimensions	43
3.3	U-tube grid and time step sensitivity test results, outlet temperature (°C)	48
3.4	Coaxial grid and time step sensitivity test results, outlet temperature (°C)	48
4.1	Parameters used for the base case tests	70
4.2	Heat transfer per unit length for heat exchangers operated intermit- tently with an inlet temperature of 25°C. Heat transfer rate averaged at a total operating time of 10 hours	109
4.3	Heat transfer per unit length for heat exchangers operated intermit- tently with an inlet temperature of 25°C. Heat transfer rate averaged at a total operating time of 6 hours	112
4.4	Operating, off, and total cycle times for 24-hour duty cycle tests . . .	119
4.5	Resistance of each heat exchanger component from simulation results	126
4.6	Properties of steel coaxial outer pipe	128
4.7	Performance of base and improved cases	128

Nomenclature

A	Area, m ²
B	Borehole spacing, m
c_p	Specific heat capacity, J/kgK
d	Diameter, m
D_h	Hydraulic diameter, m
D	Borehole starting depth, m
f	Darcy friction factor
g	gravity, m/s ²
h	Heat transfer coefficient, W/m ² K
H	Borehole length, m
k	Thermal conductivity, W/mK
L	Length, m
\dot{m}	Mass flow rate, kg/s
P	Pressure, Pa
q	Heat transfer rate, W
q'	Heat transfer rate per unit length, W/m
q''	Heat transfer rate per unit area, W/m ²
r	radius, m
r_b	Borehole radius, m or mm
R	Resistance, mK/W
s	U-tube spacing, m or mm
S	Slope
t	Time, s, hour, day, or year
t_s	Steady state time for a borehole, s

T	Temperature, °C or K
u	Fluid velocity in the axial direction, m/s
V	Volume, m ³
x	x direction
y	y direction
z	Axial direction
α	Thermal diffusivity, m ² /s
ε	Effectiveness
θ	Non-dimensional temperature
μ	Dynamic viscosity, kg/ms
ρ	Density, kg/m ³
τ	Time constant, s

Subscripts

0	Undisturbed value
ann	Annular
b	Borehole
coax	Coaxial
dur	Operating duration
exp	Experimental
f	Fluid
ground	Ground
grout	Grout
k	Face index
i	Inner radius
in	Inlet
inner	Inner
int	Interaction
io	Outer property of inner pipe
lat	Lateral
max	Maximum
num	Numerical
o	Outer radius
off	Off
oi	Inner property of outer pipe
oo	Outer property of outer pipe
out	Outlet
outer	outer
p	Pipe
s	Solid
tot	Total
transit	Transit time
u-tube	U-tube
w	Water
wall	Wall
∞	Far field

Dimensionless Groups

Fo	Fourier number
Nu	Nusselt Number
Pr	Prandtl Number
Re	Reynolds Number

Acronyms

ASHP	Air source heat pump
BHE	Borehole heat exchanger
BTES	Borehole thermal energy storage
COP	Coefficient of performance
DLSC	Drake landing solar community
DST	Duct storage
FLS	Finite line source
FEM	Finite element method
FVM	Finite volume method
GSHP	Ground source heat pump
ICS	Infinite cylindrical source
ILS	Infinite line source
PD	Percentage difference
TRT	Thermal response test
UTES	Underground thermal energy storage

Declaration of Academic Achievement

This thesis contains original research conducted by the author under the academic supervision of Drs. Lightstone and Cotton. The development of the numerical model, simulations, and data processing were all conducted by the author. This manuscript was prepared by the author, with editing contributed by Drs. Lightstone and Cotton.

Chapter 1

Introduction

1.1 Background

In cold climate countries, space heating represents a significant proportion of total energy demand. In Canada, for example, heating constitutes 63% of overall residential energy use [1]. The majority of this demand is met through unsustainable methods such as burning fossil fuels or wood [2], which contributes to greenhouse gas emissions. Much of the remaining heating is provided using electric resistance heating [2], which can be expensive and may also be generated from greenhouse gas emitting sources. Therefore, there is a need for practical sustainable alternatives for space heating that could mitigate costs and reduce emissions.

1.1.1 Geothermal technologies

Geothermal technologies such as ground source heat pumps (GSHPs) and geothermal storage are examples of such an alternative. These technologies take advantage of the



(a) Horizontal ground heat exchanger (b) Vertical ground heat exchanger

Figure 1.1: Vertical and horizontal ground heat exchanger arrangements [6]

thermal energy in the ground to provide heating without the need to burn fossil fuels.

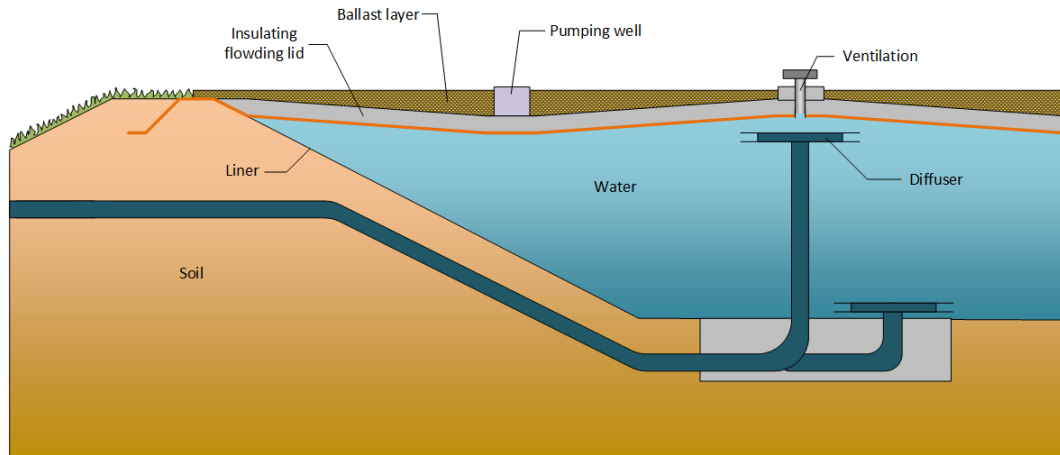
Heat pumps

Heat pumps are a sustainable alternative to electric resistance heating, since they require approximately 19 to 50% of the electricity to operate [3–5]. They are particularly effective when source-to-sink temperature differentials are moderate. Heat pumps can be used for residential heating, in both single family homes and larger buildings. The most common type of heat pump is the air source heat pump (ASHP), which relies on the ambient air as its source. Air temperatures, particularly in cold climates, can be highly variable and sometimes extreme, leading to reductions in the heat pump coefficient of performance (COP). In fact, when temperatures are low, the COP of the air source heat pump will approach 1, meaning it requires as much electricity as resistance heating. Conversely, ground source heat pumps achieve superior performance to air source heat pumps, because the ground’s moderate temperature provides a better COP.

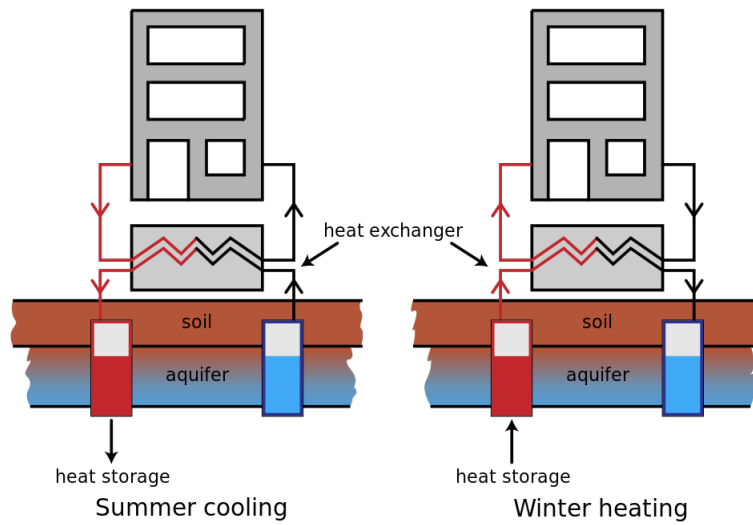
Ground source heat pump systems exchange heat with the ground using two primary methods: horizontal and vertical heat exchangers. Horizontal ground heat exchangers are installed in trenches at a depth of 1 to 2 m and can take a variety of forms, such as linear and slinky arrangements [7]. An example of a linear system is shown in Figure 1.1a. Horizontal heat exchangers require a very large area of land to install, thus making them impractical on sites with limited space. Therefore, the vertical heat exchanger, with its much smaller profile, is more versatile. This heat exchanger type, depicted in Figure 1.1b, is installed in a vertically drilled well, or borehole. The borehole heat exchangers (BHEs) are typically 10 to 15 cm in diameter and can range from 20 to 300 m in depth [8]. Many GSHP systems employ more than one borehole, with adequate spacing between them to minimize thermal interference, with a minimum spacing of 5 m [9, 10]. While vertical heat exchangers address space limitations, drilling boreholes to such depths can be costly. A significant barrier to the wider adoption of ground source heat pumps remains the high capital cost.

Geothermal storage

Geothermal storage uses the ground as the medium or location for storing heat energy. Otherwise known as underground thermal energy storage (UTES) it is often used for seasonal storage. This application takes advantage of the abundance of heat available during the summer months by collecting that energy and storing it underground. When heating is required in the winter months, the thermal energy is extracted from the ground to be used. Geothermal storage systems are typically sizeable, used for heating larger buildings or in community-scale projects.



(a) Pit thermal energy storage [11]



(b) Aquifer thermal energy storage [12]

Figure 1.2: Pit and aquifer thermal storage systems

Geothermal storage systems take a variety of forms. Some of the simplest examples are pit and aquifer thermal energy storage, which collect heat in large volumes of water held inside a cavity in the ground. Pit storage is accomplished through the excavation of a large man-made reservoir, while aquifer storage uses natural features. Both systems benefit from the high heat capacity of water and relatively quick charging or discharging. However these type of storage also have drawbacks: specifically, pit storage requires a very large area of land, and aquifer storage is constrained by the presence of pre-existing geological features [13].

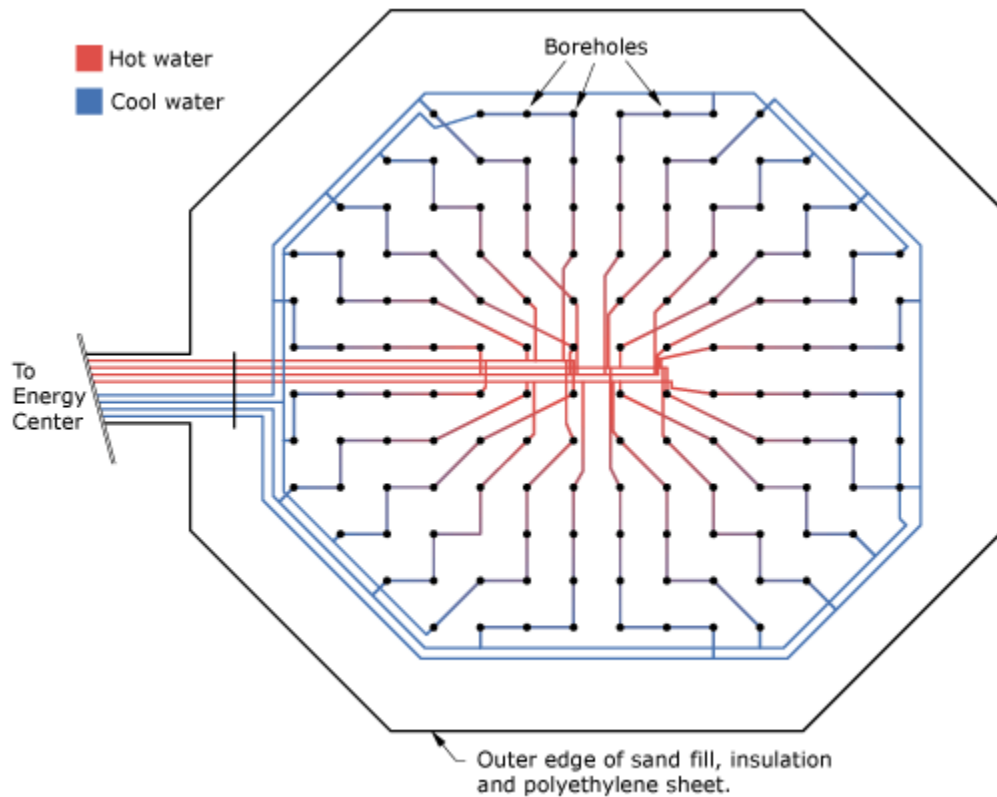


Figure 1.3: Aerial view of the Drake Landing borehole thermal energy storage field [14]

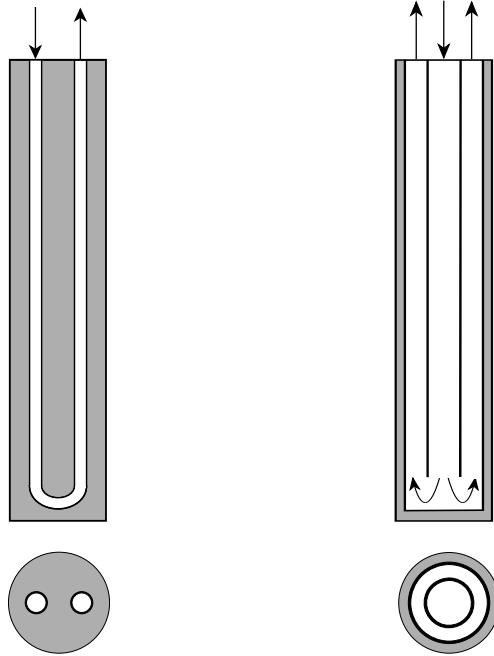
Borehole thermal energy storage (BTES) addresses both the land area and geological limitations of the other types of underground thermal storage. In BTES, the ground itself acts as the storage medium. Heat is transported into the ground using a large array of borehole heat exchangers. For seasonal storage, it is necessary to use a large number of heat exchangers grouped close together to retain heat in the borehole field. If the number of boreholes is insufficient, the ground would function as a heat sink, as it does in the case of ground source heat pumps. Research and design efforts have focussed on minimizing thermal losses. One such example of this is radial stratification, which strategically directs flow during heat injection radially outwards from the centre to the perimeter of the borehole field. This limits thermal losses by isolating the hottest temperatures in the core of the array. This configuration is depicted in Figure 1.3, showing the borehole field in the Drake Landing Solar Community (DLSC). It was established that the DLSC system has a thermal efficiency, defined as the ratio of energy deposited to the energy extracted over a year, of approximately 40 to 50% [15].

The use of vertical heat exchangers results in fewer space restrictions in comparison to pit storage, making it possible to install BTES under buildings or below park space. Some of the drawbacks of borehole thermal energy storage are slower charging and discharging rates and high initial capital cost, since the cost drilling a large quantity of boreholes is significant. Furthermore, there are some geological restrictions. For instance, BTES cannot be installed in areas with high groundwater flow, since the movement of groundwater would carry thermal energy away from the storage site.

1.1.2 Borehole Heat Exchangers

Borehole heat exchangers are the component that enables borehole thermal energy storage and many ground source heat pump systems. BHEs consist of tubing placed inside a vertical drilled well. To enhance heat transfer with the surrounding environment, the tubing within the borehole is typically surrounded by grout; however, the borehole can also be filled with gravel backfill or groundwater. A high conductivity grout material is preferred to ensure a high heat transfer rate to the ground. U-tube borehole heat exchangers are the most common design; this arrangement consists of u-shaped tubing, where fluid enters into one channel of the tube and exits up the second channel. Another common design is the coaxial, or tube-in-tube, heat exchanger which is comprised of two concentric tubes. Fluid can enter into the centre pipe, flow down to the bottom and exit up the annulus, or vice versa. Cross-sections of the coaxial and u-tube borehole designs can be seen in Figure 1.4, which are not to scale. The BHEs have typical diameters of 10 to 15 cm and depths ranging from 20 to 300 m [8].

Heat exchanger design is considered an important factor influencing the overall performance of the geothermal systems. As such, altering the configuration of borehole heat exchangers is often explored as a way to improve the performance of the heat exchanger, which could result in length reductions that would lower the cost of drilling. These efforts have led to the introduction of many novel heat exchanger designs, including the helical and double u-tube configurations. The helical design consists of a helically coiled tube placed inside the borehole, which increases the surface area for heat exchange. The double u-tube involves the addition of a second u-tube pipe, which improves surface area and allows for two independent flow circuits.



(a) U-tube heat exchanger (b) Coaxial heat exchanger

Figure 1.4: Axial and lateral cross-sections of the u-tube and coaxial heat exchanger designs, with the grout shaded in grey, not to scale

The coaxial design also aims to improve performance by enhancing the surface area for heat exchange and increasing the ratio of working fluid to the volume of grout required, thereby reducing the thermal resistance of the borehole heat exchanger.

Thermal resistance is the most common measure used to compare designs. It is possible to readily calculate this steady state term using a number of analytical models, which provides a straightforward basis of comparison for the heat exchangers. For this reason, the coaxial heat exchanger configuration is often proposed as a way to improve performance, since it has a lower thermal resistance than the u-tube due to a higher proportion of water to grout. Borehole heat exchanger performance, however, is complex and often dynamic. The heat transfer consists of conjugate heat transfer between the upward and downward legs of the fluid flow, the various heat

exchanger components, and the ground, all of which have varied conductivities and heat capacities. There are also large variations in physical scale, with the boreholes reaching depths of hundreds of metres while heat exchanger components are millimetres thick. In addition, the radial heat transfer from the heat exchanger can impact the ground temperature for significant distances. Furthermore, operation of borehole heat exchangers is often not steady. For instance, it is typical in GSHP applications to operate BHEs intermittently, turning them on to when temperature deviates from a desired set point and turning them off again when the set point is reached. As such, a steady state measure of performance is not adequate to fully capture the differences between borehole heat exchanger designs. Therefore, there is a need to compare borehole heat exchangers using detailed numerical modelling that captures the important characteristics of the heat exchangers, including conjugate heat transfer and the behaviour under transient operating conditions.

1.2 Objectives

The objectives of this study were to:

- Develop and validate a numerical model that could characterize the performance of borehole heat exchangers over a wide variety of relevant time scales thus enabling short- and long-term analysis
- Provide a comparative analysis of the performance of u-tube and coaxial heat exchangers that leads to an enhanced understanding of the differences in behaviour between the two designs
- Establish a framework to assess the performance of u-tube and coaxial heat

exchangers under intermittent operating conditions

1.3 Thesis Outline

This thesis consists of five chapters, including this introduction chapter. Chapter 2 contains a literature review, outlining the state of the art for borehole heat exchanger modelling and research on borehole design and operation. Chapter 3 describes the development of a custom detailed conjugate heat transfer model for the u-tube and coaxial heat exchangers. In Chapter 4, the experimental validation of the u-tube and coaxial heat exchanger models is presented, and the overall findings of the research study are reported and discussed. This includes an investigation of the differences in performance of u-tube and coaxial heat exchangers under continuous operating conditions and an in-depth study of the two heat exchangers when operated intermittently. This work led to a thorough understanding of the differences in performance of the u-tube and coaxial heat exchangers. The intermittent study resulted in key findings about both intermittent operation of borehole heat exchangers in general and how this operation mode caused differences in the performance of the heat exchanger designs. This chapter also explores the impact of heat exchanger design features and includes modelling of borehole fields. Finally, Chapter 5 summarizes the findings and key contributions of this research study.

Chapter 2

Literature Review

The following section outlines the state of the art pertaining to the prediction of borehole heat exchanger performance. This includes work dedicated to modelling borehole heat exchangers and research into the impact of heat exchanger design and operation on performance.

2.1 Modelling Borehole Heat Exchanger Systems

Modelling for borehole heat exchangers can be divided into two general approaches: imposed borehole wall boundary models, which consider the borehole and ground separately, and fully-coupled models that consider the borehole and the ground simultaneously. Each approach has advantages and drawbacks related to accuracy and computational cost, which will be discussed in the following literature survey.

2.1.1 Imposed borehole wall boundary models

This class of model follows a common solution approach in which a boundary condition, such as a fixed temperature or heat flux, is applied to the borehole wall to obtain the temperature response in the ground. This ground temperature response is then used to inform the solution of the borehole fluid temperatures using a separate model for the borehole heat exchanger, which is often based on steady-state resistance. As such, these models do not consider the transient behaviour of the fluid, piping, and grout and do not account for the convective effects of the fluid flow.

Ground response models

Many of the models used to predict the ground temperature response are analytical. The earliest example in the literature is the Infinite Line Source (ILS) model, which approximates the borehole as an infinitely long heat source in a homogeneous, semi-infinite medium. This one-dimensional model neglects both the borehole curvature and the end effects at the surface and bottom of the borehole. The solution to this formulation [16] involves an improper integral that can be solved numerically.

Building upon this heat source approach, the Infinite Cylindrical Source (ICS) model [17] represents the borehole as a cylindrical surface, rather than a line source. It is formulated in terms of an improper integral comprised of Bessel functions of the first and second kind, which can also be solved using numerical integration. While ICS still neglects the end and surface effects, it provides a more accurate representation of the temperature response near the borehole wall, which is important for early performance prediction.

The length of the borehole was later taken into account with the Finite Line Source

(FLS) model proposed by Eskilson [9]. It is a 2D representation constructed by numerically integrating a series of point heat sources in a solid, semi-infinite medium over the length of a borehole. The ground surface is treated as a constant temperature boundary, which is equal to the initial temperature of the ground. The FLS overcomes the 1D limitations associated with the infinite models; however, it retains the drawbacks of modelling the borehole as a line rather than a surface. Given the 2D formulation of FLS, a single representative value can be chosen for the borehole wall temperature, which may either be the temperature at the middle height of the borehole or an integral mean value [18–20].

Eskilson [9] also developed a numerical approach to predict the ground response, specifically tailored to ground source heat pump systems. This finite difference model considers a borehole of depth H and radius r_b in an infinite, homogeneous ground. The model can account for boreholes that began at a certain depth D underground and at any given angle from the vertical. Like the FLS formulation, this numerical model sets the ground surface to a constant temperature. However, unlike FLS, it also applies a constant temperature, rather than a heat flux, at the borehole wall. The boundary condition choice is significant, as the choice in borehole wall boundary condition affects long-term predictions, particularly when the solution is applied to multiple boreholes. The heat flux as a result of the applied temperature is then calculated from the temperature gradient at the borehole wall.

Eskilson expressed the temperature solution obtained from the numerical model in terms of non-dimensionalized g-function curves. The g-function can be assessed at

any time or radius from the borehole and is defined as

$$g\left(\frac{t}{t_s}, \frac{r}{H}\right) = \frac{2\pi k}{q'} \left(T\left(\frac{t}{t_s}, \frac{r}{H}\right) - T_{ground,\infty} \right) \quad (2.1.1)$$

where $T_{ground,\infty}$ is the initial or undisturbed ground temperature, k is the ground thermal conductivity, and t_s is the time for the borehole to reach steady state, defined by Eskilson as

$$t_s = \frac{H^2}{9\alpha} \quad (2.1.2)$$

where α is the ground thermal diffusivity. The characteristic time t_s coincides with a very long time period. Using the characteristic time, the Fourier number, defined as

$$Fo = \frac{\alpha t}{R^2} \quad (2.1.3)$$

can be related to the ratio between borehole radius and height, r_b/H

$$Fo = \frac{1}{9(r_b/H)^2} \quad (2.1.4)$$

Often, g-functions are presented in terms of the temperature solution at the borehole wall T_b , which gives the borehole temperature over time. Eskilson introduced the g-function curve to present the results of numerical simulations, but the results of many models, including the analytical solutions above, can be non-dimensionalized as a g-function.

Ground response models for multiple boreholes

The above solutions can also be used to solve for the temperature response of multiple boreholes grouped together. A common approach for imposed wall boundary models uses spatial superposition [9, 19, 21–24]. In this method, the solution for an individual borehole is obtained and superimposed at different locations to determine the total ground response. This superposition approach can be applied to any axisymmetric model, where the general form is

$$T_b = T_{ground,\infty} + \sum_{i=1}^N T_i(r_i, z_i, t) \quad (2.1.5)$$

with $T_i(r_i, z_i)$ being the solution for the i th borehole.

Eskilson [9] incorporated spatial superposition into the g-function curves and tabulated the results for numerous borehole field configurations. This data has since been included in commercially available software, including EED [25], GLHEPro [26], and GLD [27]. An example of the result is shown in Figure 2.1, which depicts g-functions for a 10 by 10 borehole field. The plot shows that the ground temperatures are impacted by the borehole spacing, B . As shown, the g-functions converge at small values of $\ln(t/t_s)$, where the temperature response is caused by the individual borehole heat transfer. The curves diverge when the temperature disturbances from the neighbouring boreholes begin to take effect. The time at which this occurs is dictated by the spacing. An inflection point on the g-functions can also be observed. This is associated with the time at which the inside of the borehole field becomes uniform, such that the heat transfer occurs with the borehole field acting as a single unit. The dashed line is the g-function for a single borehole.

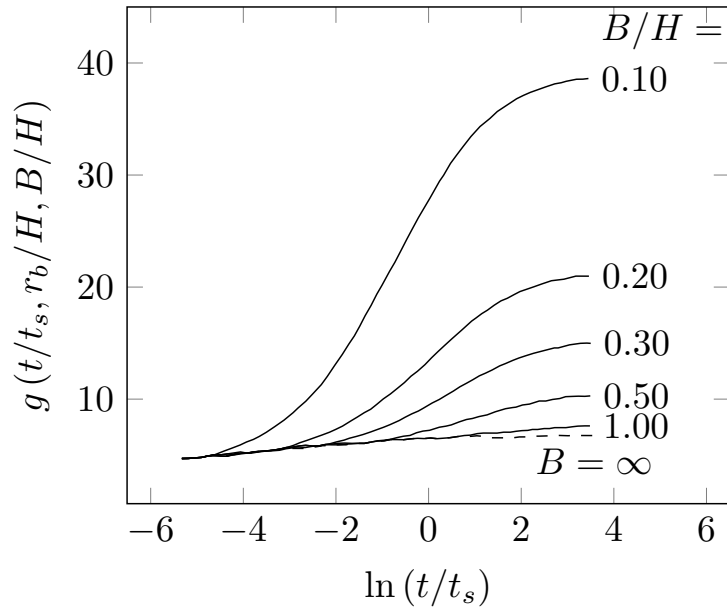


Figure 2.1: g -functions for a 10 by 10 borehole field with variable borehole spacing, digitized from Eskilson [9], where B is the borehole spacing and H is the borehole depth

The duct storage (DST) model developed by Hellström [28] is an example of a model designed specifically for borehole fields. DST is a finite difference model, which has since been implemented in the system modelling software TRNSYS [29, 30]. This model was used in the design of the Drake Landing Solar Community borehole field [31]. The DST modelling approach divides the ground into two domains: local regions close to the boreholes, and a global region encompassing the entire field. The local regions consist of hollow cylinders, where a heat flux is applied to the inner radius, representing the borehole. Local meshes can be assigned to each borehole in the field, or multiple boreholes can be grouped into a mesh; however, in this case, the boreholes are agglomerated, and the heat flux condition is still only applied at the inner radius. The fluid outlet temperature is determined using a steady resistance model of the borehole (discussed further in the following section). The heat flux at

the outer radius of the local domain is set to zero, effectively assuming a very large borehole field with symmetry at the boundaries between boreholes. The temperature at that boundary is determined by superimposing the temperature change due to adjacent boreholes. The solution of the fluid temperature in the local mesh is used to assign an average temperature to the global mesh. Modelling in the global mesh consists of an initial transient build up, a steady state component, and a periodic variation (representing the seasonal nature of the storage), which averages to a net zero heat flux.

Borehole heat exchanger modelling

With the ground temperature response established, that solution can be used to find the fluid temperatures in the borehole. Determining the fluid temperatures is essential to any design or performance prediction, since the outlet temperature will dictate the heat transfer to the load. The simplest representation of the inside of a borehole is a resistance model, which can be expressed as [28]

$$T_f = T_b - q' R_b \quad (2.1.6)$$

where R_b is the borehole thermal resistance and T_f is the fluid temperature. Expressed another way, the borehole resistance R_b is multiplied by a temperature difference between the borehole wall and the fluid to yield a heat transfer rate per unit depth.

$$q' = \frac{1}{R_b} (T_b - T_f) \quad (2.1.7)$$

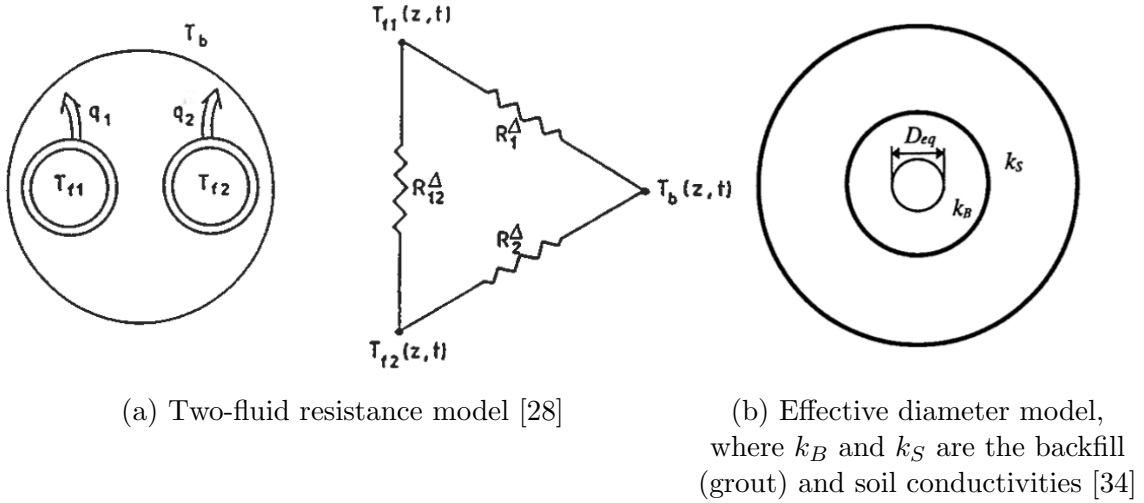


Figure 2.2: Borehole heat exchanger models

Since this approach does not include the heat capacity of the borehole components, it neglects the transient response. The resistance of the borehole can be determined analytically, numerically, or empirically. A method proposed by Paul [32] uses shape factors, established with empirical and numerical data. An alternative is the multipole method [33], which describes the borehole components as line sources to obtain a resistance value. Hellström published solutions of the multipole model for the u-tube and coaxial borehole designs. A depiction of the multipole method, which allows thermal short circuiting between inlet and outlet flows, is shown in Figure 2.2a. Gu and O’Neal [34] and Kavanaugh [35] also proposed effective diameter models that treated the u-tube channels as a single pipe concentric within the borehole, surrounded by annulus of grout, shown in Figure 2.2b.

The multipole method, developed by Bennet et al., has been demonstrated to show good agreement with numerical modelling [36, 37], and thus was selected for use in predicting the u-tube and coaxial borehole resistances in this study. This work

employs the equations derived by Hellström [28]. For all configurations, Hellström defines a three-dimensional effective resistance, R_b^* , assuming a uniform heat flux along the borehole

$$R_b^* = R_b \left(1 + \frac{H^2}{3 (\dot{m} c_p)^2 R_a R_b} \right) \quad (2.1.8)$$

where R_b is the two-dimensional borehole resistance. For the u-tube this is defined as

$$R_{b,u-tube} = \frac{1}{2} \left(\frac{1}{2\pi k_{grout}} \left[\ln \left(\frac{r_b}{r_o} \right) + \ln \left(\frac{r_b}{s} \right) + \sigma \ln \left(\frac{r_b^4}{r_b^4 - (s/2)^4} \right) \right] \right. \\ \left. + \frac{1}{2\pi k_p} \left[\ln \left(\frac{r_o}{r_i} \right) \right] + \frac{1}{2\pi r_i h} \right) \quad (2.1.9)$$

where s is the spacing between tubes, r_i and r_o are the tubing inner and outer radii, respectively, r_b is the borehole radius, and k_p is the pipe thermal conductivity. The heat transfer coefficient is h , calculated in this thesis using the Dittus Boelter correlation for cooling [38], and σ is

$$\sigma = \frac{k_{grout} - k_{ground}}{k_{grout} + k_{ground}} \quad (2.1.10)$$

The quantity R_a is the internal resistance within the heat exchanger, which is defined for the u-tube as such

$$R_{a,u-tube} = \frac{1}{\pi k_{grout}} \left[\ln \left(\frac{s}{r_o} \right) + \sigma \ln \left(\frac{r_b^2 + (s/2)^2}{r_b^2 - (s/2)^2} \right) \right] + 2 \left\{ \frac{1}{2\pi k_p} \left[\ln \left(\frac{r_o}{r_i} \right) \right] + \frac{1}{2\pi r_i h} \right\} \quad (2.1.11)$$

Hellström's model assumes a fixed heat flux from the tubes and an equal temperature for the fluids in both the downward and upward tubes.

The two-dimensional resistance for the coaxial heat exchanger is defined as

$$R_{b,coaxial} = \frac{1}{2\pi r_{oi} h_{oi}} + \frac{1}{2\pi k_p} \ln\left(\frac{r_{oo}}{r_{oi}}\right) + \frac{1}{2\pi k_{grout}} \ln\left(\frac{r_{bh}}{r_{oo}}\right) \quad (2.1.12)$$

where r_{oi} is the outer pipe inner diameter, r_{oo} is the outer pipe outer diameter, and h_{oi} is the heat transfer coefficient at the inner surface of the outer pipe.

The internal resistance is

$$R_{a,coaxial} = \frac{1}{2\pi r_{io} h_{io}} + \frac{1}{2\pi k_p} \ln\left(\frac{r_{io}}{r_{ii}}\right) + \frac{1}{2\pi r_{ii} h_{ii}} \quad (2.1.13)$$

where r_{io} and h_{io} are the radius and heat transfer coefficient for the outer surface of the inner pipe, and r_{ii} and h_{ii} are the radius and heat transfer coefficient for the inner surface of the inner pipe.

Since the steady approximation of the borehole neglects the short-term heat transfer response, authors in the literature have also proposed lumped capacitance approaches. One such example is the model by Bauer [39], which accounted for the heat capacity of the grout, but not the other components. In another example of lumped-capacitance modelling, Javed and Claesson [40] extended the effective diameter model to account for the heat capacity of the fluid. The model did not, however, account for the heat capacity of the other components of the borehole.

Challenges with imposed borehole boundary models

A fundamental drawback of imposed wall boundary models is that the wall boundary condition is not necessarily known a priori and, therefore, must be estimated. The true input conditions to the system are the fluid inlet temperature and flow rate. A heat

flux can be estimated if the heating loads for a GSHP are known or if the desired heating rate for BTES is established. For Eskilson's fixed temperature condition, a heat flux is specified by the user, from which a borehole wall temperature was calculated. Such an approach, however, does not make direct use of the known inputs.

The imposed boundary models also possess time scale limitations which could have implications on their accuracy. Line source models (i.e. ILS and FLS) are not valid at short times because they do not accurately represent the borehole wall surface [41]. Ingersoll et al. [17] imposed a lower limit of $Fo = 20$ on the ILS model, while Eskilson [9] suggested a less restrictive criterion of $Fo > 5$ for the FLS model. According to Yavuzturk and Spitler [21], this criterion corresponds with a time scale of 3-6 hours for a typical borehole. Conversely, the infinite models are not valid for very long times, because they do not consider axial effects [41]. The use of steady state resistance to represent borehole heat exchangers also neglects the transient behaviour of the heat exchanger at early times. It is important to be able to model both short and long time scales because the performance of these systems varies in time scales on the order of years, while concurrently, the systems are likely to undergo rapid changes (on the scale of minutes or hours) to the inlet conditions during normal operation. A model that accounts for both long and short time scales can therefore be critical to accurate performance predictions.

2.1.2 Coupled borehole-ground modelling

Models that couple the borehole heat exchanger to the ground address some of the limitations of the imposed borehole wall boundary models. Some of these models

consider all parts of the borehole heat exchanger, including fluid flow, while others incorporate only some parts of the heat exchanger but stop short of directly modelling the convective heat transfer.

Partial borehole coupled models

Lamarche and Beauchamp [42] extended the effective diameter model to include an analytical solution for the grout heat transfer. While it does not retain the exact geometry of a u-tube heat exchanger, it matches well with the coaxial design. The authors applied both heat flux and temperature boundary conditions to the pipe wall. This analytical model predicts shorter time scale responses without the need for numerical discretization.

Yavuzturk and Spitler [21] sought to improve upon Eskilson’s g-functions by extending the numerical model to the borehole grout and piping using the Finite Volume Method (FVM). To limit computational cost, the geometry of the grout and u-tube were mapped to a cylindrical mesh, resulting in a “pie-sector” shaped pipe. The fluid, however, was not modelled numerically. Instead, a heat flux boundary condition was applied to the inner radius of the pipes. By modelling the grout numerically, this approach accounted for shorter time scales than the original g-functions. A steady resistance term was applied to extend the fluid temperature prediction to the borehole wall in order to align their results with the long time scale g-functions. The short time step g-functions developed with this approach were then applied, using steady state borehole resistances, to make u-tube and coaxial heat exchanger performance predictions by Yavuzturk and Chiasson [43].

Some researchers have elected to model the ground response around multiple boreholes numerically, meshing the entire field. Li et al. [44] and Koochi-Fayegh and Rosen [45], applied a heat flux to the borehole wall and simulated the resulting ground response. Başer and McCartney [46] applied a heat flux to the inner pipe wall instead. This method is similar to g-functions, but eliminates the simplifications associated with spatial superposition. Kandiah and Lightstone [15] used experimental data obtained from the Drake Landing borehole field to model the ground temperature response. The model applied a temperature boundary condition to the borehole wall derived from the experimental results. The model represented the boreholes with a square rather than circular cross section. The results provided evidence that this approximation was acceptable. While this approach imposes more realistic boundary conditions than the wall heat flux models, it would not be viable for borehole fields with different geometries or operating conditions.

Fully-resolved borehole coupled models

Fully-coupled models eliminate the need to assume any boundary condition inside the borehole. Instead, the borehole or borehole field performance is predicted using only known inlet conditions: fluid inlet temperature and flow rate.

With advances in computational power, it is possible to model borehole systems in great detail. A more comprehensive approach includes modelling fluid convection within the borehole pipes coupled to the components inside and outside the borehole. Examples of high-resolution modelling are the work by Bouhacina et al. [47] and Chen et al. [48], who developed finite volume and finite element (FEM) models, respectively, for a single borehole. These models were discretized into a fine mesh, an example of

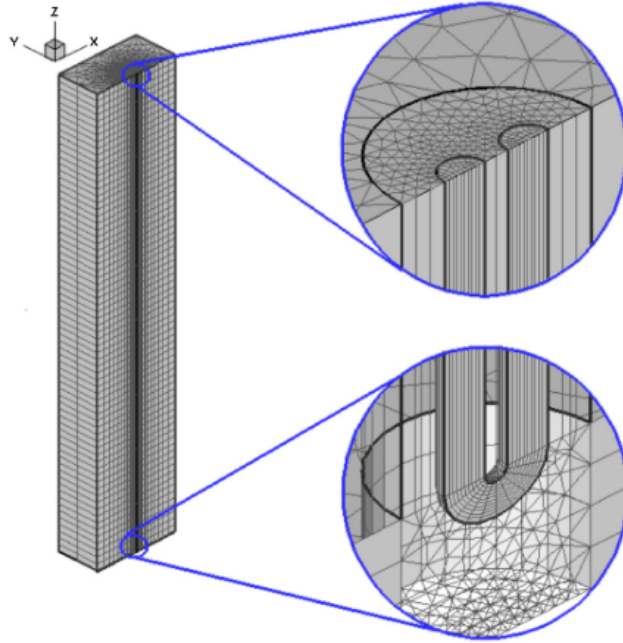


Figure 2.3: A high-resolution finite element model developed by Chen et al. [48]

which can be seen in Figure 2.3. Groundwater flow was also incorporated into these models, and the pipe flow was represented using $k-\varepsilon$ turbulence models. Bouhacina et al. simulated a period of 18 hours, and Chen et al. considered a period of 24 hours. The large number of cells used in these models result in a high computational cost. Therefore, longer-term simulations of the performance would take considerable time.

The computational cost becomes a greater challenge as the domain size increases in such detailed models. High-resolution borehole field models require refined grids near and within each borehole but must also cover thousands of cubic metres in volume. Despite these obstacles, authors in the literature have developed detailed borehole field models. J. Chen et al. [49] used FVM to model a 12-borehole field of double u-tube heat exchangers. The authors neglected groundwater flow and any thermal property variations in the ground. The fluid flow was modelled using the $k-\varepsilon$

turbulence model, and this study neglected the elbow at the bottom of the u-tube. The mesh that resolved the fluid, grout, and soil was composed of over 1.7 million cells. The authors simulated a period of 70 days and demonstrated that the results were within 1°C of experimental data. Moradi et al. [50] also developed a coupled fluid flow-conduction model. They used FEM and considered both convection and conduction in the ground. Their model discretized the fluid domain in three dimensions, applying a steady fluid flow profile to that domain. Moradi et al. modelled a smaller borehole field with only 5 boreholes, based on a laboratory-scale experimental set up which did not contain grout. The authors predicted the 8-day performance of the system. Much like their single-borehole counterparts, these high-resolution, fully-coupled borehole field models would be difficult to scale up for long term simulations, particularly in a design context.

Many authors have elected to implement simplifications to their coupled models in an effort to reduce the high computational costs. Some authors have chosen to approximate boreholes and/or their components as squares with equivalent cross-sectional areas for a simplified mesh. Zhang et al. [51] and Catolico et al. [52] modelled the borehole field at the Drake Landing Solar Community using the TOUGH2 [53] porous flow software. Both neglected the borehole grout and piping and opted to model boreholes as square cells, which were divided into inner and outer elements, representing inlet and outlet flow. The modelling of the fluid enabled the authors to consider the series arrangement of borehole strings, and the porous model meant that groundwater flow was also accounted for. The authors used very coarse grids: Catolico et al. used a 62 x 62 x 26 cell mesh, and Zhang et al. used a 30 x 20 x 8 cell mesh. This enabled them to run long-term simulations, but likely also had an impact

on accuracy. For reference, the square, soil-only mesh by Kandiah and Lightstone [15] required 1.6 million cells.

Other authors developed FEM models meant to simplify the representation of the borehole. Al-Khoury et al. [54, 55] developed a 1D element to represent the borehole. This model considered the 1D axial conduction and convection in the borehole, while still considering the radial heat transfer between the fluid and the grout. A heat transfer coefficient is used to describe the fluid heat exchange, and the piping is modelled with a resistance value. The 1D element was placed within a 3D FEM mesh of the soil. Wołoszyn and Gołaś [56] built upon the work of Al-Khoury et al. by dividing the grout into three sub-regions. This provided increased resolution of the temperature distribution inside the borehole. Wołoszyn [57] also applied this model to a borehole field.

Rees and He [37, 58] developed an FVM model that considered fine detail in the piping, grout, and soil, but simplified the fluid into a 1D flow, 2D temperature mesh. The fluid velocity was imposed at the inlet, and the heat exchange with the pipe wall was calculated with a heat transfer coefficient defined using the Dittus Boelter correlation. The fluid temperature was able to vary axially and in the azimuthal direction. This allowed for a reduction in mesh size, and could enable the modelling of borehole fields with strings, where more than one borehole is connected in series; however, when He [37] studied multiple borehole configurations, they neglected the fluid flow in those simulations.

Challenges with fully coupling boreholes and soil

The fully-coupled models provide considerable information about borehole heat transfer. This approach makes it possible to understand the complex heat transfer behaviour that arises from combining fluid flow in a small area with solid conduction in a vast domain. These models enable the investigation of how short and long time scale processes impact the performance of geothermal systems.

The drawback inherent to such detailed models, however, is their high computational cost. As a result, the majority of the fully-coupled borehole field models in the literature only simulate short periods of time. This limitation reduces the utility of these models for applications such as design, where it must be possible to predict long-term performance to assess the viability of a design.

2.2 Improvements to Borehole Heat Exchanger Design

Given the large expense of drilling borehole heat exchangers, considerable research effort has been dedicated to reducing their cost, particularly through design improvements. While the u-tube heat exchanger design is the most prevalent, many alternative heat exchanger configurations have been proposed, all of which aim to improve performance by enhancing heat exchange with the ground. These include double u-tube designs [28], u-tubes with fins added to the piping [47], and helical borehole heat exchangers [59]. Of particular interest is the coaxial heat exchanger, which has been discussed extensively [43, 60, 61] in the literature for its potential to improve borehole performance. Like many other BHE alternatives, the coaxial heat exchanger has a

lower thermal resistance than the u-tube, due to a larger ratio of water to grout compared to the u-tube. As such, it is suggested that the coaxial design could significantly improve heat exchanger performance.

Several studies have found that using a coaxial heat exchanger design is beneficial compared to the u-tube configuration. A numerical study by Yavuzturk and Chiasson [43] compared u-tube and coaxial heat exchangers subject to real building loads. The modelling predicted the borehole wall temperature using short time step g-functions developed for u-tubes [21] and applied steady state borehole resistances for each design to obtain fluid temperatures. The results of the comparative study indicated that using a coaxial heat exchanger could reduce the required borehole length by 33%. Similar findings were obtained in experiments conducted by Wang [62], in which a u-tube and coaxial heat exchanger were subjected to intermittent heat injection for 20 to 25 minutes out of each hour. The results demonstrated that a heat pump connected to a coaxial heat exchanger performed better than one connected to a u-tube, with the author predicting possible length reductions of 30 to 50% if a coaxial design was chosen.

Not every study, however, concludes that the coaxial heat exchanger outperforms the u-tube. In experimental tests by Wood et al. [63], coaxial and u-tube heat exchangers subject to a constant inlet temperature were compared. The results showed that the coaxial heat exchanger provided a lower heat output compared to the u-tube design. Poorer performance may have occurred due to the thick outer pipe employed and laminar flow observed in the coaxial annulus. Sliwa and Rosen [64] observed similar outcomes in numerical simulations comparing the two designs under constant heat loading. After a 100 hour simulation, which tested the u-tube and coaxial heat

exchangers of the same depth and diameter, it was found that the coaxial outlet temperature was 3°C warmer than that of the u-tube. One potential reason for this difference could be the large volume of grout used in the coaxial design, where grout thickness exceeded 4 cm.

There are many challenges involved in comparing different borehole heat exchanger designs. A reliable assessment of the differences between heat exchanger performance requires a controlled and methodical approach. One difficulty is maintaining consistent sizing while using heat exchangers of differing geometries. For instance, in their resistance-based study, Desmedt et al. [65] compared 115 mm diameter u-tubes against coaxial heat exchangers with a diameter of 180 mm. A variation in borehole diameter makes it difficult to compare borehole performance because the surface area in contact with the ground is not the same for each heat exchanger. This could result in differences in heat exchanger performance that are not directly attributable to the design.

Maintaining comparable flow rates and flow regimes presents an additional challenge. Some studies, such as the experiments conducted by Wang [62], use different flow rates for the different designs (14.5 gpm for the coaxial and 11 gpm for the u-tube). This helps achieve the desired flow regime within each heat exchanger and may also arise due to differing pressure drops in the heat exchangers, but could make it difficult to ascertain whether a difference in performance was due to the flow or the design. Even when the flow rates are consistent, it is difficult to compare borehole designs because the heat exchangers have dissimilar flow areas, which can result in differing flow regimes. This was true in the study by Wang; even with the higher flow rate, the coaxial heat exchanger had a Reynolds number of 7000, while the u-tube

had a Reynolds number equal to 19,000. In the experiments by Wood et al. [63], the Reynolds number in the coaxial annulus was consistently below 2000, while the u-tube flow rate was in the transition regime for much of the test. A lower coaxial heat transfer rate due to flow in a laminar regime could explain why Wood et al. concluded that the coaxial design did not provide a benefit over the u-tube.

Although it is often suggested that the coaxial heat exchanger has a lower thermal resistance than the u-tube, this is not always the case. A study by Desmedt et al. [65] included three coaxial designs that had higher resistances than the u-tube in the investigation. Some of the studies that indicated poorer performance from the coaxial design included elements that would lead to higher resistance, such as the thick outer pipe in the study by Wood et al. [63] and the thick layer of grout in the simulations performed by Sliwa and Rosen [64]. These high-resistance features could also impact performance differences between the u-tube and coaxial designs.

In the aggregate, these studies do not conclusively show that one heat exchanger consistently performs best. Despite the anticipated performance advantage due to a lower resistance, the coaxial heat exchanger did not always outperform the u-tube. This unexpected result could be because the coaxial design does not necessarily guarantee a lower resistance, or it could be due to other factors, such as differences in borehole sizing, fluid flow, or operating conditions. As such, this study aims to compare the u-tube and coaxial designs using consistent geometry and flow conditions to provide a clear understanding of the differences in performance between the u-tube and coaxial heat exchanger designs.

2.3 Intermittent Operation of Borehole Heat Exchangers

Several of the studies that compared the u-tube and coaxial heat exchangers considered intermittent loading conditions. This was the case in the experimental results published by Wang [62], where the average heat transfer rate supplied to the boreholes followed a square wave pattern, with heat injection for 20 to 25 minutes per hour-long cycle. In the study by Yavuzturk and Chiasson, the loading pattern was determined for a specific small office building. In both these studies, the coaxial outperformed the u-tube leading to significant length reduction predictions for the coaxial design. A numerical study by Quaggiotto et al. [66], which considered double, rather than single, u-tubes, also found that the coaxial performed best when subject to a realistic intermittent building load. Jalaluddin and Miyara [67] conducted a comprehensive numerical study on u-tube, double u-tube, and coaxial BHE designs under a variety of intermittent operating conditions. This study tested intermittent operating cycles of two hours on and two hours off, 6 and 12 hours per day, as well as 2-hour alternate heating and cooling cycles. The findings indicated that for all operating modes tested, including continuous operation, the coaxial heat exchanger performed best.

In contrast to research described above, Wood [63] found that the u-tube heat exchanger provided better performance than the coaxial during an intermittent test. This test, however, was only partly intermittent because it involved a short, 45 minute recovery time during the entire 8 hour experiment. There were also other confounding factors, such as the laminar flow in the annulus and the thick outer pipe, that may have contributed to this finding.

Some research has focussed on the specifics of how intermittent operation affects borehole heat exchanger performance. A study by Li et al. [68] showed that a borehole field had better ground temperature recovery when a shorter but higher thermal load was applied, compared to a longer but lower heating load. Cao et al. [69] examined the effects of fixed ratios of operating and recovery times on u-tube and coaxial heat exchangers. The numerical study, which modelled the borehole heat exchanger using a steady thermal resistance, established that increasing the proportion of recovery time (when the heat exchanger was off) to operating time improved the heat flux per unit length achieved by the borehole and reduced the radius of temperature disturbance in the soil around the heat exchanger. Baek et al. [70] used detailed finite difference modelling to test the response of a u-tube heat exchanger to varying ratios of operating to recovery time. This study also found that increasing the amount of recovery time compared to operating time improved the ground temperature.

Since many intermittent studies indicate better performance from the coaxial design, further investigation is needed to establish whether intermittent operation affects the performance of the borehole heat exchanger designs differently. While some of the studies above look at multiple BHE configurations under intermittent loading, a systematic study over a broad range of operating cycles is needed to fully understand how intermittent operation affects the difference in performance between heat exchanger designs. In particular, this study must identify the key transient time scales of the heat exchangers in order to establish how intermittency influences heat exchanger performance. Such a study would also shed more light into how the parameters of intermittent operation impact heat exchanger performance.

2.4 Summary

Several approaches to modelling borehole heat exchangers have been developed. The least computationally expensive option to predict borehole heat exchanger performance is the imposed wall boundary approach, as was used in the ILS, FLS, DST, and Eskilson’s numerical g-functions. This modelling strategy uses a numerical or analytical solution for the ground temperature response, governed by a fixed boundary condition at the borehole wall. The borehole heat exchanger performance is then predicted using a separate model, typically a steady state resistance. While fast, the fixed wall boundary condition may not completely capture the conjugate heat transfer between the borehole and the ground, and, further, steady state borehole resistance models cannot predict transient changes in the borehole heat exchange. Partially and fully coupled models were developed to address the conjugate heat transfer and time scale limitations. While partial coupling accounts for the transient behaviour of some borehole components, fully coupled models resolve all elements in the system, from the convective heat transfer in the working fluid, to the conduction in the tubing, grout, and ground. The high fidelity of these fully coupled models results in a higher computational cost; however, this is necessary to accurately capture the borehole heat exchanger behaviour under a wide range of time scales.

In particular, a high fidelity, fully coupled numerical model can be used to establish differences in performance between different borehole heat exchanger designs. Several experimental and numerical studies have compared different heat exchanger designs, with a focus on comparing the commonplace u-tube and coaxial configurations. It is broadly expected for the coaxial heat exchanger to exhibit better performance than the u-tube due to its lower borehole thermal resistance; however, the literature

provides conflicting results. In some cases the coaxial outperformed the u-tube, as expected, while in others, the u-tube performed best. These discrepancies may be due, in part, to the difficulty in comparing the heat exchangers on equal terms. As such, the first phase of this study aims to establish the differences in performance between the u-tube and coaxial designs. The use of a detailed fully coupled numerical model will allow for a thorough and strategic comparison of the u-tube and coaxial heat exchangers while maintaining consistency between their geometry and operating conditions.

Some of the comparison studies between u-tube and coaxial designs examined the heat exchangers under intermittent operating conditions. Since many of these studies indicated that the coaxial configuration performed best under this operating mode, there is a need to investigate how intermittent operation might affect the borehole designs differently. While some studies have considered the impact of intermittent operation on borehole heat exchangers in general, and others have investigated the different designs under a limited range of intermittent operating conditions, none have thoroughly explored how intermittency impacts heat exchanger design. This is an ideal application of a detailed numerical model, since intermittent operation could occur at time scales below the time it takes for the heat exchangers to reach steady state. This portion of the study will focus first on establishing a framework for examining heat exchanger performance during intermittent operation. A detailed comparative analysis of the borehole heat exchanger designs under intermittent operation will subsequently be conducted.

Overall, this study will provide insight into the differences between borehole heat exchanger design, taking into account a broad range of time scales and operating

conditions. By focussing on the direct effect of the components of the heat exchangers, a deeper understanding of the mechanisms causing differences in performance can be revealed.

Chapter 3

Methodology

A numerical model for borehole heat exchangers was developed in OpenFOAM [71], an open source computational fluid dynamics library. The modelling accounted for two heat exchanger designs: a u-tube and a coaxial configuration. All components of the heat exchangers are incorporated, including working fluids, tubing, grout, and soil. This high level of detail enables the modelling to fully capture the complex conjugate nature of the heat exchange within the boreholes at a wide array of time scales: from the first seconds after the system is switched on to years into operation. The following chapter details the approach to the numerical modelling of the borehole heat exchangers, including the geometry and mesh selection, and the numerical methods used to implement the models.

3.1 Geometry and Mesh

Each heat exchanger was modelled as a borehole, containing tubing, fluid, and grout, surrounded by the ground. For testing on the scale of days, such as the u-tube and

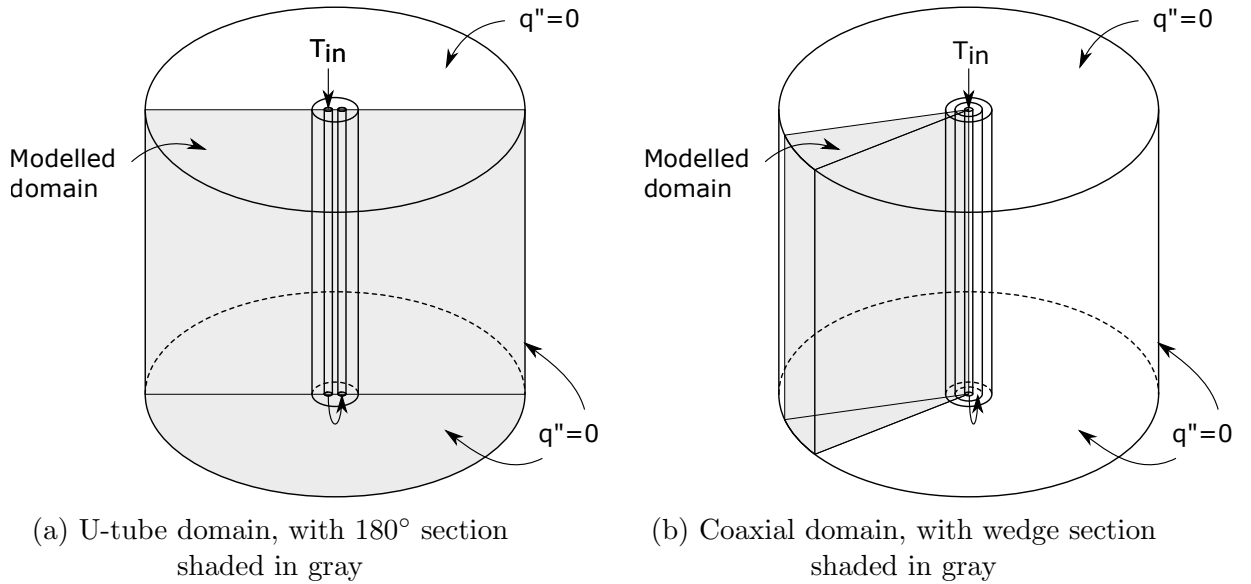


Figure 3.1: Model domains and boundary conditions for the u-tube and coaxial heat exchangers

coaxial continuous and intermittent studies discussed in Chapter 4, heat transfer is predominantly in the radial direction. The ground below the borehole heat exchangers has an impact on the time scale of years. As such, in these tests, the volume of soil below the boreholes can be neglected. This is supported by experimental validation, which shows very good agreement between the models and experimental data over a 72 hour time period. The piping at bottom of the heat exchanger where the flow reverses direction is neglected to simplify modelling. This is an acceptable assumption, since this portion of the piping represents a very small percentage of the overall heat exchanger length. All fluids in the heat exchangers are modelled in one dimension using heat transfer coefficients. Both u-tube and coaxial models take advantage of symmetry to reduce domain size. The u-tube and coaxial domains, as well as temperature and flow boundaries are depicted in Figure 3.1.

3.1.1 U-tube mesh

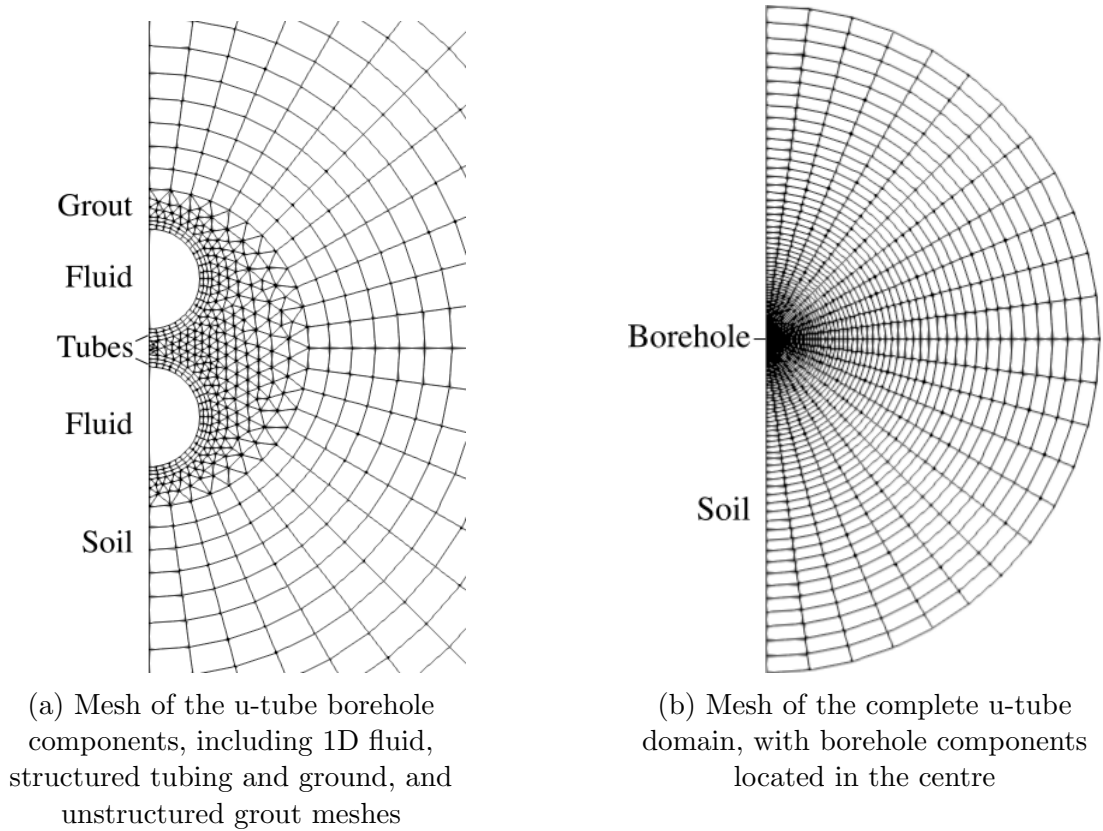


Figure 3.2: Mesh of the u-tube domain

The u-tube heat exchanger is symmetric about the plane intersecting the two tubes, making it possible to reduce the domain in half to lower computational cost. As such, only 180° of the u-tube and soil are resolved, as is shown in Figure 3.1a.

The tubing, grout, ground meshes for the u-tube heat exchanger were created using the open source meshing tool gmsh. Figure 3.2 shows the u-tube mesh in the x - y plane, with the detail inside the borehole depicted in Figure 3.2a. In this model, the mesh on the x - y plane is extruded uniformly in the z -direction. Hexahedral uniform meshing was applied in all possible components, namely the tubing and soil. A custom

Table 3.1: U-tube dimensions

Parameter	Dimension
Pipe OD	42.16 mm
Pipe thickness	4.06 mm
Borehole diameter	107.95 mm
Borehole length	182.9 m

1D mesh was used in the fluid domains to maintain the cross section and surface area of the circular pipes. An unstructured tetrahedral mesh was employed in the grout to conform to its complex shape. Within the ground, a radial expansion rate of 5% was used to reduce the number of cells in the domain. This enabled refinement near the borehole, where temperature gradients are expected to be high, while reducing mesh density at the outer limits of the soil domain, where no heat transfer occurs.

A summary of the u-tube dimensions used throughout this study can be found in Table 3.1. The resulting u-tube mesh has 269,400 cells: 193,536 cells in the ground domain, 57,216 cells in the grout, 9,216 cells for each tube, and 128 cells in each fluid domain. The u-tube mesh was tested for grid sensitivity, which is discussed in detail in Section 3.1.6.

1D circular pipe mesh

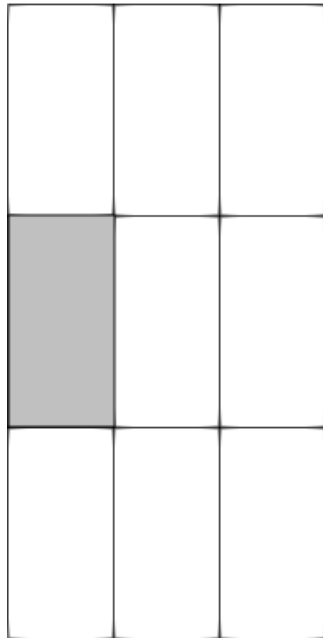
Since the fluid in the heat exchangers is modelled as one-dimensional, a custom mesh was required for the u-tube fluid. This mesh was developed to be one dimensional in the axial direction, while conforming to the rounded tube surface. The result is a semi-circular 1D mesh, with a single cell in the x - y direction and many faces along the tube wall to correctly capture both the curvature and cross-sectional area of the pipe.

The fluid mesh consists of an array of polyhedral cells stacked in the axial direction of the pipe. OpenFOAM defines polyhedral cells such that it is possible to generate a cell with an unlimited number of faces [72]. While this generalized definition of a cell makes it possible to create highly conformal 1D meshes, it is not readily achievable using commercial meshing software. As such, it was necessary to employ a novel meshing protocol.

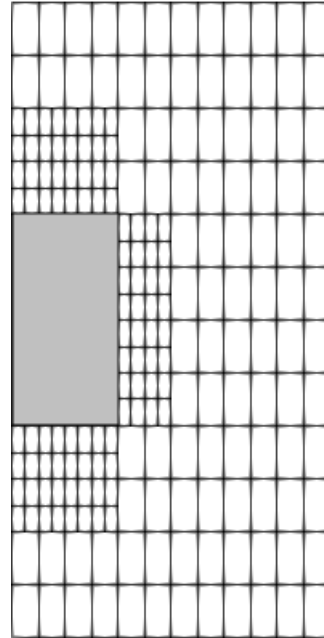
To ensure that the mesh could be interpreted by the OpenFOAM solver, the base 1D mesh was generated using the OpenFOAM-based meshing tool, blockMesh. For this step, 3x3 cell mesh was created for which the width of the cells matched the radius of the circular pipe and the height of the cells matched the diameter. Only a single cell remains at the end of the mesh creation. The 3x3 mesh can be seen in Figure 3.3a. The final cell that remains after processing is shaded in grey.

At this stage, the desired final cell has four faces: one which will become the symmetry plane of the semi-circle and the remainder will make up the curved pipe surface. The OpenFOAM-based tool refineMesh is used to refine the cells adjacent to the three faces designated to the curved surface, demonstrated in Figure 3.3b. The cells are refined until the number of faces is sufficient to generate a faceted curved surface. Next, the subSetMesh tool is used to remove the extraneous cells around the final cell, leaving a square cell with multiple faces on three sides (Figure 3.3c).

Finally, a script was developed to remap the square cell points to a semi-circular profile. The final product is shown in Figure 3.3d. This mesh meets the requirement of being compatible with OpenFOAM's solvers while having only a single cell in the x - y direction, but with several faces curved to match the surface of the u-tube piping.



(a) 3x3 grid made with blockMesh, final cell shaded in grey



(b) refineMesh used in cells surrounding final cell to create extra faces



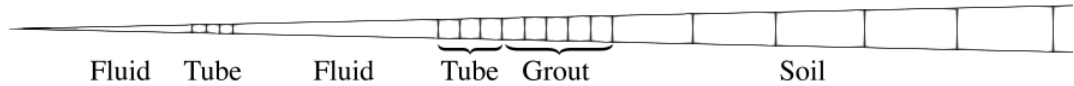
(c) Final cell isolated with subSetMesh, square shaped



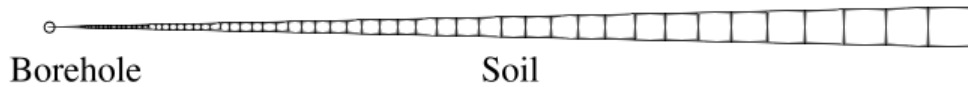
(d) Completed final cell with semi-circular profile

Figure 3.3: 1D semi-circular mesh development

3.1.2 Coaxial mesh



(a) Mesh of the coaxial components. From left to right: 1D inner fluid, inner tube, 1D outer fluid, outer tube, grout, and the ground



(b) Mesh of the complete wedge-shaped coaxial domain, with borehole components located at the centreline of the wedge

Figure 3.4: Mesh of the coaxial domain

The coaxial heat exchanger is axisymmetric, enabling the use of a much smaller and more computationally efficient domain. A 2.5° wedge of the coaxial heat exchanger and surrounding ground is modelled, with symmetry boundary conditions applied to each face of the wedge. All the meshes in the coaxial heat exchanger model were generated using the OpenFOAM tool blockMesh. The resulting mesh is depicted in Figure 3.4, with the details inside the borehole shown in Figure 3.4a.

With this modelling approach, all meshes have a single cell in the azimuthal direction. All cells in the coaxial model are hexahedral, except for the tetrahedral cells in the central fluid. The tubes and grout use a uniform mesh in the radial direction, while the mesh in the ground employs an radial expansion rate of 5%, the same as the u-tube ground mesh. All components have a uniform mesh in the axial direction.

The dimensions of the coaxial heat exchanger are listed in Table 3.2. The coaxial

Table 3.2: Coaxial dimensions

Parameter	Dimension
Outer pipe OD	88.21 mm
Outer pipe thickness	5.74 mm
Inner pipe OD	40 mm
Inner pipe thickness	3.6 mm
Borehole diameter	107.95 mm
Borehole length	182.9 m

mesh size is considerably smaller due to its symmetry properties. The mesh has 128 cells in each fluid, 384 cells in the tubes, 640 cells in the grout, and 8064 cells in the ground, adding up to a total of 10496 cells in the coaxial mesh. Details of grid sensitivity testing for the coaxial mesh are discussed in Section 3.1.6.

3.1.3 Multiple borehole modelling

This thesis includes case studies of multiple boreholes in the same ground domain, with the goal of understanding how borehole heat exchangers interact when modelled together. In these simulations, the long-term performance is most critical, since borehole interaction occurs over long time scales. As such, the internal components of the heat exchangers can be neglected. The resulting domain consists only of the boreholes in the ground. The ground beneath the boreholes is included in the domain to account for any axial heat transfer at the bottom of the borehole field. As shown in Figure 3.5, symmetry conditions at the centre of the field are used to limit domain size. A reduced scale is employed to further lower computational cost.

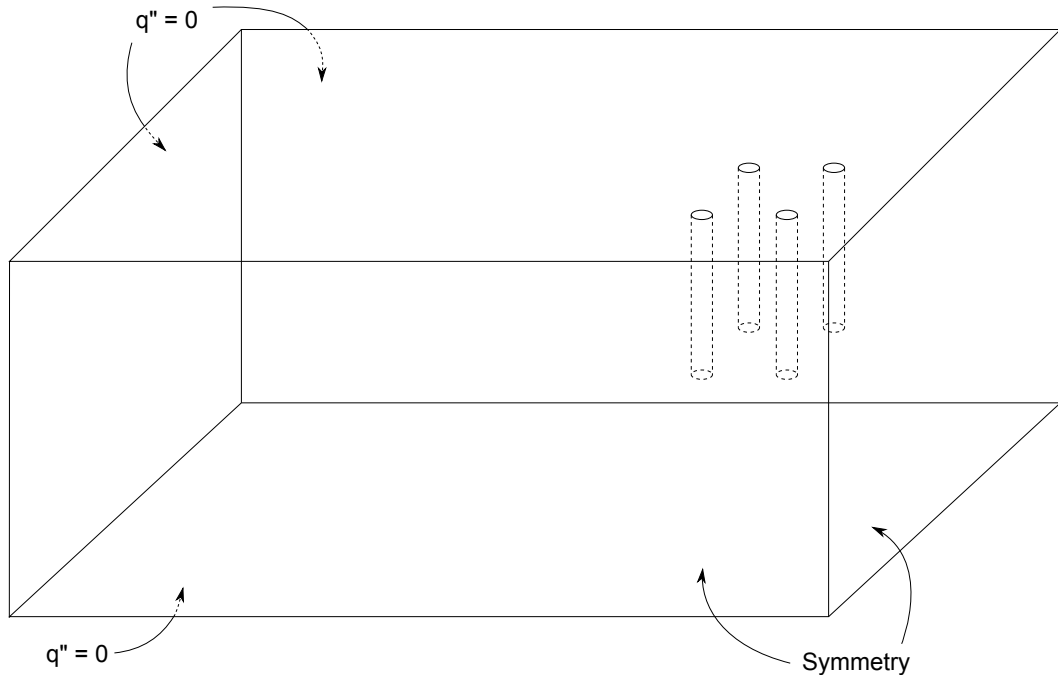


Figure 3.5: Multiple borehole domain

3.1.4 Boundary conditions

The boundary conditions for the singular u-tube and coaxial models are illustrated in Figure 3.1. In these models, the surface boundary and bottom boundaries are set to have a zero heat flux condition for all solid components. At the outer radial boundary in the ground, the heat flux is also set to zero, assuming that no heat reaches the far field of the domain. The validity of this boundary condition is maintained by ensuring that the radius of the ground domain remains large enough that the temperature at the far field is never disturbed. An automatic check was implemented during the simulations to ensure this condition was always met. If the temperature at the outer boundary of the domain exceeded $1 \times 10^{-5} \text{°C}$ above the initial temperature, the simulation was automatically stopped so that the domain size could be increased.

The inlet fluid condition is case dependent. Two inlet boundary condition types

are employed in this study: constant temperature and constant heat injection rate. A constant temperature inlet boundary is self-explanatory. The constant heat injection rate is achieved by setting the inlet temperature a constant ΔT above the outlet temperature, according to the desired heat transfer rate, where

$$\Delta T = \frac{q}{\dot{m}c_p} \quad (3.1.1)$$

This results in a persistent rise in both inlet and outlet temperatures during heat injection.

The coaxial inlet location was selected to be the centre of the pipe. While it may be expected that the choice of inlet location would have an effect on performance, Beier et al. [61] demonstrated that the varying the coaxial inlet location did not affect the outlet temperature of the heat exchanger, as is shown in Figure 3.6.

As described above, the reversal of flow at the bottom of the heat exchangers is simplified and not directly captured in the mesh. Instead, the fluid flow at the bottom is modelled such that the inlet temperature of the upward flow is exactly equal to the outlet temperature of the downward flow, disregarding any small temperature change that could have occurred as the flow turned.

There are also coupling boundary conditions between each component of the system. The coupling approach is described in detail in Section 3.2.5.

The boundary conditions in the multiple borehole domain are shown in Figure 3.5. The surface boundary condition is case dependent, while the far field and bottom surfaces are set to have a zero heat flux condition. Symmetry conditions are employed along the x and y axes in the centre of the field.

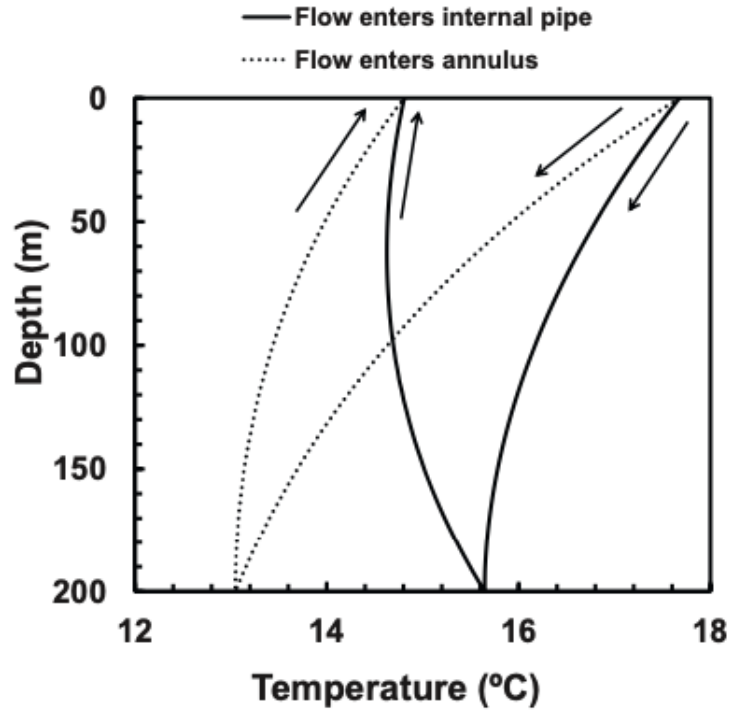


Figure 3.6: Results from Beier et al. demonstrating the effect of coaxial inlet location [61]

3.1.5 Initial conditions

All components, including the fluids, are initialized to the same temperature, assuming that the borehole and ground will share the same temperature at the beginning of the test. It is assumed that the temperature of the ground is uniform, with no increase in temperature with depth. This is a common assumption employed in the literature [45, 73, 74], supported by the small temperature changes over the depths considered in this study.

3.1.6 Grid and time step sensitivity study

A grid sensitivity study was undertaken to ensure all meshes were adequately refined. The sensitivity study was considered one component at a time, with each test targeting the mesh refinement in a single direction. This testing was complicated in the u-tube by the coupling between each component, since refining the mesh in one component, such as the tubes, may impact others, like the fluid and grout. The grid sensitivity testing protocol was as follows for the u-tube:

Test of the tube meshes:

- Refine in the radial direction
- Refine in the azimuthal direction (note: affects fluid and grout)

Test of the grout mesh:

- Refine cells along symmetry boundaries
- Refine azimuthally at the borehole wall boundary (note: affects the soil)

Test of the soil mesh:

- Refine in the radial direction

Test of the axial refinement of all meshes

The coaxial grid sensitivity tests were more straightforward and involved refining each individual component in the radial direction.

With the exception of the expanding grids, each mesh refinement represented a doubling of the number of cells in the given direction. When refining the expanding grids, the smallest cell was halved in size in the given direction. The mesh was considered acceptable when doubling the mesh did not influence the outlet temperature

Table 3.3: U-tube grid and time step sensitivity test results, outlet temperature ($^{\circ}\text{C}$)

Refinement	Time (hr)			
	6.5	13	19.5	26
Base case	19.78	21.30	22.14	22.72
Tube radial	19.78	21.30	22.14	22.72
Tube azimuthal	19.80	21.32	22.16	22.75
Grout symmetry boundary	19.79	21.30	22.14	22.72
Borehole wall azimuthal	19.80	21.31	22.16	22.74
Soil radial	19.78	21.30	22.14	22.72
All axial	19.78	21.30	22.14	22.72
Time step	19.79	21.30	22.14	22.72

Table 3.4: Coaxial grid and time step sensitivity test results, outlet temperature ($^{\circ}\text{C}$)

Refinement	Time (hr)			
	6.5	13	19.5	26
Base case	19.23	20.75	21.60	22.18
Outer tube radial	19.23	20.75	21.59	22.17
Inner tube radial	19.23	20.75	21.60	22.18
Grout radial	19.23	20.75	21.59	22.18
Soil radial	19.23	20.75	21.59	22.18
All axial	19.23	20.75	21.59	22.17
Time step	19.23	20.76	21.60	22.19

of the heat exchanger.

Similarly, time step sensitivity was tested by halving the time step. A value for the time step was selected such that if it was halved, it would not change the outlet temperature of the heat exchanger. The grid and time step sensitivity data for the u-tube and coaxial models are shown in Tables 3.3 and 3.4.

3.2 Numerical Modelling

The heat transfer problem within the borehole heat exchangers consists of pure conduction in the solid components combined with convection heat transfer in the working fluid. While the heat transfer in the solid components is three-dimensional, the fluid undergoes flow in a straight pipe, which can be simplified down to one dimension. This integration of 1D convection and 3D conduction required the creation of a custom code in OpenFOAM [71], developed based on the `chtMultiRegion` solver, a conjugate heat transfer package. In this model, the borehole components and the ground are each represented separately in their own domain and a segregated solution approach is used to resolve the entire system.

The following section outlines the numerical approach to solving this heat transfer problem, including the governing equations for solid and fluid components and the coupling strategy employed.

3.2.1 Implementation in OpenFOAM

Several changes were needed to implement this modelling strategy using the existing OpenFOAM package, `chtMultiRegionFoam`. OpenFOAM uses a symbolic representation of partial differential equations that is similar to the way they are expressed mathematically, making it straightforward to change the code to solve any desired equation. Changes were made to establish the required governing equations for the the fluid and solid components, described below in Section 3.2.2. Routines were developed to calculate heat transfer coefficients that depended upon both the geometry (circular or annular pipes) and the flow velocity. Furthermore, code was written to calculate the change in flow velocity during intermittent operation. This included

ramp up and ramp down velocities computed from the unsteady Bernoulli equation (see Section 3.2.2) and the development of a routine to solve the ramp up equation using a fourth-order Runge Kutta scheme.

Additionally, since the `chtMultiRegionFoam` algorithm consisted of the successive solution of each component domain, it was possible for the coupling at the interface to be non-conservative, as the code was written. While the coupling boundary condition specified that both the temperature and heat transfer rate across an interface must be equal in each domain, some domains were computed using the old wall temperature value of the neighbouring domain, while others were calculated using the updated value. Therefore, a routine was written to ensure interfacial energy conservation. This involved computing the heat transfer rates across each interface, and iterating the solution of each domain until the difference in heat transfer rate across the surface fell below a set threshold.

Case set up scripts were also developed in Perl to maintain consistency of testing by ensuring that all values were correctly updated in each OpenFOAM case directory. This was critical because each component domain had an individual set of case files, which included files detailing initial conditions, flow conditions, thermophysical properties, meshing, numerical schemes, and solver controls. As a result, each case directory contained dozens of files that needed to be correctly updated for each test. The set up scripts were written to replace text to correctly assign all necessary properties from a central input file, examples of which is included in Appendix A. This script updated initial, flow, and thermophysical properties, updated meshes by executing meshing programs from parametric mesh files, and made calculations to suggest the appropriate time step given the Courant number of the flow. This

ensured that consistent testing methodology was maintained at all times.

3.2.2 Governing equations

Solid

The solid components consist of the tubing, grout, and ground. The heat transfer within each solid component is modelled as 3D transient convection, defined as

$$\frac{\partial T_s}{\partial t} - \alpha_s \nabla^2 T_s = 0 \quad (3.2.1)$$

where T_s is the temperature of the solid component and α_s is the thermal diffusivity.

Fluid

In the fluids, heat transfer is modelled as 1D convection, with heat exchange between the fluid and the tube walls accounted for using empirical correlations. The heat transfer is assumed to be pure convection, neglecting the effect of axial conduction within the fluid. The transient convection relationship, including the empirical heat transfer coefficient, h , is

$$\rho_f c_{p,f} \frac{\partial T_f}{\partial t} + \rho_f c_{p,f} u \frac{\partial T_f}{\partial x} = \frac{4h}{d_i} (\bar{T}_{wall} - T_f) \quad (3.2.2)$$

where ρ_f and $c_{p,f}$ are the fluid density and heat capacity, u is the fluid velocity (in the axial direction), and T_f is the fluid temperature. \bar{T}_{wall} is the area-weighted average of the wall temperature. This is calculated using the area and temperature at each

facet of the curved fluid surface

$$\bar{T}_{wall} = \frac{\sum_i T_{wall,i} A_i}{\sum_i A_i} \quad (3.2.3)$$

where i refers to a single face on the surface, from which the surface area A_i and the wall temperature $T_{wall,i}$ are obtained.

Flow calculations

The initial tests in this study concern continuous operation of the BHEs, during which hot fluid is constantly supplied and the fluid velocity remains uniform in time. In the second phase of this study, the intermittent operation of borehole heat exchangers is tested. In the case of intermittent operation, fluid is pumped into the heat exchangers for a defined period of time before the pumping is stopped, allowing the flow to become stationary. This process is repeated several times during a test. When the system is turned off, it is assumed that the inlet temperature is equal to that of the outlet. To capture this flow behaviour in the models, it was necessary to develop a 1D time dependent fluid velocity profile.

Using the unsteady Bernoulli equation, it was possible to account for the ramping up of the flow when a pump is switched on and the corresponding ramping down of flow when that pump is switched off. This gives a more conservative prediction of the achievable heat transfer during an intermittent operating mode. The unsteady Bernoulli equation is defined along a streamline as [75]

$$\int_a^b \rho \frac{\partial u_s}{\partial t} ds + \left(P + \frac{1}{2} \rho u_s^2 + \rho g z \right)_b - \left(P + \frac{1}{2} \rho u_s^2 + \rho g z \right)_a = 0 \quad (3.2.4)$$

where u_s is the velocity along the streamline s , P is the pressure, and z is the height. The borehole system can be characterized by Figure 3.7. The two points, a and b are close enough to one another that their height difference is small compared to the total length of the system. For this analysis, it is also assumed that the pressure drop is due to major losses only, and that the friction due to the pump and piping outside the borehole is negligible compared to that from the borehole itself. Because the fluid is incompressible and the piping diameter consistent between a and b , the kinetic energy term can be eliminated.

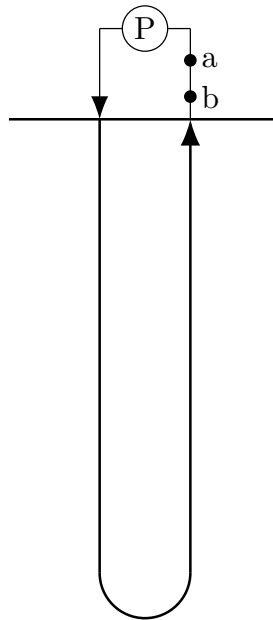


Figure 3.7: Diagram of the borehole heat exchanger system for unsteady Bernoulli analysis

The ramp up velocity represents the transient increase in velocity as a response to the pump starting. As such, the pressure difference across the system consists of two components: the pressure increase induced by the pump and the pressure drop due to friction losses. Assuming that the pump is sized to meet the maximum velocity in

the system, the pressure change due to the pump can be expressed as

$$\Delta P = f \frac{\rho u_{max}^2 L}{2 d} \quad (3.2.5)$$

and the friction factor can be approximated using the Blasius equation

$$f = 0.316 Re^{-0.25} \quad (3.2.6)$$

The pressure drop due to friction losses is defined using the instantaneous velocity in the system

$$\Delta P = f \frac{\rho u_s^2 L}{2 d} \quad (3.2.7)$$

Thus, the unsteady Bernoulli equation can be expressed as

$$\int_a^b \rho \frac{\partial u_s}{\partial t} ds = P_1 - P_2 \quad (3.2.8)$$

$$\int_a^b \rho \frac{\partial u_s}{\partial t} ds = 0.316 \left(\frac{\rho u_{max} d}{\mu} \right)^{-1/4} \frac{\rho u_{max}^2 L}{2 d} - 0.316 \left(\frac{\rho u_s d}{\mu} \right)^{-1/4} \frac{\rho u_s^2 L}{2 d} \quad (3.2.9)$$

In this instance, the left hand term can be integrated, simplifying the expression to

$$\frac{\partial u_s}{\partial t} = 0.158 \left(\frac{\rho d^5}{\mu} \right)^{-1/4} (u_{max}^{7/4} - u_s^{7/4}) \quad (3.2.10)$$

This expression is solved using a fourth-order Runge-Kutta scheme to determine the velocity during the ramp up phase before the maximum velocity u_{max} is reached. For a flow rate of 0.87 kg/s in a u-tube heat exchanger, the fluid velocity reaches 95% of the maximum velocity within seven seconds and reaches 99% of u_{max} after 10 seconds.

The ramp down velocity, representing the flow after the pump has switched off, is similarly defined. In this case, pressure across the system is only affected by friction loss, making the solution more straightforward. The unsteady Bernoulli equation for this scenario is expressed as

$$\int_a^b \rho \frac{\partial u_s}{\partial t} ds = P_1 - P_2 = 0.316 \left(\frac{\rho u_s d}{\mu} \right)^{-1/4} \frac{L}{d} \frac{\rho u_s^2}{2} \quad (3.2.11)$$

which simplifies to

$$\frac{\partial u_s}{\partial t} = 0.158 \left(\frac{\rho d^5}{\mu} \right)^{-1/4} u_s^{7/4} \quad (3.2.12)$$

and can be solved directly to give the expression for the ramp-down flow velocity

$$u = \left[0.1185 \left(\frac{\rho d^5}{\mu} \right)^{-1/4} (t - t_{off}) + u_{max}^{-3/4} \right]^{-4/3} \quad (3.2.13)$$

where t_{off} is the time at which the pump is shut off. Using a flow rate of 0.87 kg/s in a u-tube, the flow reaches 1% of the maximum velocity after 127 seconds (roughly 2 minutes). It takes 732 seconds (just over 12 minutes) for the flow to reach 0.1% of the maximum velocity.

3.2.3 Numerical Schemes

A number of different numerical schemes were applied to calculate the differential equations for the fluid and solid domains. Each domain type had defined numerical schemes for time differentiation, cell-to-cell interpolation, and surface-to-cell interpolation. A divergence scheme was selected for the fluids, and a Laplacian scheme was used for the solids. In both the fluid and solid domains, the time discretization

method was selected to be the Euler scheme, which is first-order and implicit. In the fluid, a Gauss upwinding scheme was selected for the divergence. This first-order, bounded method sets the cell face value to the upstream value. In the solid, Gaussian discretization was selected for the Laplacian term, which requires interpolation between the cell faces and centres. Limited non-orthogonal correction was applied to the Gaussian discretization to improve stability. For both domain types, linear interpolation was used for interpolation between cell centres. For surface-to-cell interpolation, linear interpolation was applied for the fluids, and limited linear interpolation was applied for the solids to improve stability.

3.2.4 Heat Transfer Correlations

The heat transfer coefficient used to represent the heat transfer between the fluid and the tube wall was determined using empirical correlations. Several heat transfer correlations were required to account for the various pipe geometries and also the variation of fluid velocity when the heat exchangers were operated intermittently. The heat transfer coefficient h is defined as

$$h = \frac{Nu k_f}{D_h} \quad (3.2.14)$$

where Nu is the Nusselt number, k_f is the fluid thermal conductivity, and D_h is the hydraulic diameter of the pipe. The hydraulic diameter is defined as simply the pipe diameter for a circular pipe, and for a concentric annulus can be computed from the inner diameter of the outer pipe d_{oi} and the outer diameter of the inner pipe d_{io}

$$D_h = d_{oi} - d_{io} \quad (3.2.15)$$

The heat transfer correlations used to determine the Nusselt number depended upon both geometry and flow regime. For the u-tube and coaxial centre pipe, when the flow is turbulent, the Nusselt number Nu is determined using the Gnielinski correlation [76] for flow in circular pipes, which is valid for $2300 < Re < 10^6$ and $0.6 < Pr < 10^5$.

$$Nu = \frac{(f/8)(Re - 1000)Pr}{1 + 12.7 \left(Pr^{2/3} - 1 \right) \sqrt{f/8}} \quad (3.2.16)$$

The friction factor f is calculated using the Filonenko correlation [77]

$$f = (0.79 \log Re - 1.64)^{-2} \quad (3.2.17)$$

where Re is the Reynolds number of the flow.

When the flow is laminar ($Re < 2300$) in the circular pipes, the Nusselt number is defined as a constant value, 3.66 [78].

$$Nu = 3.66 \quad (3.2.18)$$

A fourth-order fit is used to determine the Nusselt number in the transition regime, when Reynolds numbers were between 2300 and 10,000. The relationship between the Nusselt number and Reynolds number is shown in Figure 3.8.

In the annular flow of the coaxial heat exchanger, the Nusselt number was established using the Gnielinski correlation [79] for turbulent flow in an annulus. This correlation is valid for $10^4 < Re < 10^6$ and $0.6 < Pr < 1000$.

$$Nu = \frac{(f_{ann}/8) Re Pr}{k_1 + 12.7 \sqrt{f_{ann}/8} \left(Pr^{2/3} - 1 \right)} \left[1 + \left(\frac{D_h}{L} \right)^{2/3} \right] F_{ann} \quad (3.2.19)$$

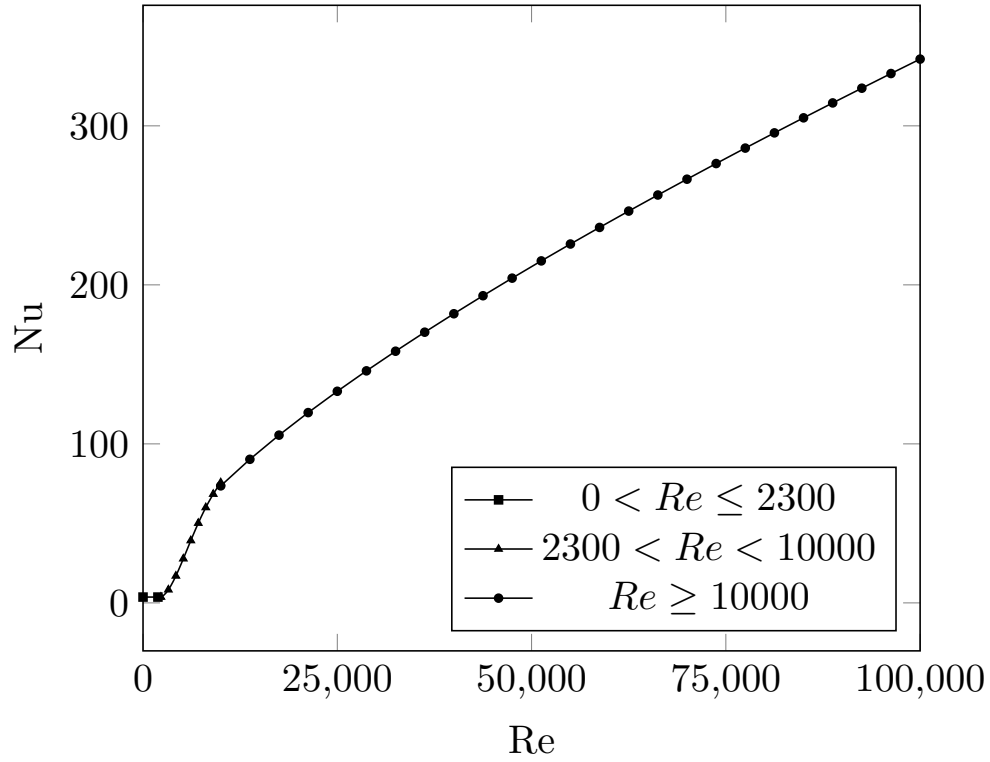


Figure 3.8: Relationship between Nusselt number and Reynolds number for circular cross section

where L is the length of the pipe and k_1 is

$$k_1 = 1.07 + \frac{900}{Re} - \frac{0.63}{1 + 10Pr} \quad (3.2.20)$$

and

$$F_{ann} = \frac{0.75a^{-0.17} + (0.9 - 0.15a^{0.6})}{1 + a} \quad (3.2.21)$$

The annular friction factor is defined as

$$f_{ann} = (1.8 \log(Re^*) - 1.5)^{-2} \quad (3.2.22)$$

with

$$Re^* = Re \frac{(1 + a^2) \ln a + (1 - a^2)}{(1 - a^2) \ln a} \quad (3.2.23)$$

and a is defined as

$$a = \frac{d_{io}}{d_{oi}} \quad (3.2.24)$$

where d_{io} is the outer diameter of the inner pipe and d_{oi} is the inner diameter of the outer pipe.

For annular flow with $3000 < Re < 10^4$, a relationship from Foust and Christian [80] was used for the Nusselt number

$$Nu = \frac{0.04a}{(a + 1)^{0.2}} Re^{0.8} Pr^{0.4} \quad (3.2.25)$$

where a is

$$a = \frac{d_o}{d_i} \quad (3.2.26)$$

For laminar Reynolds numbers (below 2300) in the annulus, the Nusselt number was [81]

$$Nu_{oi} = 5.70 \quad (3.2.27)$$

for the inner radius of the annulus. For the outer radius of the annulus, the Nusselt number was [81]

$$Nu_{oo} = 4.45 \quad (3.2.28)$$

A fourth-order fit was used to establish the Nusselt number for Reynolds numbers between 2300 and 3000.

3.2.5 Coupling

Each component of the system was represented numerically in its own domain. This meant that the fluid or solid governing equation was solved separately for each individual part, with heat transfer at the boundaries between components accounted for using a coupled boundary condition. The coupled boundary specified that the temperature was equal on each side of the interface

$$T|_{left} = T|_{right} \quad (3.2.29)$$

and also that the temperature gradient was the same at this interface.

$$k_{left} \frac{\partial T}{\partial \eta} \Big|_{left} = k_{right} \frac{\partial T}{\partial \eta} \Big|_{right} \quad (3.2.30)$$

Each domain is computed successively, starting with the downward and then upward fluid and moving radially outwards through the solid domains. This solution approach results in time inconsistencies in the coupling boundaries. For instance, for a tube in the u-tube model, the inner boundary temperature will be based on the fluid temperature calculated at the current time step, while the outer boundary will be calculated using the grout temperature at the previous time step. To address this, the temperature solutions are iterated multiple times until conservation is achieved at each interface.

Chapter 4

Results and Discussion

The following chapter presents and discusses the results of this study. The results in Sections 4.1 and 4.3 are described in a journal article entitled “Analysis of the transient performance of coaxial and u-tube borehole heat exchangers”, published in the journal *Geothermics*. A second paper, entitled “A numerical study on the intermittent operation of u-tube and coaxial borehole heat exchangers”, outlines the results presented in Section 4.4. This paper is currently under review. The chapter that follows presents the results of this study in a full-thesis style.

4.1 Experimental Validation

Both the u-tube and coaxial heat exchanger models were validated using experimental data from thermal response tests (TRTs). TRTs use a heater to provide a roughly constant amount of heat to a working fluid pumped into a borehole. They are used to establish the thermal conductivity of the ground in situ. The outlet temperatures of these TRTs were used to compare results, with the error between the model and

the experiment defined as

$$\text{Error}(t) = \frac{T_{exp}(t) - T_{num}(t)}{T_{in}(t) - T_{ground,\infty}} \quad (4.1.1)$$

where $T_{exp}(t)$ is the experimental temperature, $T_{num}(t)$ is the temperature from the numerical simulation, $T_{in}(t)$ is the inlet temperature of the borehole and $T_{ground,\infty}$ is the undisturbed ground temperature.

4.1.1 U-tube

The u-tube model was experimentally validated using data supplied by an industry partner, GeoSource Energy. In this test, approximately 11 kW of heat was used to warm fluid that was supplied to the u-tube at a flow rate of 0.56 kg/s. The borehole was 182.88 m (600 ft) deep with a diameter of 98.4 mm (3 7/8 in), and the ground temperature was 10.1°C at the start of the test. The inlet and outlet temperature measurements had an accuracy of 0.1°C and the flow rate measurement error was 0.2%.

The thermal conductivity of the ground was determined from the data to be 3.77 W/mK. This can be found by plotting the average of the inlet and outlet temperature against the logarithm of time. The ground conductivity is established from the slope of the curve after the transient borehole warming period, in this case after 12 hours. Ground conductivity is defined as [82]

$$k_{ground} = \frac{q'}{4\pi S} \quad (4.1.2)$$

where q' is the heat transfer rate per unit length in W/m and S is the slope of the

average temperature plotted against $\log(t)$.

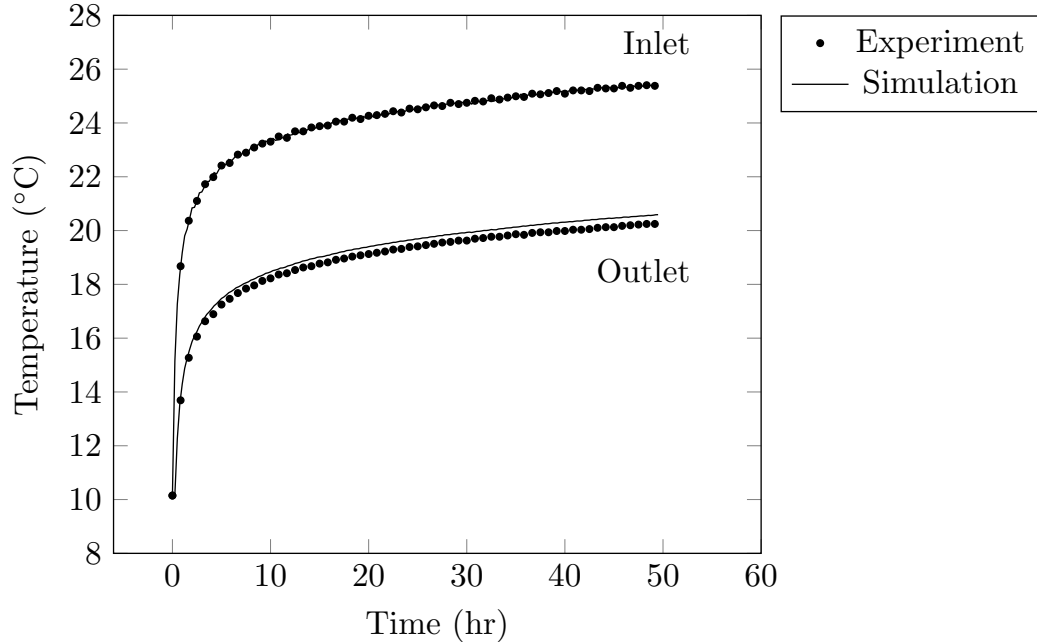


Figure 4.1: Experimental validation of the u-tube model, with a fixed flow rate of 0.56 kg/s, a ground conductivity of 3.77 W/mK, and inlet temperatures taken from experimental data. Experimental results provided by GeoSource Energy

A comparison between the experiment and the numerical simulation is shown in Figure 4.1. The numerical simulation was conducted using the experimental inlet temperature. The result, shown in Figure 4.1, demonstrates good agreement, with an error of -2.1% at the end of the two-day test.

4.1.2 Coaxial

The coaxial model was validated using experimental data published by Beier et al. [61]. The experimental data was obtained from an 78-hour thermal response test, with a heat input rate of 6360 W. The borehole diameter was 115 m and the active heat exchanger length was reported to be between 165 m to 171 m. A length of 171 m

was selected for the numerical simulation. The working fluid was water, which had a flow rate of 0.58 L/s, and the initial ground temperature was 8.4°C. The authors reported a temperature measurement uncertainty of ± 0.1 K using a fibre optic cable.

Beier et al. calculated a ground conductivity of 3.25 W/mK. Analysis of the published temperature data, however, indicated that a thermal conductivity of 3.8 W/mK demonstrated better agreement. This is established by examining the average temperature curve against logarithmic time after 10.5 hours, adequate time to achieve steady heat transfer within the borehole. From this, it can be shown that a thermal conductivity of 3.8 W/mK produces an RMS error of 0.05 K, while using a thermal conductivity of 3.25 W/mK results in an error of 0.11 K. As such, the ground conductivity for the numerical simulation was selected to be 3.8 W/mK.

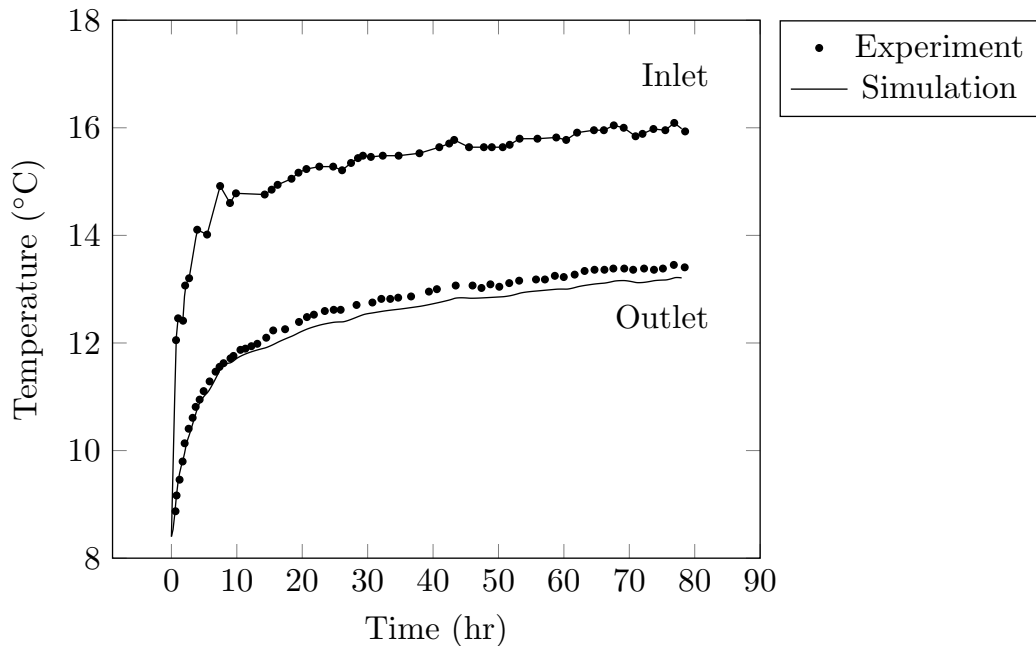


Figure 4.2: Experimental validation of the coaxial model using data published by Beier et al. [61]. Modelling uses a fixed flow rate of 0.58 kg/s, a ground conductivity of 3.8 W/mK, and inlet data from the experiment.

The numerical simulation was conducted with inlet temperatures from the thermal response test. Figure 4.2 shows the numerical simulation results compared with experiment. The plot indicates that the simulation outlet temperature slightly exceeds that of the experiment; however the result is within an acceptable error of 5% at the end of the test.

4.2 Strategies for comparing borehole heat exchanger designs

One objective of this thesis is to provide a systematic comparison between u-tube and coaxial borehole heat exchanger. Comparisons between borehole heat exchanger designs can be broadly categorized as property-based and performance-based. Property-based comparisons use the thermal properties of the heat exchanger configurations to make predictions about their performance, while performance-based comparisons use data to draw conclusions about differences in performance. Predictions about borehole performance can be made from both thermal resistance and thermal mass, calculated from thermophysical properties and geometry. Metrics for comparing performance data between borehole designs include heat transfer rate and heat exchanger effectiveness.

4.2.1 Borehole thermal resistance

It is commonplace to quantify the efficacy of a borehole heat exchanger configuration using its thermal resistance. The borehole thermal resistance is defined as the resistance between the fluid and the borehole wall, caused by all components inside of the

borehole, including the working fluid, tubing, and grout

$$R_b = \frac{\bar{T}_f - \bar{T}_b}{q'} \quad (4.2.1)$$

where q' is the heat transfer rate per unit length, equal to

$$q' = \frac{\dot{m}c_p(T_{f,in} - T_{f,out})}{H} \quad (4.2.2)$$

and H is the borehole height. The average fluid temperature \bar{T}_f is

$$\bar{T}_f = \frac{T_{f,in} + T_{f,out}}{2} \quad (4.2.3)$$

and the borehole average temperature, \bar{T}_b , is the temperature at the borehole wall averaged over its surface area.

The u-tube and coaxial BHE configurations have differing ratios of fluid, tubing, and grout, resulting in different thermal resistances. The coaxial design has less grout and more fluid compared to the u-tube, giving the coaxial a lower thermal resistance, in general. As such, it is often suggested that the lower resistance of the coaxial design will result in better performance than the u-tube [43, 83, 61].

The thermal resistance of a borehole can be obtained through thermal response testing and can also be predicted using a variety of different models. In this document, Hellstrom's solution for the multipole method [28] is used to predict the borehole resistances. A full description of this method can be found in Section 2.1.1 of Chapter 2. The effective u-tube resistance calculated using this method is 0.0902 mK/W, and the coaxial resistance is predicted to be 0.0832 mK/W, confirming that the coaxial

resistance is in fact smaller.

4.2.2 Borehole thermal mass

The thermal mass of the heat exchangers dictates their transient response. A larger thermal mass will slow the heat exchanger's response to a change in temperature, increasing the time to steady state and dampening the effects of sudden changes. Under heat injection, a greater borehole thermal mass will result in cooler temperatures during the early transient phase. The borehole thermal mass per unit depth can be defined using a cross-sectional area average

$$\left(\frac{(\rho c_p A)_f + (\rho c_p A)_p + (\rho c_p A)_{grout}}{A_f + A_p + A_{grout}} \right) \frac{V_{bh}}{H} \quad (4.2.4)$$

where A_f , A_p , and A_{grout} are the fluid, piping, and grout cross-sectional areas, respectively. Using the dimensions outlined in Table 4.1, the u-tube thermal mass per unit depth was calculated to be 3.33×10^4 J/mK, while the coaxial value was 5% greater, at 3.50×10^4 J/mK.

4.2.3 Outlet temperature

The outlet temperature can be used as a general indicator of performance. When heat is injected into a borehole, a lower outlet temperature represents better performance, because heat has been more effectively carried away from the working fluid.

4.2.4 Heat transfer rate

Where data is available, it is possible to make accurate comparisons between designs based on their performance. For this, it is necessary to establish consistent metrics as a basis for comparison. Under the correct conditions, the heat transfer rate of the BHEs is helpful for comparison. The heat transfer rate of a borehole heat exchanger is defined in equation 4.2.2, based on the mass flow rate and inlet and outlet temperatures of the heat exchanger. The heat transfer rate cannot, however, be employed to compare cases where q' is fixed, such as thermal response tests.

4.2.5 Effectiveness

In this thesis, heat exchanger effectiveness is proposed as an alternate measure of performance suitable for any inlet condition. The heat exchanger effectiveness is the ratio of the actual rate of heat transfer compared with the maximum possible heat transfer rate that can be achieved. A value of one represents the best performance theoretically possible. Effectiveness can be used to compare heat exchangers with constant heat transfer rates as well as any other inlet condition. Since most heat exchangers contain two working fluids, effectiveness is usually defined based on the inlet and outlet temperatures of each flow. Borehole heat exchangers are unique, however, in that they use a single fluid. Thus, effectiveness in a borehole must be defined relative to the ground temperature, wherein the maximum theoretical heat transfer rate is achieved when the outlet temperature of the heat exchanger reaches the undisturbed ground temperature. This is expressed as

$$\varepsilon = \frac{T_{in} - T_{out}}{T_{in} - T_{ground,\infty}} \quad (4.2.5)$$

4.2.6 Pressure drop

Although pressure drop is not critical for a study of heat transfer performance, it is also important to consider when comparing heat exchanger designs. If the mass flow rate is kept the same for the u-tube and coaxial configurations, the larger flow areas in the coaxial design will result in lower velocities and, therefore, a lower pressure drop. Using the parameters listed in Table 4.1, the pressure drop can be calculated using the major losses in each heat exchanger. For the u-tube, the pressure drop is 112.6 kPa, which is 36% greater than the coaxial pressure drop of 72.3 kPa.

4.3 Comparative Study of U-tube and Coaxial Heat Exchangers Under Continuous Loading

The u-tube and coaxial designs were first compared under a continuous load, with no interruptions in operation. The objective of this testing is to provide a medium-term comparison between the two configurations, beyond the time it takes for the heat exchangers to reach steady state. For these purposes, 72-hour tests were conducted. Two different tests were carried out: a thermal response-type test, where the heat transfer rate was held constant during the simulation, and a constant inlet temperature test.

To provide an equal comparison between the different designs, consistency between the two heat exchangers was maintained as much as possible. Each borehole had the same length of 182.88 m and 107.95 mm diameter. For all tests, the ground properties were assumed to be homogeneous with pure conduction heat transfer. The dimensions and thermophysical properties of the u-tube and coaxial components were selected

Table 4.1: Parameters used for the base case tests

Parameter	Symbol	Value
Heat injection rate (const. q case)	q	9 kW
Inlet temperature (const. T case)	T_{in}	25°C
Flow rate	\dot{m}	0.87 kg/s
Undisturbed ground temperature	T_0	11°C
Borehole diameter	d_b	107.95 mm
Borehole length	H	182.9 m
U-tube pipe OD	d_o	42.16 mm
U-tube pipe thickness		4.06 mm
Coaxial outer pipe OD	d_{oo}	88.21 mm
Coaxial outer pipe thickness		5.74 mm
Coaxial inner pipe OD	d_{io}	40 mm
Coaxial inner pipe thickness		3.6 mm
Ground thermal conductivity	k_{ground}	2.1 W/mK
Ground density	ρ_{ground}	2115 kg/m ³
Ground specific heat	$c_{p,ground}$	795 J/kgK
Grout thermal conductivity	k_{grout}	1.5 W/mK
Grout density	ρ_{grout}	1300 kg/m ³
Grout specific heat	$c_{p,grout}$	3100 J/kgK
Piping thermal conductivity	k_p	0.45 W/mK
Piping density	ρ_p	950 kg/m ³
Piping specific heat	$c_{p,p}$	1900 J/kgK
Water thermal conductivity	k_w	0.697 W/mK
Water density	ρ_w	997 kg/m ³
Water specific heat	$c_{p,w}$	4184 J/kgK
Water dynamic viscosity	μ_w	8.91E-4 kg/ms
Water Prandtl number	Pr_w	6.14

based on what would be reasonably expected for each design. The working fluid was water with a flow rate of 0.87 kg/s. Both heat exchangers used polyethylene tubing and bentonite grout [84]. All dimensions and thermophysical properties of the tests are detailed in Table 4.1.

4.3.1 Constant heat transfer rate comparison

For this testing, the borehole heat exchangers were subject to a constant heat transfer rate of 9 kW, which corresponds to approximately 50 W/m. This was implemented in the simulation by setting the fluid inlet temperature relative to the outlet temperature by a step increase corresponding to the rate of heat transfer

$$\Delta T = \frac{q}{\dot{m}c_p} \quad (4.3.1)$$

In this case, the fluid inlet temperature was 2.47°C greater than the outlet. As result, both the inlet and outlet temperatures continually rise in these tests.

The inlet and outlet temperatures of the u-tube and coaxial heat exchangers as a result of heat injection are shown in Figure 4.3. The plot shows a consistent difference between the inlet and outlet temperatures of each heat exchanger, representing the constant heat transfer rate. The results show a rapid increase in temperature at the start of the tests and a levelling off as the simulation progresses.

From Figure 4.3, it can be seen that the coaxial heat exchanger produces lower temperatures than the u-tube. This can be attributed to the lower thermal resistance of the heat exchanger. It is clear, however, that the difference between the u-tube and coaxial temperatures is small. At the end of the 72-hour test, the coaxial outlet temperature is only 0.54°C lower than that of the u-tube.

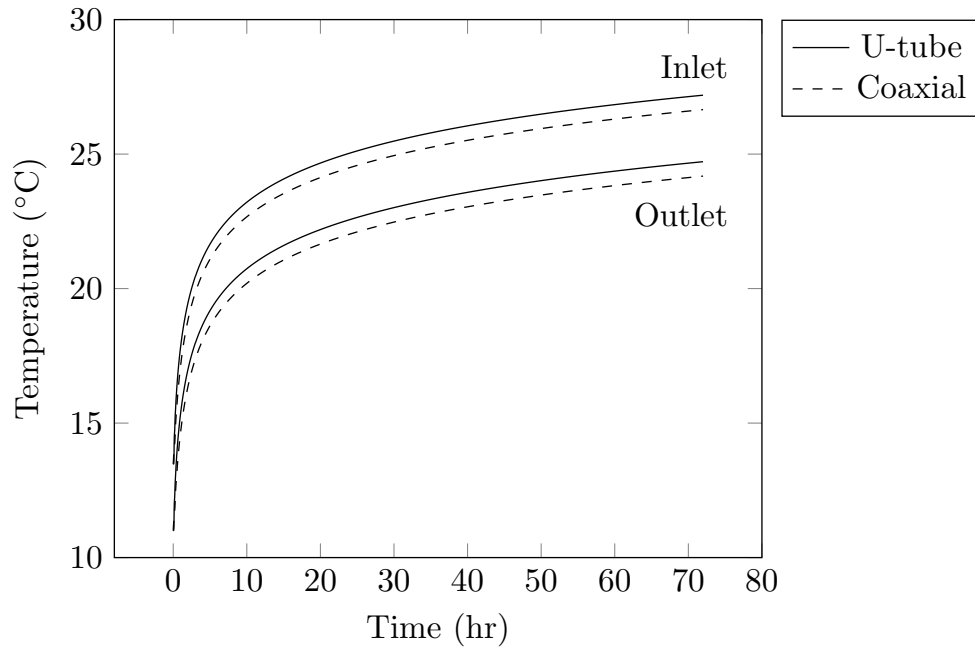


Figure 4.3: U-tube and coaxial inlet and outlet temperatures during a thermal response test, for a case with a constant heat injection rate of 50 W/m

Figures 4.4 and 4.5 illustrate how the temperatures inside the heat exchangers and ground change over the course of the simulation. The u-tube heat exchanger is depicted in Figure 4.4, featuring a top view and a side view of the heat exchanger cross-section near the surface of the ground. The u-tube plots demonstrate the temperature difference between the inlet and the outlet that persists throughout the test, with the inlet tube on the left and the outlet tube on the right. The temperature plots highlight how the asymmetrical geometry of the u-tube heat exchanger results in warmer temperatures near the inlet flow. The effect of the asymmetry, however, is limited to a small radius in the ground around the heat exchanger. Figure 4.5 shows the coaxial top and side views, with a warmer inlet in the centre of the heat exchanger and cooler outlet in the annulus. These plots show how heating is first restricted to

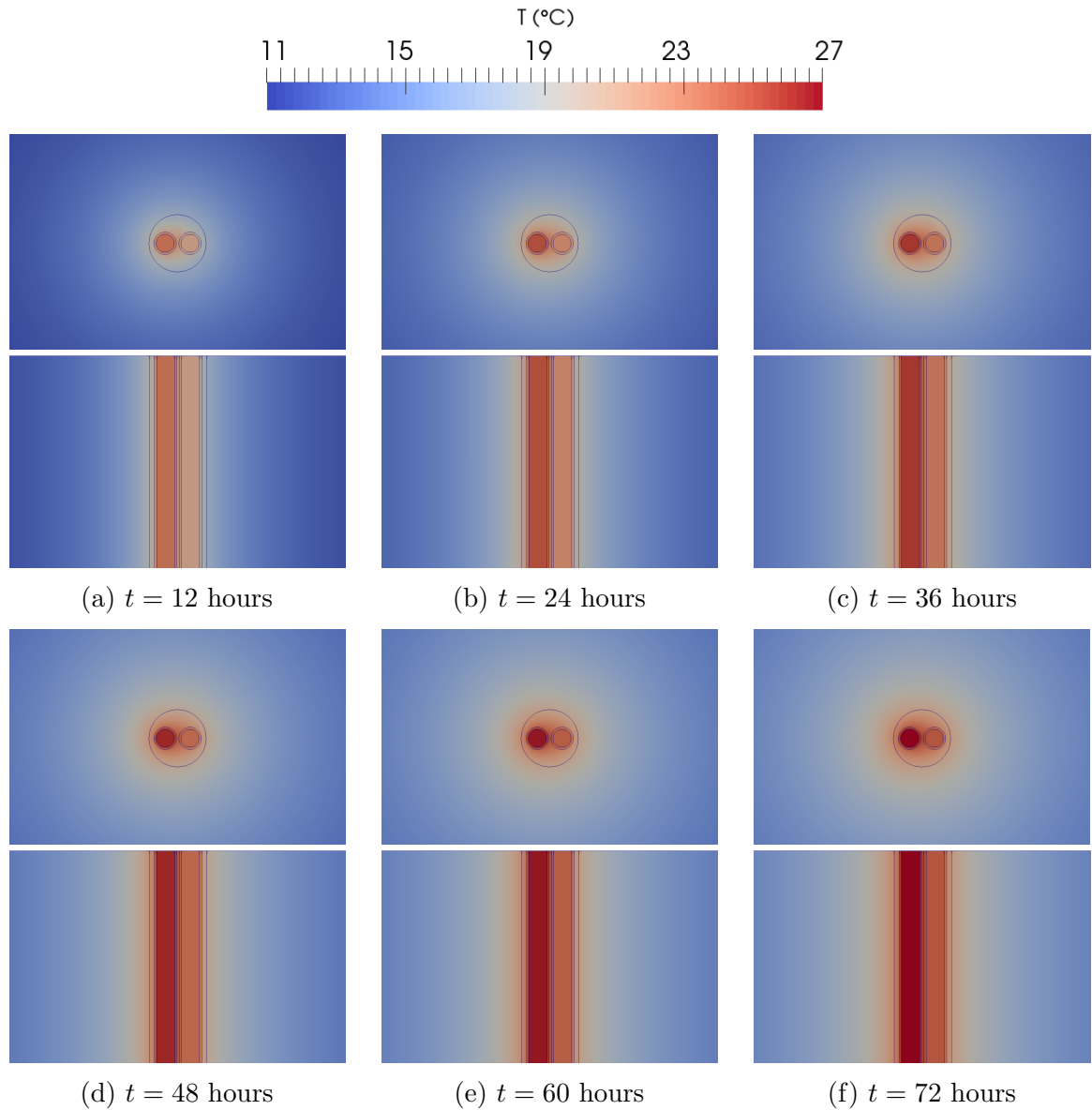


Figure 4.4: U-tube temperatures over time, for a case with a constant heat injection rate of 50 W/m. Top view and side view taken at the top of the domain, near the ground surface

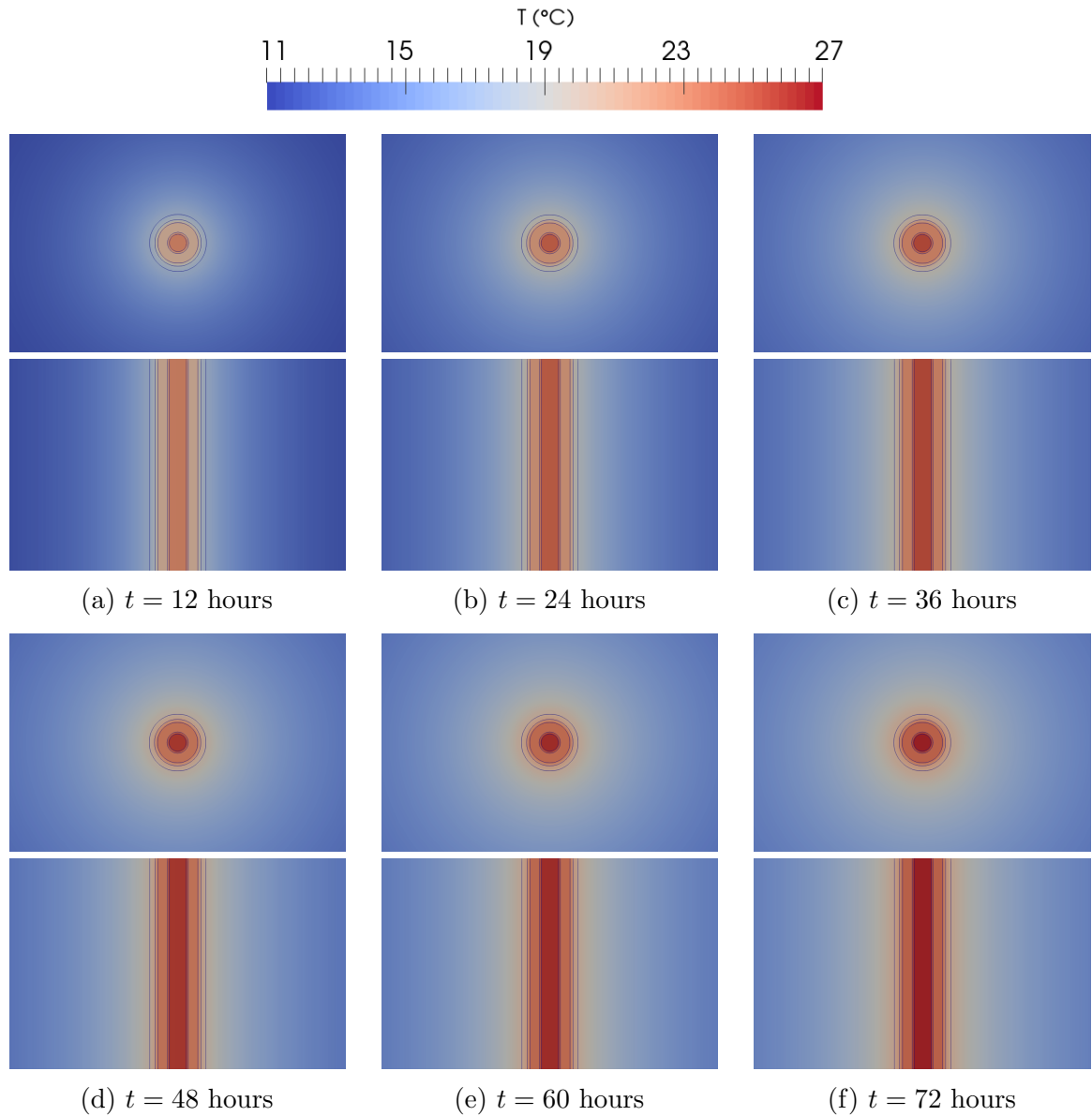


Figure 4.5: Coaxial temperatures over time, for a case with a constant heat injection rate of 50 W/m . Top view and side view taken at the top of the domain, near the ground surface

the heat exchanger and the ground immediately adjacent to the borehole wall. Over time, the ground further away from the borehole wall begins to warm while the temperatures inside the heat exchangers progressively rise. This reflects the results in Figure 4.3, which shows that a difference is maintained between the inlet and outlet temperatures as they continually rise for the duration of the test.

Further insight can be gathered by examining the temperature response in the first hours of operation, shown in Figure 4.6. This plot highlights complex early transient behaviour in both heat exchangers, with clear differences between them at the very start of operation. For the first minutes of operation, the u-tube temperature remains flat. This is followed by a sudden increase in temperature and subsequent oscillations in the temperature curve before it takes on a logarithmic shape, which persists through the remainder of the test. In contrast, the coaxial temperature rises immediately at the start of operation. The coaxial BHE also undergoes a jump in temperature, though it is both smaller and occurs later than that of the u-tube. After this transient behaviour, the coaxial curve smooths, and settles to a temperature consistently below the u-tube temperature.

The distinct behaviour of both heat exchangers can be explained by their differences in geometry and flow. At the beginning of the test, the outlet temperature of both heat exchangers is equal to the undisturbed ground temperature. When hot fluid is injected at the inlet, the outlet temperature should not instantly change, because it takes time for the injected fluid to reach the outlet. This transit time is 381 s (≈ 0.11 hours) for the u-tube and 883 s (≈ 0.25 hours) for the coaxial. The u-tube outlet temperature clearly shows this delay; the temperature remains low until hot fluid reaches the outlet. When this happens, the outlet temperature jumps, causing

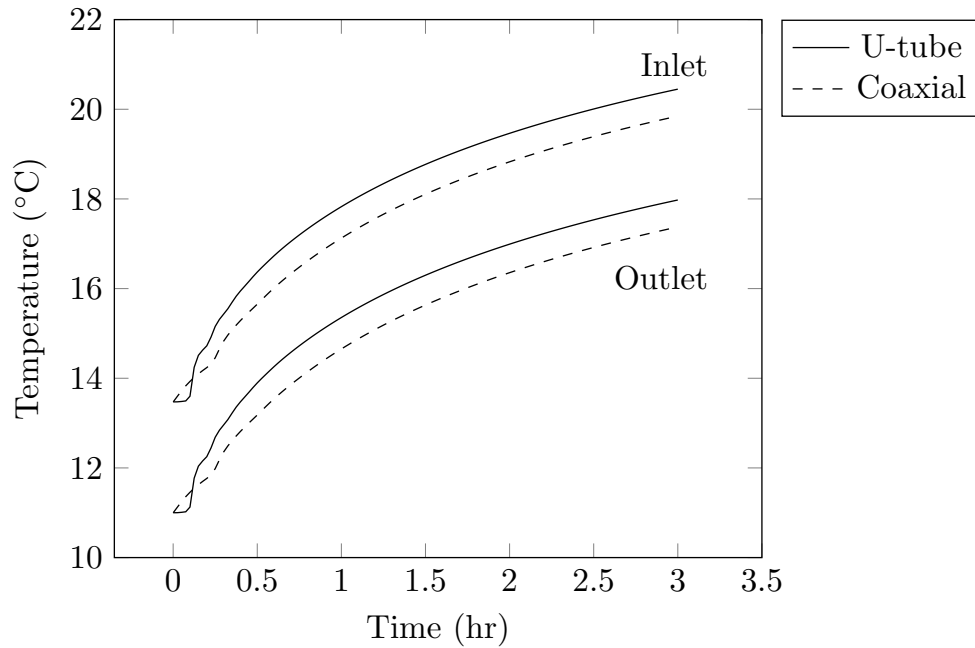


Figure 4.6: U-tube and coaxial inlet and outlet temperatures during the first three hours of a thermal response test, for a case with a constant heat injection rate of 50 W/m

a commensurate rise in the inlet temperature, which is coupled to the outlet by the simulated heater. This sudden jump in the inlet temperature is then reflected in the outlet temperature at 762 s (twice the transit time) after the start of operation. This oscillation is repeated a third time, after which the effect is damped out.

The coaxial outlet temperature appears to rise much sooner, despite its longer transit time. This occurs because there is significant lateral heat transfer between the inlet and outlet flows across the centre pipe, warming the outlet temperature before the first inlet fluid reaches the outlet. The same early lateral heat transfer is not observed in the u-tube because the tubes are spaced apart, with a volume of grout in between. As a result, the coaxial outlet temperature is in fact greater than that of the u-tube in the first minutes of operation. Once the u-tube transit time

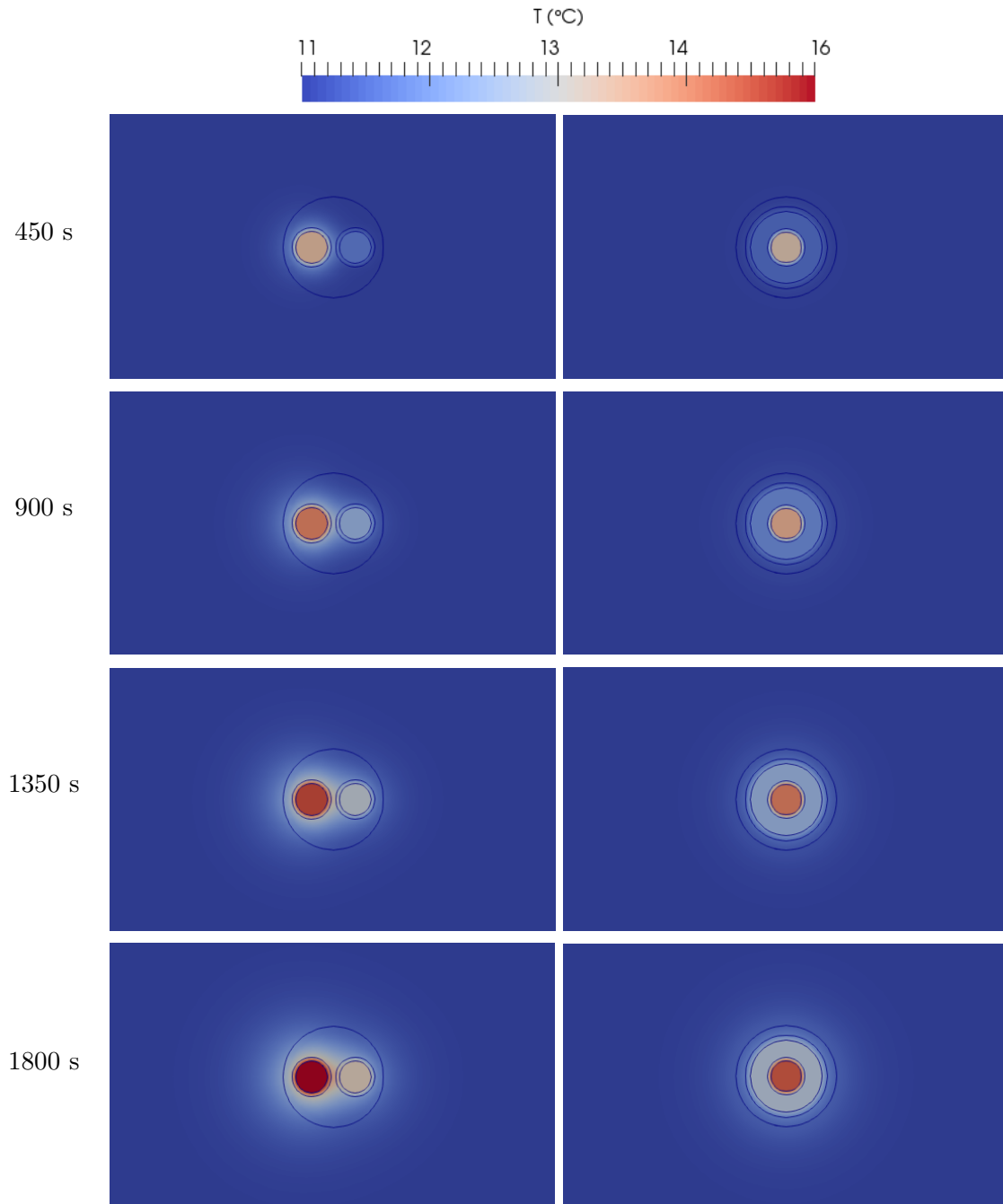


Figure 4.7: Cross-sections of the u-tube and coaxial heat exchangers over the first 30 minutes of operation during a thermal response test with a heat injection rate of 50 W/m. Cross-sections taken at the top surface of the domain

is reached, however, the u-tube outlet temperature quickly jumps and overtakes the coaxial value. The u-tube temperatures remain higher for the remainder of the test.

A comparison of the heat exchangers' early temperature behaviour can also be seen in Figure 4.7. The temperature field plots show how the u-tube inlet and outlet temperatures are higher than that of the coaxial when below the coaxial transit time. The effect of asymmetry in the u-tube can be clearly seen over these early times, with higher temperatures in the grout, tubing, and soil surrounding the outlet tube. Furthermore, the plots highlight that, due to the differences in geometry, the grout and ground temperatures are disturbed sooner in the u-tube case compared to the coaxial. The coaxial outer fluid acts as a buffer between the inlet flow and the ground, creating a delay in the rise in grout and ground temperatures. Overall, this figure emphasises how the u-tube inlet and outlet temperatures rise higher than the coaxial temperatures during the first 30 minutes of operation.

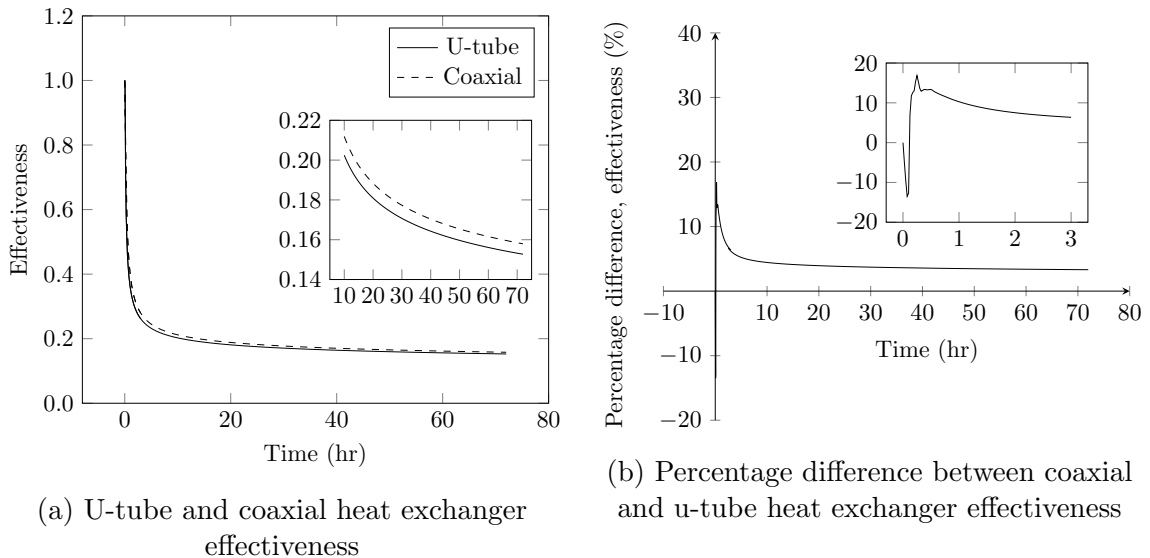


Figure 4.8: Effectiveness and percentage difference of effectiveness for u-tube and coaxial heat exchangers during a thermal response test with a constant heat injection rate of 50 W/m

Effectiveness is used to quantify the impact of these differing temperatures on performance. Figure 4.8a shows that both the u-tube and coaxial heat exchangers have very similar effectiveness curves. At the start of the test, each has an effectiveness of one, the maximum possible value, because the outlet temperatures begin equal to the undisturbed ground temperature. After the start of the test, the effectiveness rapidly drops, before levelling off at approximately 10 hours and experiencing much more gradual decreases for the remainder of the test. The inset plot shows the detail of the effectiveness curve after the large drop, demonstrating more clearly that the coaxial BHE has a slightly larger effectiveness than the u-tube.

Examining the percentage difference between the u-tube and coaxial effectiveness sheds more light on how the performance of the two heat exchangers differs. The percentage difference in effectiveness is defined as

$$PD = 100 \left(\frac{\varepsilon_{coax} - \varepsilon_{u-tube}}{\varepsilon_{coax}} \right) \quad (4.3.2)$$

where ε_{coax} and ε_{u-tube} are the coaxial and u-tube effectivenesses, respectively. Figure 4.8b indicates that, while the u-tube and coaxial performance is close through most of the test, there are significant variances at the beginning of operation that are not apparent from the effectiveness plot alone. The inset plot, in particular, reflects the transient temperature changes observed in Figure 4.6. The initial negative percentage difference occurs because the coaxial outlet temperature rises from the start, above the u-tube outlet, which remains flat. The coaxial begins to outperform the u-tube once the u-tube transit time is reached, and its outlet temperature rises suddenly. After this point, the coaxial effectiveness exceeds that of the u-tube, reaching a maximum difference of 17% at 15 minutes. Subsequently, the performance advantage of the

coaxial heat exchanger drops. By the end of the test, the coaxial has an effectiveness 3.3% greater than the u-tube. These results clearly show that the largest difference in the coaxial and u-tube performance occurs at the beginning of operation.

4.3.2 Constant inlet temperature comparison

In addition to the thermal response test, a case was established with a fixed inlet temperature of 25°C, rather than a fixed heat injection rate. The initial temperature of the borehole and ground was 11°C. With a constant inlet boundary condition, it was possible to compare the heat transfer rate achieved by each heat exchanger design. The heat transfer rate per unit length is calculated using the relationship

$$q' = \frac{\dot{m}c_p(T_{out} - T_{in})}{H} \quad (4.3.3)$$

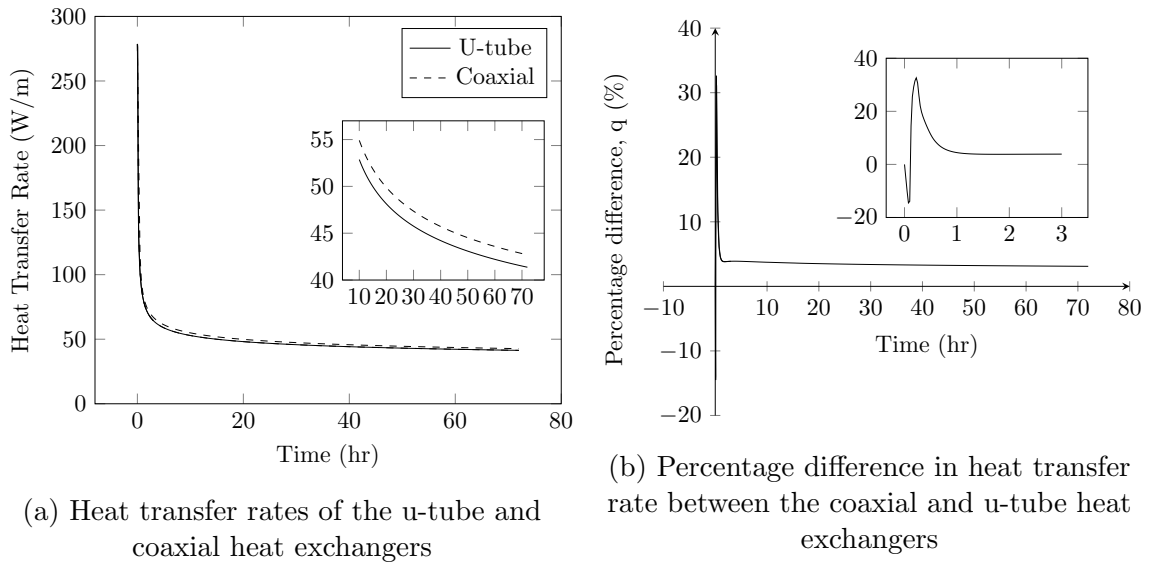


Figure 4.9: Heat transfer rate and percentage difference of heat transfer rate for u-tube and coaxial heat exchangers subject to an inlet temperature of 25°C

Figure 4.9a shows the heat transfer rates achieved by both heat exchangers. While the coaxial heat transfer rate is slightly higher, the u-tube and coaxial heat transfer rates are close. There are, however, notable differences early in the operation. Since the inlet temperature is held constant, the heat transfer rate begins high; for the first time step, the u-tube and coaxial have a equivalent heat transfer rate of 278.7 W/m. After, the heat transfer rate drops quickly at first, before decreasing more gradually for the rest of the simulation. During the early transience, the u-tube briefly has a higher heat transfer rate, before the coaxial performance becomes significantly better than the u-tube. Fifteen minutes into the test, the coaxial heat transfer rate is 31% higher than the u-tube, detailed in Figure 4.9b, with a coaxial q of 186.8 W/m. This represents the maximum difference between the performance of the two designs during this test, after which the heat transfer rates become much closer. At the end of the test, the u-tube BHE has a heat transfer rate of 41.4 W/m and the coaxial has a rate of 42.7 W/m, a difference of 1.3 W/m or 3.1%.

Comparing the heat transfer rates to the effectiveness, very similar behaviour is observed. The effectiveness in Figure 4.10a follows the same pattern of a rapid drop, followed by gradual decrease. As with the heat transfer rates, the effectiveness of the coaxial is higher, though the differences are small, particularly over longer periods. In Figure 4.10b, the percentage difference in effectiveness matches very closely with that of the heat transfer rate in Figure 4.9b. The coaxial effectiveness is 31% greater than the u-tube at 15 minutes, and the test concludes with a difference in effectiveness of 3.1%.

The similarity in the findings for heat transfer rate and effectiveness points to the usefulness of employing effectiveness as a measure of BHE performance. While q is

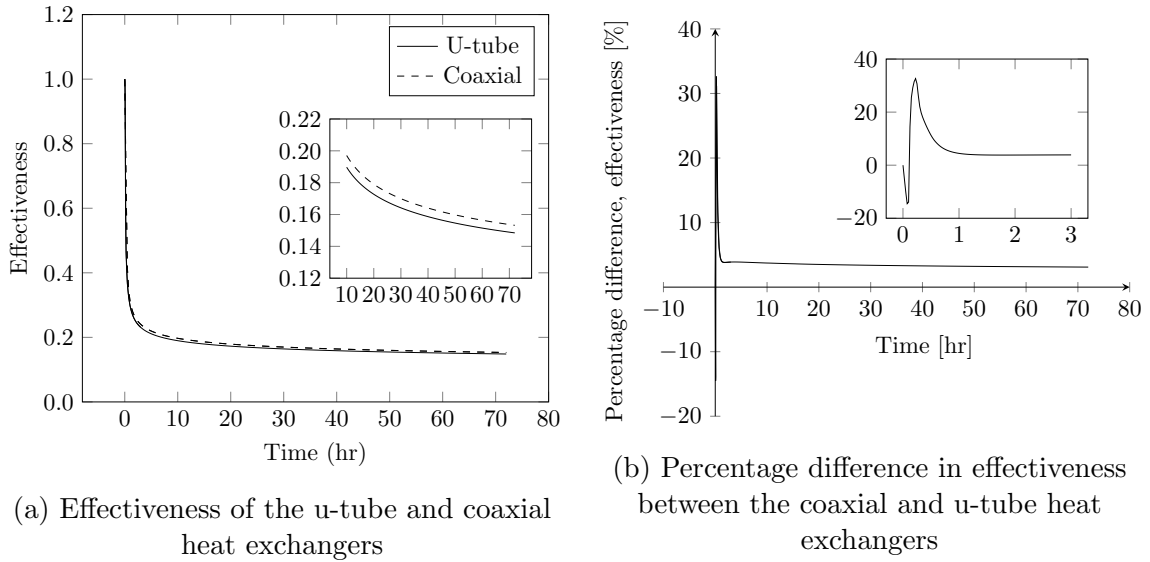


Figure 4.10: Effectiveness and percentage difference of effectiveness for u-tube and coaxial heat exchangers subject to a constant inlet temperature of 25°C

the most direct measure of the ability of a heat exchanger to transfer heat, it is not possible to use it to measure performance in cases where the rate is fixed, such as a TRT. Since the effectiveness curve leads to exactly the same conclusions as the heat transfer rate, it is, therefore, possible to use effectiveness as a measure of performance for all inlet conditions.

4.3.3 Temperature profiles inside the borehole heat exchanger

The detailed nature of the numerical modelling makes it possible to more closely examine the heat transfer and temperature profiles within the borehole heat exchangers. In this section, the results from the constant heat transfer rate case, where heat was injected at a rate of 50 W/m, were investigated in depth. This analysis looks at the temperatures laterally across the inside of the boreholes and the axial temperature profiles of the fluids flowing in the heat exchangers. Lateral temperature profiles are

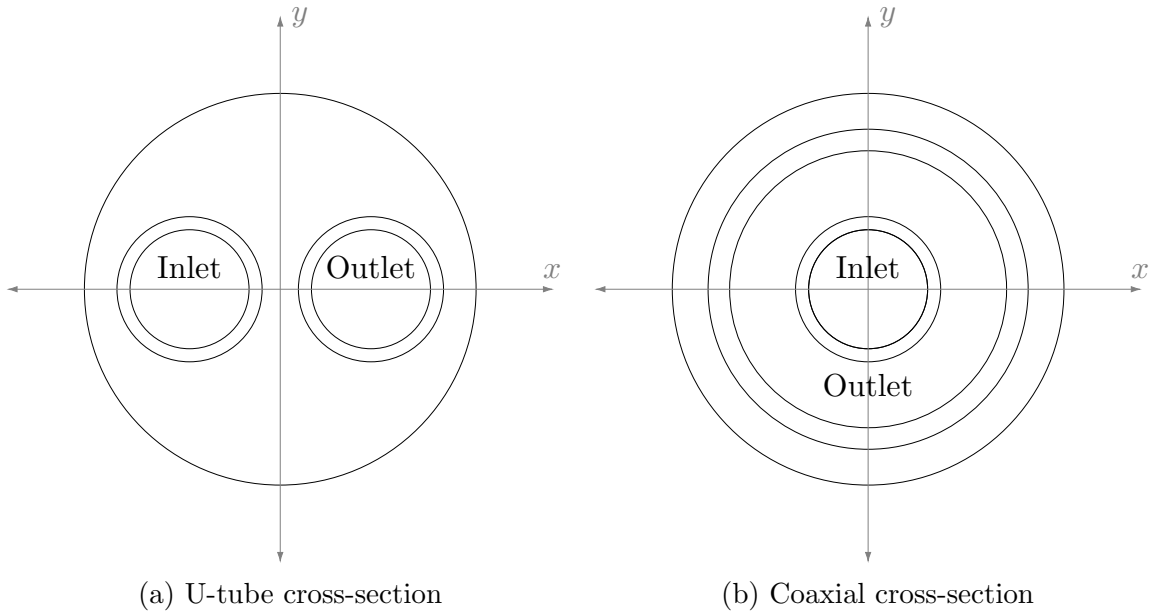
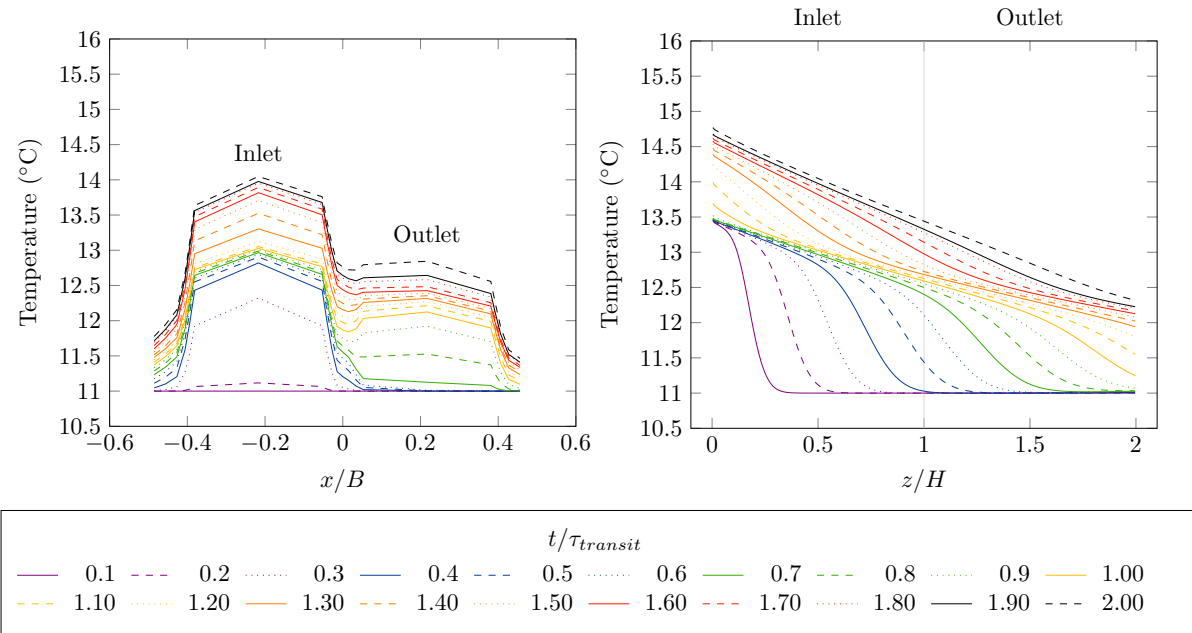


Figure 4.11: U-tube and coaxial radial borehole temperatures are taken along the x -axis at a depth of $H/2$

taken at a depth of $H/2$ along a line that bisects both the inlet and outlet flows, depicted as the x -axis in Figure 4.11. Temperature profiles are taken at several different times early in operation. For the purposes of comparison, the times are expressed as a fraction of the transit time $\tau_{transit}$ for each borehole (381 s for the u-tube and 883 seconds for the coaxial). Thus, it was necessary to linearly interpolate between time steps to obtain results at a consistent interval relative to the transit time. Due to the differences between the transit time for the two heat exchangers, the total time examined ($2 \tau_{transit}$) differs for each design. The time range considered for the u-tube is 762 s, while the time range for the coaxial is 1766 s.

Figure 4.12a shows the temperatures laterally across the borehole taken at a height of $H/2$. The plot highlights the characteristic asymmetry across the u-tube due to differences between the inlet and outlet fluids. This results in a temperature gradient



(a) Radial temperature profiles inside the u-tube borehole heat exchanger at a depth of $H/2$

(b) Axial fluid temperature profiles inside the u-tube borehole heat exchanger

Figure 4.12: U-tube radial borehole temperatures and axial fluid temperatures for a case with a constant heat injection rate of 50 W/m , $\tau_{transit}=381 \text{ s}$

between the inlet and outlet pipes, causing heat transfer between the two fluids. This asymmetry is also reflected in the borehole wall temperature at $x/B = \pm 0.5$, which varies azimuthally. At a time of $2 \tau_{transit}$ the temperature variation across the borehole wall reaches a difference of 0.31°C .

Figure 4.12a also demonstrates the transient progression of the temperature profiles, as hot fluid injected into the heat exchanger reaches the middle height of the borehole in each pipe. The first fluid injected into the borehole is expected to reach the midpoint of the inlet pipe at $0.25 \tau_{transit}$. As can be seen in the figure, there is a very small increase in the inlet pipe temperature at $0.2 \tau_{transit}$. This can be explained by the relatively long axial length of the one-dimensional cells in the pipes causing

elevated temperatures slightly sooner than expected. A more significant rise in inlet temperature is seen at $0.3\tau_{transit}$. The inlet temperature rises further over the subsequent time intervals, at first jumping rapidly before the rate of increase begins to stall. Concurrently, the fluid in the outlet pipe undergoes small increases in temperature. These early temperature increases can be attributed to heat transfer laterally across the heat exchanger, because the temperature of the fluid in the outlet pipe is not expected to rise before a time of $0.75 \tau_{transit}$, when the first hot fluid reaches the middle height of the outlet pipe. After $t = 0.75 \tau_{transit}$, the rise in outlet fluid temperatures is more significant, caused by convection of the hot fluid. The constant heat injection inlet condition results is achieved by coupling the fluid in the inlet pipe to the outlet by a fixed ΔT . As such, when the hot fluid reaches the exit at a time of $1 \tau_{transit}$, the inlet temperature jumps. This causes a second jump in the fluid temperature in the inlet pipe at $1.3 \tau_{transit}$, before the temperature rises begin to diminish again. These variations are also reflected in the oscillations in the inlet and outlet temperature depicted in Figure 4.6.

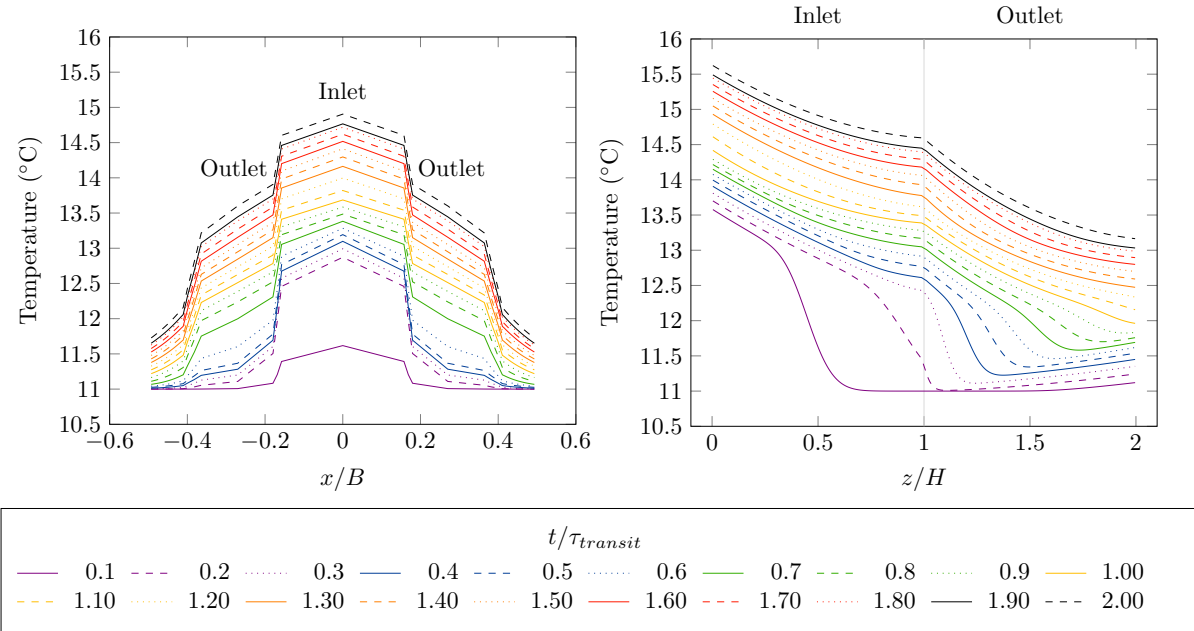
It is interesting to note the changes in the temperature profile at the centre of the borehole. When lateral heat transfer from the inlet to the outlet pipe dominates at the beginning of the test, the slope in temperature across the centre of the borehole is negative. After $0.75 \tau_{transit}$, the centre temperature profile inverts into a u-shape, since the fluid in the outlet pipe is now warmer than the centre. At a time of $1.6 \tau_{transit}$, the temperature profile becomes negative again, due to warming of the centre of the borehole relative to the outlet pipe.

Figure 4.12b shows the axial temperature profiles of the inlet and outlet pipe fluids over the same time periods. The inlet fluid is shown on the x -axis from $0 < z/H < 1$

and the outlet fluid is shown from $1 < z/H < 2$. The plot clearly demonstrates how the hot fluid injected into the heat exchanger progresses through the pipes. It can be seen that the fluid temperature remains at the initial temperature until the first injected fluid arrives at a given height. The first rise in fluid temperature at the bottom of the heat exchanger is seen at $0.5 \tau_{transit}$, as expected, and the temperature at the outlet first rises at $1 \tau_{transit}$, when the injected fluid has travelled the full length of the heat exchanger. A very slight increase in the outlet temperature, and consequently the inlet temperature, is seen before a time of $1 \tau_{transit}$. This can be attributed to lateral heat exchange across the borehole. A bump in the inlet temperature can be seen after $1 \tau_{transit}$, caused by the coupling between the inlet and outlet temperatures, due to the fixed heat input condition. This jump in fluid temperature is propagated through the piping until it reaches the outlet at $2 \tau_{transit}$. At this point in time, the axial temperature profile takes on a relatively linear shape.

Figure 4.13a shows the temperature profile laterally across the coaxial heat exchanger. In contrast to the u-tube configuration, the temperature profiles across the coaxial borehole are axisymmetric due to the annular coaxial design. This plot also highlights how the annular configuration encourages lateral heat transfer between the inlet and outlet fluids, since all radial heat transfer from the inlet pipe must travel towards the fluid in the outlet pipe.

Differences in the cross-sectional areas of the inner pipe and outer annulus lead to different flow velocities and, therefore, different transit times through the two pipes. While the total transit time for the coaxial heat exchanger is 883 s, the transit time of the inner inlet pipe is 177 s (20% of $\tau_{transit}$), while the larger outer annulus has a transit time of 706 s (80% of $\tau_{transit}$). Therefore, the first fluid injected into the heat



(a) Radial temperature profiles inside the coaxial borehole heat exchanger at a depth of $H/2$

(b) Axial fluid temperature profiles inside the coaxial borehole heat exchanger

Figure 4.13: Coaxial radial borehole temperatures and axial fluid temperatures for a case with a constant heat injection rate of 50 W/m , $\tau_{transit}=883 \text{ s}$

exchanger is expected to reach the midpoint of the inner pipe at a time of $0.1 \tau_{transit}$, while the midpoint of the outlet pipe should be reached at a time of $0.6 \tau_{transit}$. Figure 4.13a shows a rise in the inlet temperature at a time of $0.1 \tau_{transit}$ as expected, with a more significant jump in the fluid temperature in the inner pipe at $0.2 \tau_{transit}$. Compared with the u-tube, temperatures of the fluid in the coaxial outlet pipe can be seen to rise more significantly before the expected time of $0.6 \tau_{transit}$. This is caused by a larger proportion of lateral heat transfer between the inlet and outlet pipes. This is also indicated by the steep slope of the temperature profile in the pipe separating the inner inlet fluid from the outlet fluid in the annulus. A further increase in the annulus fluid temperature is seen when the injected fluid reaches the midpoint of the

outlet pipe. Unlike the u-tube, there is much less significant oscillation in the coaxial inlet temperature. This is due to the lateral heat transfer between the inlet and outlet pipes damping the oscillatory effect.

Figure 4.13b shows the axial temperature profiles of the fluids in the inner pipe and outer annulus of the coaxial heat exchanger. While some of the fluid in the outer annulus remains at the initial temperature before the injected fluid arrives, there is clear evidence of significant warming of the annular fluid due to lateral heat transfer. This effect is particularly noticeable near the outlet of the flow, because the temperature difference between the inner pipe and outer annulus is greatest at this location. The plot shows that the hot injected fluid reaches the bottom of the inner pipe at the expected time of $0.2 \tau_{transit}$, and that it reaches the outlet of the flow at $1 \tau_{transit}$. Interestingly, the figure also shows a significant difference in the slope of the temperature profiles in the inner pipe and outer annulus. This difference was not present between the inlet and outlet pipes in the u-tube. This discrepancy can be explained by the annular configuration of the coaxial heat exchanger. When fluid is in the inner pipe, it is surrounded by the outer pipe, which contains warm fluid that will act to effectively insulate the inner pipe. When the fluid reaches the outer annulus, it is suddenly exposed to the cooler surroundings. As such, the fluid in the outer annulus experiences a more dramatic drop in temperature due to greater rates of heat exchange with the outer surface.

4.3.4 Lateral heat transfer across the borehole heat exchangers

The internal u-tube and coaxial temperature profiles clearly indicate that there is some lateral heat transfer that occurs between the hot inlet pipe and the cooler outlet pipe. As such, it is important to consider the effect of this heat exchange on the performance of the heat exchangers. Lateral heat transfer can be identified by examining the outlet pipe and fluid. In the case of continuous heating, it is expected that heat should flow away from the outlet pipe. If there is lateral heat transfer, however, there will be some portion of the outlet pipe that experiences heat flow into the fluid. Therefore, if lateral heat transfer is present at a given axial location, the temperature of the inner wall of the outlet pipe will be hotter than the fluid inside.

$$T_{p,i}(\theta, z) > T_{f,out}(z) \quad (4.3.4)$$

The heat transfer rate between the pipe and the fluid can be calculated for each face on the pipe wall using the relationship for convection heat transfer

$$q_k(\theta, z) = hA_k (T_{p,i}(\theta, z) - T_{f,out}(z)) \quad (4.3.5)$$

where $q_k(\theta, z)$ is the heat transfer rate at a given cell face, $T_{p,i}(\theta, z)$ is the temperature of the inner wall of the outlet pipe, $T_{f,out}(z)$ is the fluid temperature in the outlet pipe, h is the heat transfer coefficient, and A_k is the area of a cell face. Lateral heat transfer q_{lat} is quantified by summing the heat transfer rate for each cell face at which

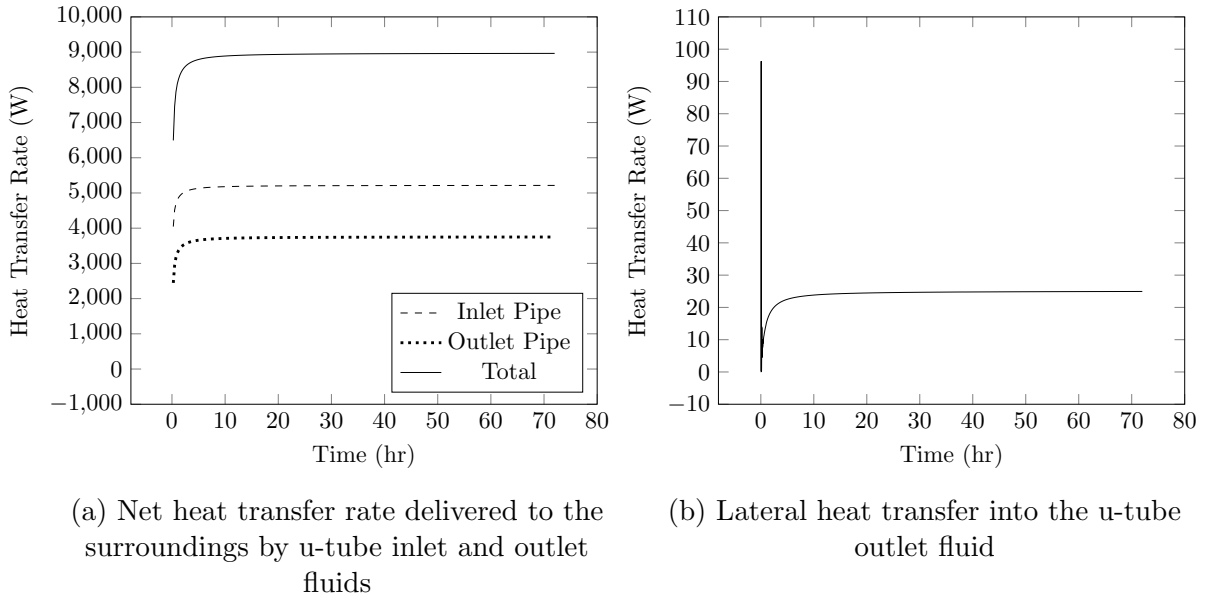


Figure 4.14: Net heat transfer rate delivered by the inlet and outlet fluids and lateral heat transfer into the outlet fluid of a u-tube heat exchanger, for a case with a constant heat injection rate of 50 W/m

there is positive heat flow into the fluid

$$q_{lat} = \sum_k q_k [q_k > 0] \quad (4.3.6)$$

Figure 4.14 shows the lateral heat transfer into the outlet pipe alongside a breakdown of the net heat transfer from the inlet and outlet fluids in the u-tube. Figure 4.14a demonstrates that roughly 58% of the heat being delivered to the ground comes from the inlet fluid, compared with 42% from the outlet fluid. This makes sense, since the inlet fluid is warmer than the fluid in the outlet pipe. In total, 9 kW of heat is delivered to the ground from the u-tube, which agrees with the inlet conditions. Figure 4.14b shows how much heat is transferred laterally from the inlet fluid to the outlet fluid. The plot shows that lateral heat transfer spikes at the start of

the test, when the temperature difference between the inlet and outlet fluids is at its highest. The rate of lateral heat transfer then rapidly drops, due to an equalization between the inlet and outlet fluid temperatures, before it begins to rise again. Lateral heat transfer peaks at a value of 96.3 W and plateaus to a value of 24.9 W by the end of the test. It is clear from these results that lateral heat transfer represents a very small fraction of the net heat transfer rate from the u-tube overall.

This conclusion is supported by calculating the percentage of net heat transfer in the outlet pipe due to lateral heat exchange, shown in Figure 4.15. The percentage of heat transfer due to lateral heat exchange is computed as

$$\left| \frac{q_{lat}}{q_{net,out}} \right| \quad (4.3.7)$$

The plot shows that lateral heat transfer is responsible for 100% of the heat exchange in the outlet pipe very early in the test. This is because it takes some time before the hot fluid initially injected into the heat exchanger reaches the outlet pipe. Once the hot fluid is convected into the outlet pipe, the percentage due lateral heat transfer drops considerably. At 2.75 hours, the percentage of heat transfer in the outlet pipe due to lateral heat exchange is 0.57%. After 72 hours, the percentage is 0.66%. Figure 4.15 also plots the percentage of the surface area of the outlet pipe that experiences lateral heat transfer. Interestingly, a larger proportion of the surface experiences lateral heat exchange in comparison with the percentage of heat transfer. The percentage of surface area due to lateral heat exchange is 4.5% at 2.75 hours and 5.1% at 72 hours. This is because the temperature difference between the inlet and outlet pipes is smaller than the temperature difference between the pipes and the surrounding grout and ground. In effect, the surface area experiencing lateral

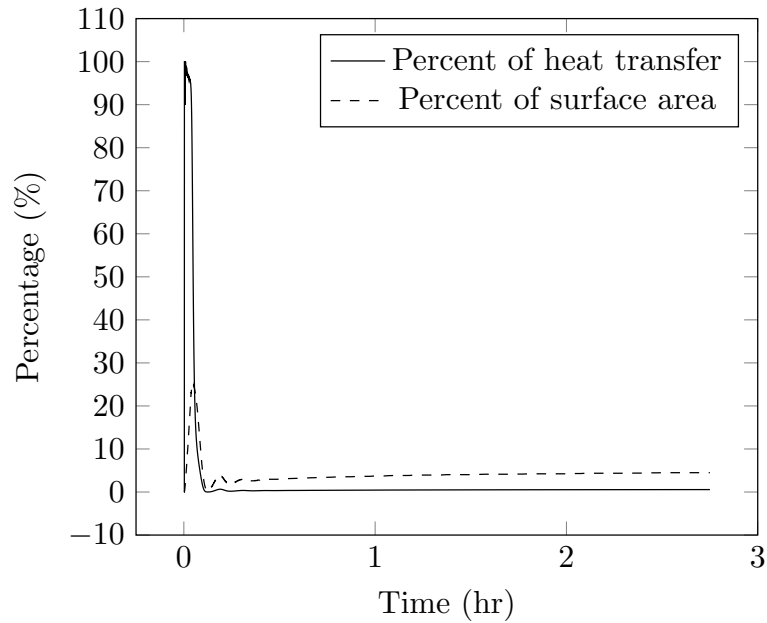
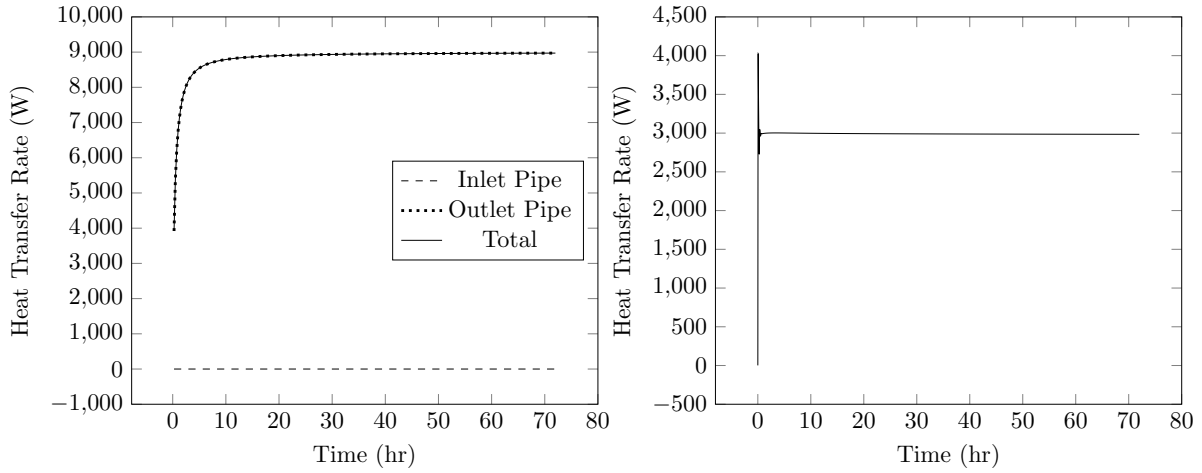


Figure 4.15: Percentage of heat transfer and surface area in outlet pipe due to lateral heat transfer

heat flow serves to insulate the space between the inlet and outlet pipes, since it represents such a small quantity of heat transfer over a more significant portion of the surface area. Therefore, one can conclude that the addition of insulation to prevent lateral heat exchange would have little impact on the performance of the u-tube heat exchanger.

Figure 4.16a shows the net heat delivered to the ground from the inlet and outlet fluids of the coaxial heat exchanger. The plot shows that 100% of the heat delivered to the ground comes from the outlet pipe, the outer annulus. This due to the annular design, in which all the heat travelling radially out of the inner pipe must first flow through the outer annulus before it reaches the ground. As a consequence of this design, lateral heat transfer is a much more significant proportion of the total heat transfer rate of the coaxial heat transfer. Figure 4.16b shows that the lateral heat



(a) Net heat transfer rate delivered to the surroundings by the coaxial inlet and outlet fluids

(b) Lateral heat transfer into the coaxial outer annulus

Figure 4.16: Net heat transfer rate delivered by the inlet and outlet fluids and lateral heat transfer into the outer annulus of a coaxial heat exchanger, for a case with a constant input heat transfer rate of 50 W/m

transfer rate in the coaxial heat exchanger also peaks before reaching a plateau. The lateral heat transfer rate peaks at a value of 4025 W and plateaus at 2984 W by the end of the test. This represents 33% of the total heat transfer rate of the coaxial heat exchanger.

4.3.5 Transient thermal resistance

It has been previously discussed how borehole thermal resistance is used to make predictions about how different heat exchanger designs will perform. It is clear, however, that differences in the thermal resistance do not guarantee a significant performance benefit. This can be understood by investigating how the thermal resistance of a borehole heat exchanger system changes with time. This approach is unique in the

literature; resistance is typically used as a steady state measure. By analysing resistance over time for the whole system, however, it is possible to glean further insight into why a borehole with a small thermal resistance could perform similarly to a borehole with a higher resistance. A plot of resistance over time will incorporate the transient effects due to factors such as thermal mass and fluid flow early in operation. A transient analysis of resistance also demonstrates when components reach steady state. This approach provides a clearer visualization of how u-tube and coaxial heat exchangers differ over the course of operation.

A borehole system can be divided into two sources of thermal resistance: the borehole heat exchanger and the ground.

$$R_{tot} = R_b + R_{ground} \quad (4.3.8)$$

The resistance inside the borehole is due to all components between the working fluid and the borehole wall, including fluid, tubing, and grout. For the purposes of this study, an effective resistance is employed. This is defined using the mean of the fluid inlet and outlet temperatures \bar{T}_f to give the resistance of the entire borehole. The effective borehole resistance is expressed as

$$R_b = \frac{\bar{T}_f - \bar{T}_b}{q'} \quad (4.3.9)$$

where \bar{T}_b is the temperature averaged over the surface of the borehole wall and q' is the heat transfer rate per unit length. The resistance due to the ground is taken

between the borehole wall and the undisturbed ground

$$R_{ground} = \frac{\bar{T}_b - T_{ground,\infty}}{q'} \quad (4.3.10)$$

where $T_{ground,\infty}$ is the initial temperature of the ground before heat exchange occurs.

Using the results of the simulated TRT (described in Section 4.3.1), it is possible to examine the resistance of both the borehole and the ground over the duration of the simulation. In Figure 4.17a, these are plotted alongside the total resistance of the system for both the u-tube and coaxial configurations. This figure clearly demonstrates the dynamic nature of the thermal resistance in the BHE system. Initially, all resistance terms are low. Once hot fluid is injected into the boreholes, the borehole resistances rise very rapidly. Quickly afterwards, the borehole resistances plateau, approaching their steady state values within the first few hours of operation. In the u-tube, the borehole resistance reaches 95% of its value at the end of the test within 4 hours. The coaxial resistance reaches 95% of its final value within 4.5 hours. The gap between the u-tube and coaxial resistances remains consistent throughout the remainder of the test and reflects the fact that the u-tube has a higher thermal resistance.

The thermal resistance settling times are consistent with Eskilson's predictions for when boreholes reach steady state. Eskilson [9] states that the borehole heat exchangers become steady at a time scale of $5r_b^2/\alpha_{ground}$ is reached. For this test, that corresponds to a time of 3.24 hours, which is similar to, though slightly shorter than, the values predicted in the numerical simulation for the u-tube and coaxial.

It is also interesting to note that the heat exchangers reach their steady values faster in the constant inlet temperature test. In that case, both the u-tube and coaxial

reached 95% of their final value within 1.5 hours. This can be attributed to the higher early heat transfer rates in this test.

The steady values of borehole resistance obtained from the numerical simulations can be compared with analytical predictions made using Hellström’s approach [28]. Using this analytical method, the u-tube resistance is predicted to be 0.0902 mK/W and the coaxial resistance is predicted as 0.0832 mK/W. These compare well with the values calculated from the numerical results. The u-tube value from the simulation was 0.0966 mK/W, 6.6% higher than the analytical prediction, and the coaxial value from the simulation was 0.0847 mK/W, 1.8% higher than the analytical value. These findings confirm that the numerical model at steady state matches well with analytical approaches to modelling borehole resistance.

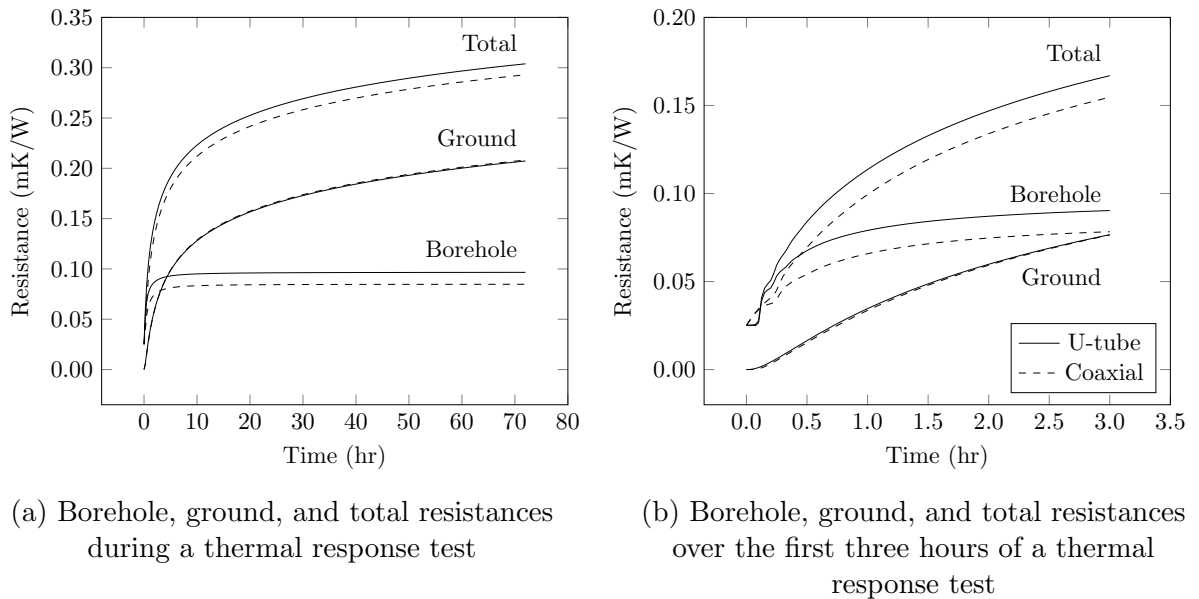


Figure 4.17: U-tube and coaxial system resistances during a thermal response test for a case with a constant heat injection rate of 50 W/m

At the start of the test the ground resistance is zero. This is because the temperature of the borehole wall is initially equal to the undisturbed ground temperature. As such, the ground resistance is initially lower than the borehole resistance. As heat injection causes the borehole wall temperature to rise, so does the ground resistance. This eventually leads to the ground resistance exceeding that of both boreholes and dominating the total system resistance. Since the ground is an infinite sink, and heat is continuously injected into the ground during the TRT, the ground resistance persistently rises throughout the test, becoming increasingly larger than the relatively constant borehole resistances.

The ground resistance is effectively equivalent for the u-tube and coaxial tests. A slight difference between the two resistances can be seen in Figure 4.17a, which is attributable to the variation in borehole wall temperatures caused by the differing designs. As such, any difference in performance between the two designs is caused by the difference in resistance of the heat exchangers. Once the borehole resistances plateau, this difference is steady and easily predicted using models for steady state borehole resistance. However, the variations in borehole resistance are neither steady nor easy to predict analytically during the rapid changes at the beginning of the test.

The detailed numerical models used in this study provide unique insight into the transient behaviour of the BHEs. Since the fluid flow and the thermal mass of the heat exchanger components are considered, the models provide useful insight into how the heat exchangers react to heat injection at very small time scales. This is reflected in Figure 4.17b, showing the system resistances during the first three hours of the TRT. While the ground resistance is initially zero, the borehole resistances are non-zero from the start due to the temperature of the inlet flow. The borehole

resistances reflect the temperature data discussed in Section 4.3.1. While the u-tube outlet temperature experiences a lag due to the transit time for the inlet fluid, the coaxial outlet temperature rises faster due to lateral heat transfer between the inlet and outlet flows. Consequently, the u-tube resistance is temporarily lower than the coaxial resistance. The sudden jump in u-tube outlet temperature and subsequent oscillations are also indicated in the resistance plot. Additionally, the coaxial heat exchanger has a higher thermal mass due to a larger volume of water in the heat exchanger, which causes its temperature to rise more slowly. As a result, the coaxial resistance takes longer to reach steady state. This further contributes to the larger differences between borehole resistances observed early in the test.

Figures 4.17a and 4.17b show how the ground resistance intersects with borehole resistances, before rising continuously for the remainder the test. Since the coaxial borehole resistance is consistently lower after transit time, the ground resistance reaches it first, exceeding the coaxial value at a time of 3.25 hours. The ground resistance exceeds the u-tube borehole resistance at 4.5 hours.

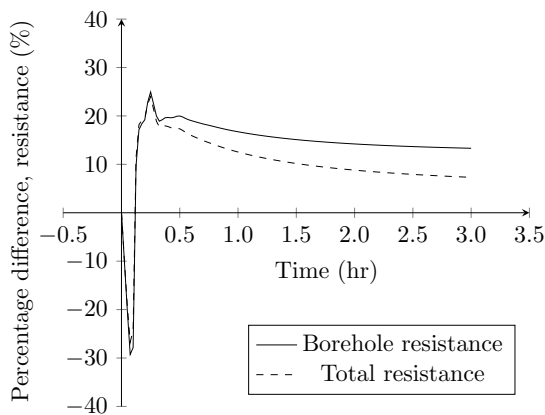
Percentage difference can be used to more clearly understand how the u-tube and coaxial resistances vary relative to one another over time. For this analysis, the percentage difference of the borehole resistance is defined as

$$PD = 100 \left(\frac{R_{u-tube} - R_{coax}}{R_{u-tube}} \right) \quad (4.3.11)$$

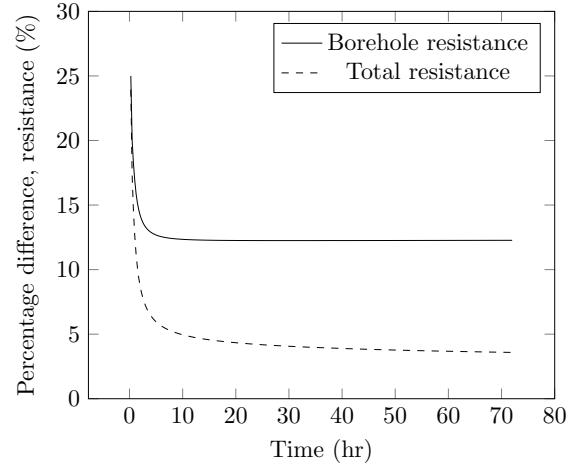
In Figure 4.18, the percentage difference between the u-tube and coaxial resistances is presented. The plots show both the difference between the borehole resistances and the difference between the total system resistances for the two configurations.

Figure 4.18a shows that the resistances vary significantly over the first three hours

of operation. The initial negative value corresponds with the lower u-tube resistance at the start. Once the u-tube resistance rises above the coaxial value, there is a significant (over 20%) difference between the u-tube and coaxial resistances. This drops as the borehole resistances approach their plateau. The final difference in borehole resistance at the end of the test, shown in Figure 4.18b is 12%. The early results also show that the difference between the borehole resistances and the system resistances are very similar over the first hours of operation.



(a) Percentage difference at the start of the thermal response test



(b) Percentage difference over the thermal response test

Figure 4.18: Percentage difference between u-tube and coaxial total and borehole resistances for a thermal response test with a constant heat injection rate of 50 W/m

In Figure 4.18, the differences between the borehole and system resistances are presented for the full 72-hour test. The results show that, after the initial spike in the difference between the u-tube and the coaxial resistances, the gap between them drops. The difference between borehole resistances plateaus after the two heat exchangers reach steady state, approaching a value of 12% at the end of the test. The percentage difference between the system resistances, however, continues to drop

after the BHEs become steady. At the end of the test, the u-tube system resistance is 3.6% higher than that of the coaxial system.

Figure 4.18 provides a clear illustration of why the u-tube and coaxial performance differs the most at early times. At the beginning of the test, the system resistance is almost completely due to the borehole heat exchanger. Further, the differences between the borehole resistances is very high early on due to the transit time and thermal mass effects seen early in operation. These factors combined mean that the difference between the borehole performances is very high near the start of operation. After the system has been running for some time, however, the differences diminish because the system resistance is no longer wholly dependent on the borehole resistance. A larger proportion of the system resistance is caused by the ground. As is seen in Figure 4.17a, the ground resistance continually rises as heat is injected, growing while the borehole resistance remains steady. As such, the total resistance of the system is more dependent on the ground as time progresses, and the differences between u-tube and coaxial system resistances diminish. Therefore, the borehole resistance is most critical to performance in the first hours of operation.

4.4 Intermittent Operation of U-tube and Coaxial Heat Exchangers

The results in Section 4.3 clearly establish that performance differs much more significantly between borehole heat exchanger configurations during the early stages of operation. While this means that BHE design is less critical for long-term or continuously operating systems, design may play a much more important role in systems that

rely upon shorter operating periods, such as those that operate intermittently. This is particularly important for ground source heat pump applications, where the heat pump may operate intermittently for short periods of time. Therefore, this portion of the study aims to systematically examine the impacts of intermittently operating the u-tube and coaxial heat exchangers. This section details the effect of a variety of intermittent operating conditions on borehole performance and uses these findings to establish how intermittency affects each heat exchanger design differently. This investigation is carried out by analysing three key intermittent parameters: operating duration, recovery time, and duty cycle.

4.4.1 Simulation of intermittent operation

In this study, intermittent operation is considered as a period of heat injection, followed by a period of dormancy. When heat injection occurs, the model behaves as if the pump supplying the working fluid is turned on, and the fluid inlet is set to a constant temperature of 25°C. When heat injection stops, that pump is turned off and the inlet temperature to the heat exchanger is assumed to be equal to the outlet temperature. All dimensions and thermophysical properties of the system components are detailed in Table 4.1.

Intermittent flow velocity

The impact of switching the pump on and off was accounted for in the fluid velocity. In the numerical models, the flow velocity is uniform throughout the length of the heat exchanger, but can vary with time. The ramping up and down of the flow when the pump is switched on or off is computed using the unsteady Bernoulli equation,

as explained in Section 3.2.2.

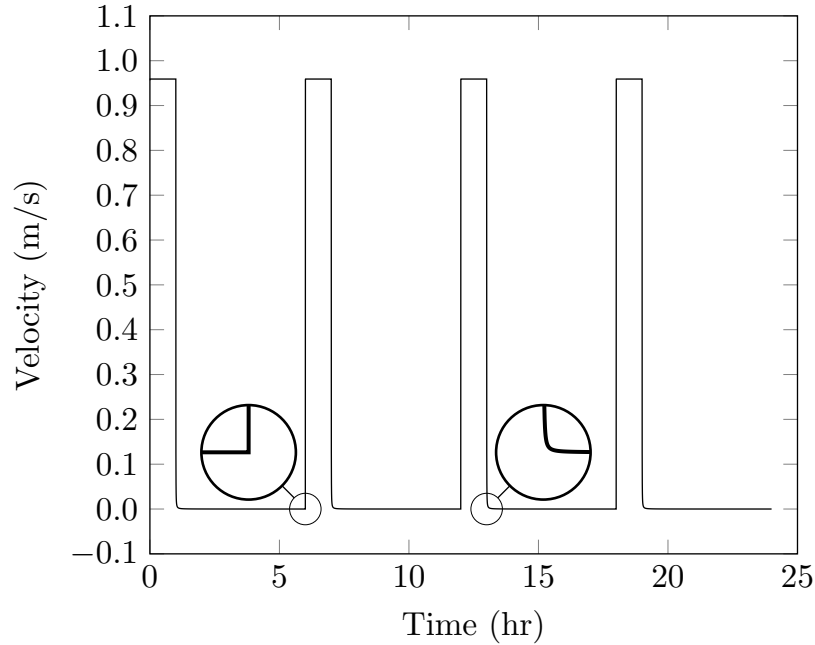


Figure 4.19: Fluid velocity for a case where flow is on for one out of every six hours. The plot shows the ramp up and down of velocity during the intermittent cycles

Figure 4.19 shows the velocity profile for a case where the pump operates for one in every six hours. The fluid ramps up rapidly, reaching a constant target velocity during the operating period before quickly dropping during the dormant phase. For the tested flow rate of 0.87 kg/s, the fluid velocity reaches 95% of the maximum value within seven seconds and 99% of u_{max} within 10 seconds while ramping up. While slowing down, the fluid takes take 127 s (\approx two minutes) for the flow to reach 1% of the maximum velocity. It takes 732 s (just over 12 minutes) for the flow to reach 0.1% of u_{max} . While the scale of the ramp down time is longer than that of the ramp up, both time scales are small and should have a minimal effect on the overall heat transfer rates, but are included for thoroughness.

Intermittent operation case study

Several intermittent operating profiles were simulated in this study. To illustrate the behaviour of the heat exchangers under intermittent loading, one case is examined here in detail. In this case, the u-tube and coaxial heat exchangers are operated for one hour, before being shut off for ten hours. The total operating period is 11 hours, and the duty cycle is 9%.

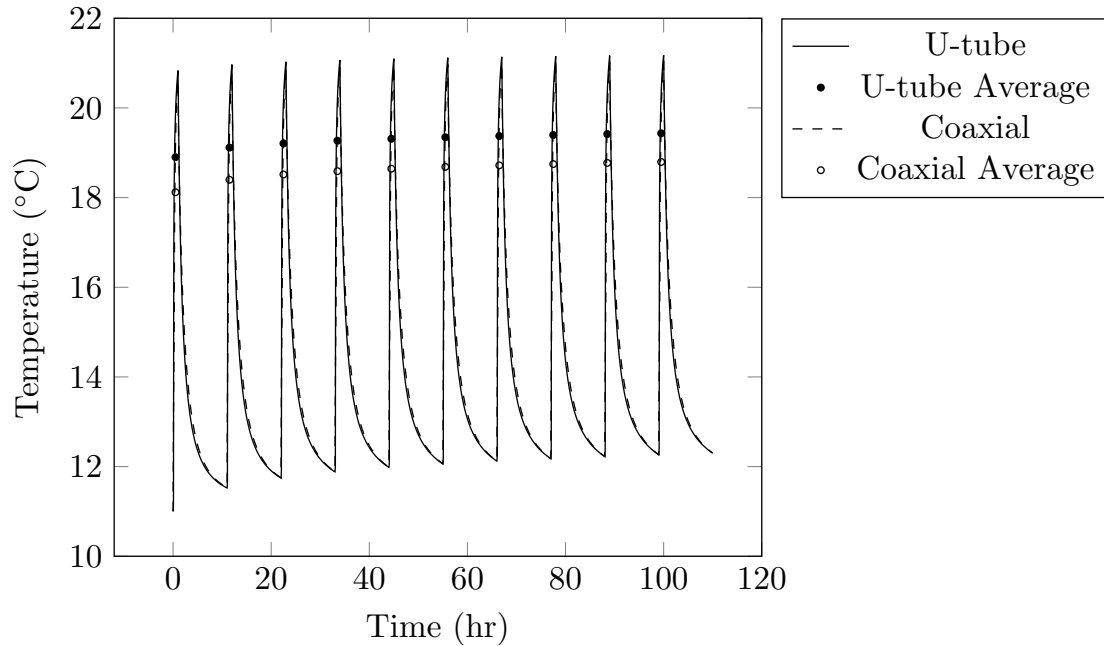


Figure 4.20: Outlet temperatures and average outlet temperatures during operation for a u-tube and coaxial heat exchanger operated intermittently with an inlet temperature of 25°C for one out of 11 hours

Figure 4.20 shows the outlet temperatures of both heat exchangers, alongside the average operating temperature. The average operating temperature is computed as the temperature average taken exclusively over the time the system is running; the outlet temperature during the recovery time is not considered in this term. The outlet temperatures shown take a sawtooth-like profile, rising rapidly when the system is

switched on and dropping when the flow and heat injection is stopped. The plot shows that, while the u-tube and coaxial outlet temperatures appear quite close, there is some deviation between the average temperatures during operation. The u-tube average temperature is 19.4°C during the last operating period of the 110-hour test, and the coaxial average temperature was 18.8°C , a difference of 0.6°C .

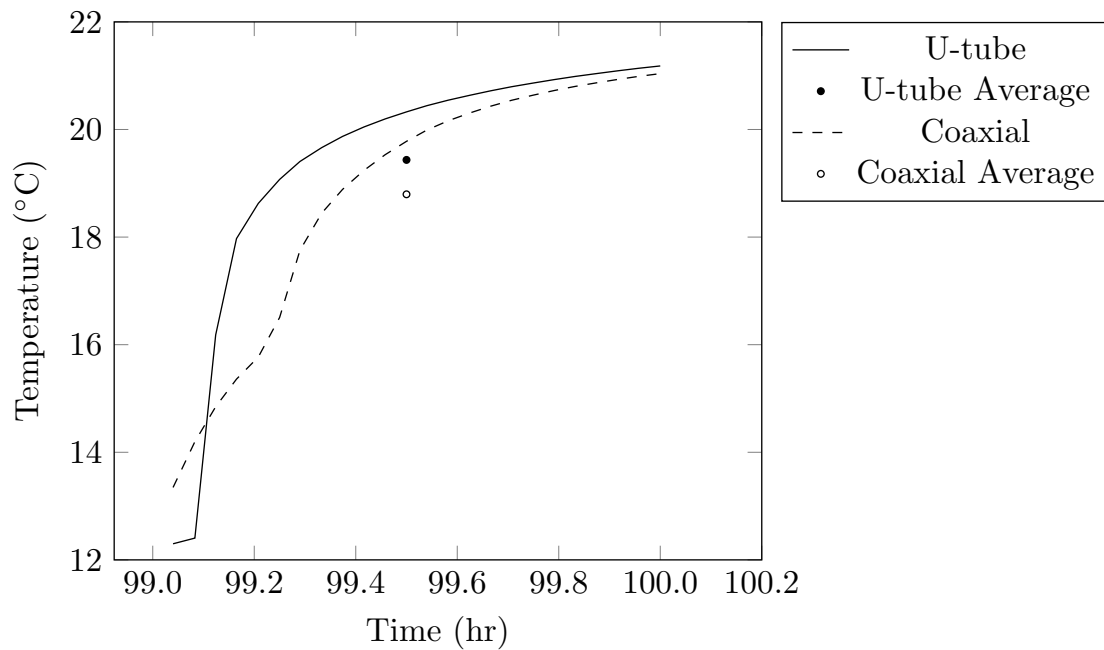


Figure 4.21: Outlet temperatures and average outlet temperatures during the last operating period of the intermittent operation test with an inlet temperature of 25°C for one out of 11 hours

A better understanding of the differences between the u-tube and coaxial temperature responses can be obtained by examining a single operating duration. This is shown in Figure 4.21. This plot bears a significant resemblance to the early temperature profiles shown in Figure 4.6, because the same flow and heat transfer dynamics are at play. The plot demonstrates the latency period in the u-tube before the transit time is reached at 6.35 minutes, after which the outlet temperature jumps rapidly.

Additionally, the more gradual but immediate increase in the coaxial temperature is shown, caused by the significant lateral heat transfer between the inlet and outlet flows. A smaller jump in coaxial outlet temperature is also observed when its transit time is reached at 14.7 minutes. The overall slower rise in the coaxial outlet temperature over the hour of operation can be attributed to the higher thermal mass of the heat exchanger, which slows the heat exchanger’s response to changes in temperature and results in the lower average operating temperature observed in the coaxial BHE.

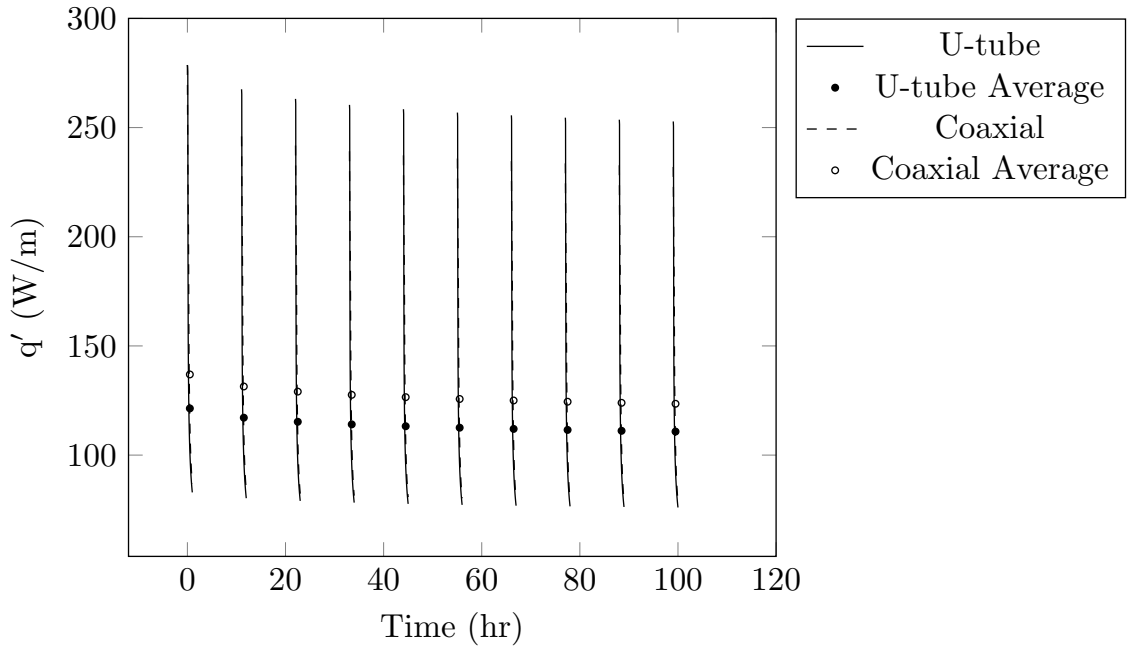


Figure 4.22: Heat transfer rates per unit length and cycle averages during operation for a u-tube and coaxial heat exchanger operated intermittently with an inlet temperature of 25°C for one out of 11 hours

The implications of these differences in temperature response can be seen in Figure 4.22, which shows the heat transfer rates of the BHEs. The heat transfer per unit

length is calculated using the inlet and outlet temperatures.

$$q' = \frac{\dot{m}c_p(T_{out} - T_{in})}{H} \quad (4.4.1)$$

The plot includes the transient heat transfer rate over each operating period and the average heat transfer rate during operation. For clarity, the heat transfer rate during off times is not plotted, since the energy injected into the fluid, and thus the difference between the inlet and outlet temperatures, is equal to zero. This plot shows that the heat transfer rate begins high at the start of each operating period but drops rapidly; and, while the two heat exchangers have similar heat transfer profiles, the average coaxial heat transfer rate is greater than the u-tube. At the end of the 110-hour test (and after 10 hours total operating time), the u-tube transferred an average of 111 W/m during the final cycle, versus the coaxial rate of 124 W/m, a difference of 11%.

Figure 4.23 clarifies what occurs during the swift drop in heat transfer over a single operating duration in the last cycle of the test. The heat transfer rates mirror the temperature responses. The heat transfer rate from the borehole heat exchanger is high for both heat exchangers at the start of the operating period, equal to 253 W/m for the u-tube and 232 W/m for the coaxial. This is because the outlet temperatures are low at the start of operation, due to the cooling that occurred in the borehole during the recovery time. Since the u-tube outlet temperature does not immediately rise when hot fluid is first injected into the heat exchanger, the heat transfer rate remains high, before a sudden drop corresponding to the transit time. The internal lateral heat transfer in the coaxial heat exchanger causes the heat transfer rate to drop sooner, with further losses in the heat transfer rate observed at the coaxial transit

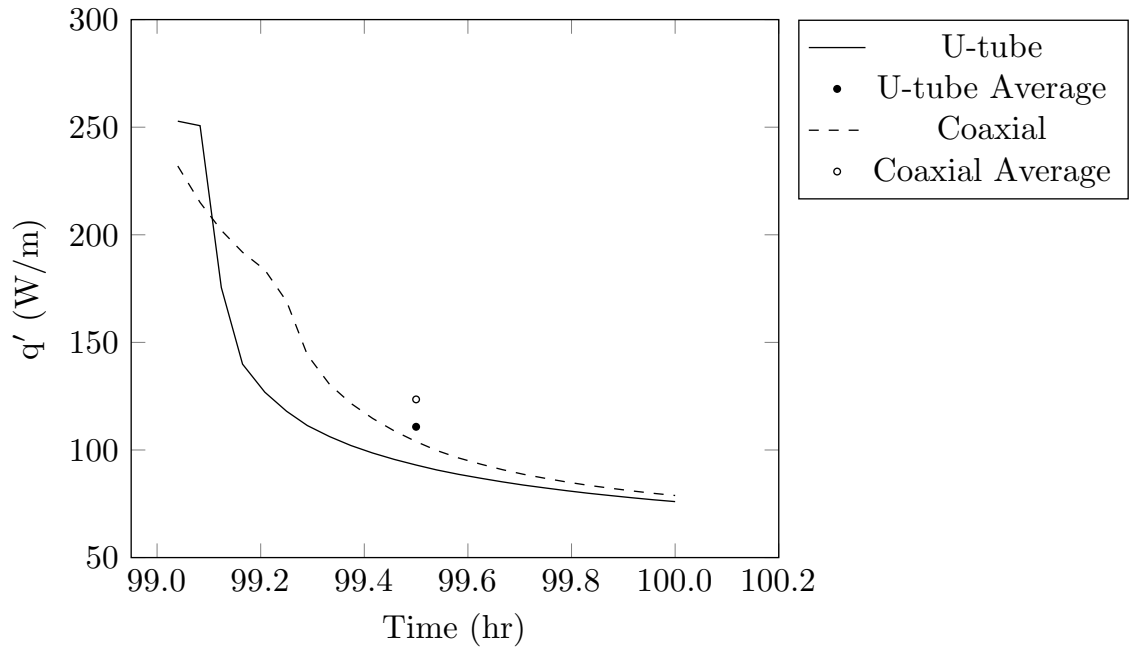


Figure 4.23: Heat transfer rates per unit length and cycle averages during the last operating period of the intermittent operation test with a inlet temperature of 25°C for one out of 11 hours

time. Over the duration of the operating time, the average coaxial heat transfer rate exceeds that of the u-tube: 124 W/m for the coaxial and 111 W/m for the u-tube. While the u-tube heat transfer rate is initially much higher than the coaxial, the slower rate of decrease in heat transfer in the coaxial BHE is ultimately more influential on the average operating q' .

4.4.2 Duration of operation

In this document, the length of time that the heat exchanger is on during an intermittent period is referred to as the operating duration. The first objective in this investigation was to isolate for the effect of operating duration to establish its influence on heat exchanger performance. This was considered by changing the duration

of time that the heat exchanger ran per cycle while maintaining the same recovery period. The simulations were conducted such that the total operating time for each test was consistent throughout this portion of the study. As a result, the number of cycles and the total duration of each test was variable. This approach ensures a consistent duration of heat injection for each test.

Durations above the transit time

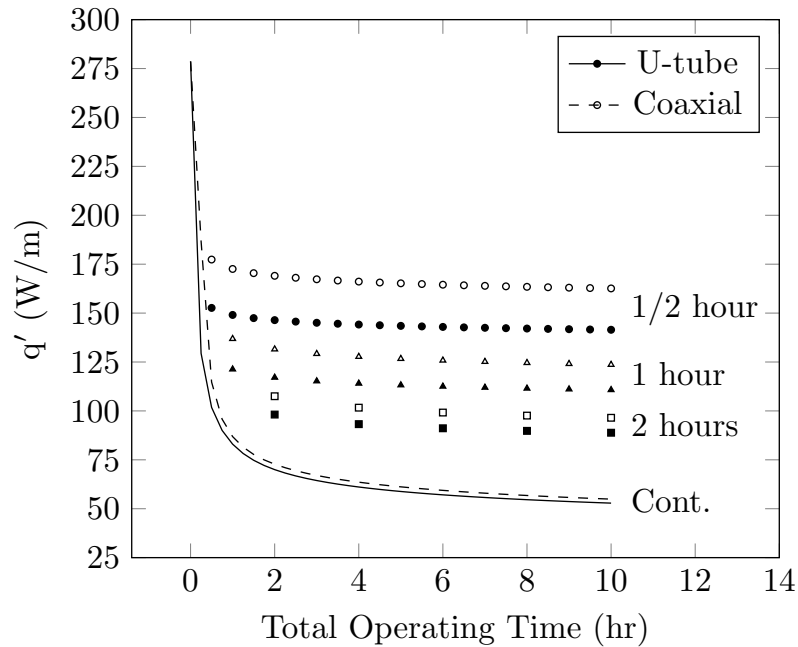


Figure 4.24: Heat transfer per unit length averaged over operating duration for 1/2 hour, 1 hour, and 2 hour durations compared with q' for continuously operated u-tube and coaxial heat exchangers. All cases are operated with a constant inlet temperature of 25°C

Figure 4.24 compares the average operating heat transfer rates for the u-tube and coaxial heat exchangers for operating times of 1/2 hour, 1 hour, and 2 hours. In each case, the systems are off for 10 hours per cycle, sufficient to enable ground

Table 4.2: Heat transfer per unit length for heat exchangers operated intermittently with an inlet temperature of 25°C. Heat transfer rate averaged at a total operating time of 10 hours

Cycle operating duration (hr)	Average u-tube q' (W/m)	Average coaxial q' (W/m)	Percentage difference (%)
0.5	141.6	162.5	12.9
1	110.8	123.5	10.3
2	88.9	96.4	7.8
Continuous	52.9	54.9	3.7

temperature recovery. The x -axis of the plot is the total operating time, which does not include the time for recovery. As such, each case is compared for the same duration of heat injection. The figure also considers the heat transfer rates during continuous operation. The plot shows that the average heat transfer rates all follow a similar trend, starting high when the ground and borehole are initially cool, before dropping and levelling out as time progresses. Significantly, the heat transfer rates approach different values as they stabilize. For example, when the u-tube is operated for a half hour at a time, the average rate approaches 145.5 W/m after a total of 10 hours on. When the same u-tube is operated for 2 hours at a time, the average q' approaches 88.9 W/m. Table 4.2 summarizes all of the average heat transfer rates for each operating duration after 10 hours of total heat exchange. In this table, percentage difference is defined as

$$PD = \frac{q'_{coax} - q'_{u-tube}}{q'_{coax}} \quad (4.4.2)$$

Figure 4.24 and Table 4.2 also highlight the differences between the u-tube and coaxial heat exchangers over these operating durations. Notably, decreasing the operating duration increases the difference between the coaxial and u-tube heat transfer

rates. To illustrate, the percentage difference between the coaxial and u-tube average heat transfer rates is 12.9% with a half-hour operating time and 7.8% with a 2 hour operating time. When the heat exchangers are operated continuously, the difference is only 3.7%. This trend can be explained by the higher thermal mass of the coaxial heat exchanger. As was seen in Figures 4.21 and 4.23, above, the higher coaxial thermal mass slowed the response of the heat exchanger to changes in temperature, decreasing its outlet temperature and increasing its heat transfer rate. Reducing the amount of time that the coaxial BHE is on per cycle further enhances this benefit, since the heat exchanger has had even less time to warm in response to the heat injection.

Durations near or below the transit time

In Figure 4.24, all of the operating times were significantly above the heat exchanger transit times (u-tube: 6.35 minutes, coaxial: 14.7 minutes). Since considerable change occurs within the heat exchangers in and around the transit times, it is important to examine operating durations of that time scale. In Figure 4.25 operating times of 5, 10, and 20 minutes are presented over a total operating period of 6 hours. Each case considered a recovery time of 3 hours per cycle. This plot reinforces the finding that decreasing the operating duration provides a pronounced benefit to the heat transfer rate. The differences between the u-tube and coaxial heat transfer rates in this figure, however, are quite distinct from the behaviour observed in the longer operating times. At 20 minutes of operation, above both transit times, the coaxial outperforms the u-tube, as was seen previously. When the operating time is lowered to 10 minutes, the performance of the two heat exchangers is, in fact, closer, opposite to the trend seen

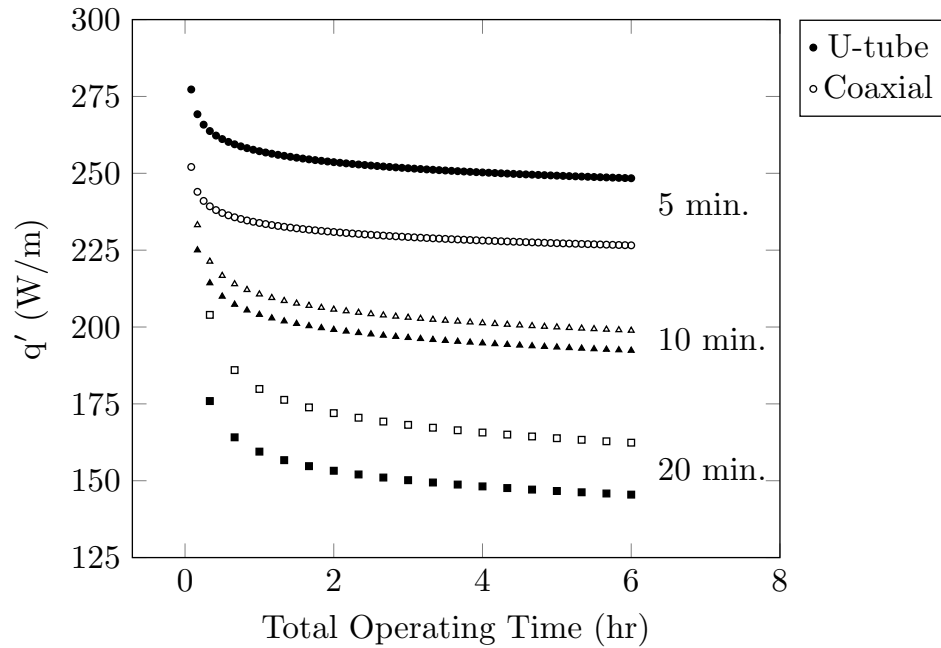


Figure 4.25: Heat transfer per unit length averaged over operating duration for 5, 10, and 20 minute durations, where the u-tube transit time is 6.35 minutes and the coaxial transit time is 14.7 minutes. All cases are operated with a constant inlet temperature of 25°C

in Figure 4.24. At this operating time, the coaxial is below its transit time, but the u-tube is not. Further reducing the operating time to 5 minutes results in a reversal, in which the u-tube performs significantly better than the coaxial. These results are summarized in Table 4.3, which includes the percentage differences between the designs.

These results indicate that intermittent operation for durations similar to the transit time of a heat exchanger has a distinct effect on its performance. When a heat exchanger is operated for a duration longer than the transit time, the hot fluid that entered at the beginning of operation has enough time to travel the full length of the piping and exit the heat exchanger. While this hot fluid travels, it warms the

Table 4.3: Heat transfer per unit length for heat exchangers operated intermittently with an inlet temperature of 25°C. Heat transfer rate averaged at a total operating time of 6 hours

Cycle operating duration (min)	Average u-tube q' (W/m)	Average coaxial q' (W/m)	Percentage difference (%)
5	248.4	226.6	-9.6
10	192.4	198.9	3.3
20	145.5	162.4	10.4

tubing and grout surrounding the fluid. If operation is halted before reaching the transit time of a heat exchanger, the hot fluid that entered at the start of operation does not have an opportunity to exit. As such, the tubing and grout near the outlet do not warm up, since they have not been in contact with hot fluid. Additionally, the fluid that exits has had time to cool inside the heat exchanger between operation periods. As a result, operating a heat exchanger below its transit time should result in a significant improvement in performance, with lower outlet temperatures during heat injection and higher heat transfer rates.

Examining the coaxial performance when its operating duration drops from above to below the transit time, however, does not confirm this effect. When the operating time is lowered from 20 minutes to 10 minutes, the coaxial performance, in fact, gets closer to that of the u-tube. The resulting difference is similar to that observed in the continuous case. It would be expected from the physics described above, that the coaxial configuration would have a significant advantage when operated below its transit time and while the u-tube is above its transit time. This counterintuitive result can be explained by the geometry of the coaxial heat exchanger. In this design, the inlet and outlet flows are separated by the wall of the inner pipe. This wall allows for heat exchange between the inlet and outlet flows along the entire length of the

heat exchanger. This is in contrast with the u-tube design, where there is tubing and a volume of grout separating the inlet and outlet flows. As a consequence, the outlet flow in the coaxial configuration rises in temperature well in advance of the transit time. This results in warming of the tubing and grout surrounding the outlet flow, and mitigating the benefit of operating below the transit time in the coaxial BHE.

The benefit of operating below the transit time is more clearly demonstrated with the u-tube. Since the tubes are separated by grout, there is more thermal mass between them, and lateral heat transfer occurs a longer time scales. This is seen directly in the 5 minute case, where the u-tube heat transfer rates are 9.6% greater than in the coaxial. When the u-tube is operated for 5 minute intervals, the outlet temperature always remains in the plateau observed at the beginning of the test in Figure 4.21. As such, the area around the outlet stays cool, even after 6 hours of operation.

4.4.3 Recovery time

The recovery time is the period of time over which the heat exchanger is off during an intermittent cycle. Recovery time has been shown in the literature to be an important factor affecting the performance of intermittently operated BHEs [69, 70]. An understanding of how recovery time impacts the heat exchanger designs differently, however, has not been established. This portion of the study focusses on comparing the response of the u-tube and coaxial configurations to varying recovery periods.

In the previous section, it was established that, above the u-tube transit time, the coaxial heat exchanger outperforms the u-tube given the same operating duration. As such, for this portion of the study it was necessary to compare the u-tube and

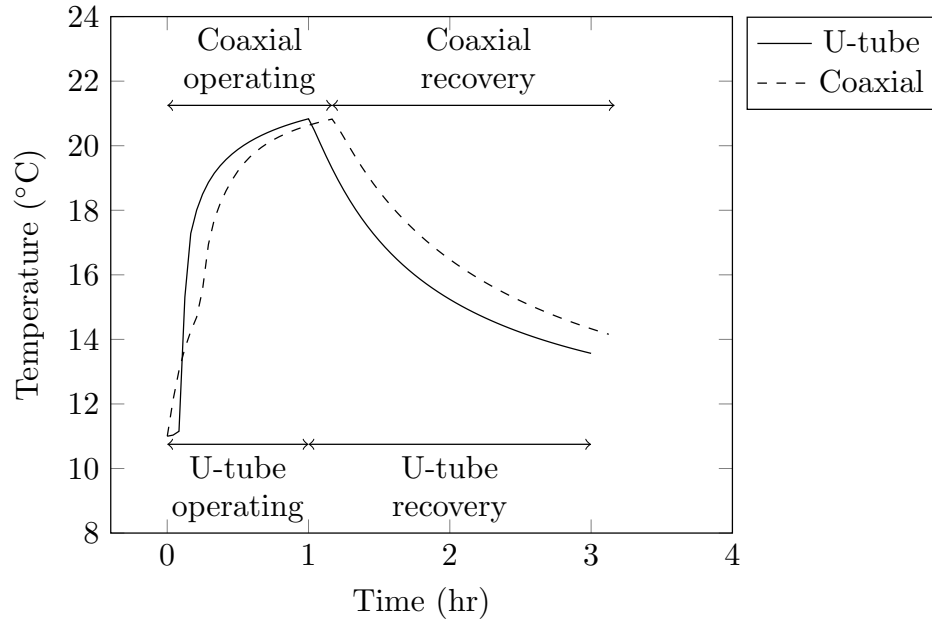


Figure 4.26: Outlet temperatures during the first cycle of a two-hour recovery time test, where the undisturbed ground temperature is 11°C. Both heat exchangers are operated at a constant inlet temperature of 25°C, with the u-tube heat exchanger operated for 1 hour and the coaxial heat exchanger operated for 1.17 hours

coaxial heat exchangers over an equivalent, rather than equal, operating time. An operating duration of one hour was selected for the u-tube heat exchanger. The coaxial equivalent operating time was then found by running the coaxial model for slightly longer, until the outlet temperature exactly matched that of the u-tube at the end of its operation. Therefore, an operating time of 1.17 hours (4200 s) was selected as the coaxial operating duration. The first cycle of the test is presented in Figure 4.26, which demonstrates the slightly longer operating time of the coaxial heat exchanger.

During the recovery period, the pump driving flow is stopped, causing the fluid to slow until it is stationary, and no hot fluid is injected into the heat exchanger. During this time thermal energy is dissipated from the heat exchanger and the ground

surrounding it, allowing temperatures to decline before operation is started again. This temperature recovery allows the heat exchanger to start heat injection again at a lower temperature, resulting in enhanced performance.

The benefits of recovery can be seen in Figure 4.26, which shows a full intermittent cycle, including the operating and recovery time. At the end of their respective operating periods, the u-tube and coaxial have the same outlet temperature. When operation is stopped, the outlet temperatures fall. It can be seen that the u-tube temperature declines faster than the coaxial outlet. This is caused by the higher thermal mass of the coaxial heat exchanger. This high thermal mass benefits the coaxial at the start of operation, slowing the rise in temperature; however, thermal mass also slows the dissipation of heat during recovery. As a result, the coaxial outlet temperature is 0.8°C degrees warmer than the u-tube at the end of the first recovery time.

To understand the full impact of the recovery time, a long term simulation was carried out. The results are presented in Figure 4.27. This figure shows the minimum, average, and maximum temperature for each operating cycle. A total of 35 cycles are plotted, representing a simulation time of 4.4 days for the u-tube and 4.6 days for the coaxial. The two heat exchangers have clear differences in the minimum temperature, which corresponds to the temperature at the end of the recovery time. This confirms that the high thermal mass of the coaxial design will prevent it from cooling as much as the u-tube over the course of several intermittent cycles. Interestingly, the average and maximum temperatures do not differ significantly between the u-tube and coaxial designs. This suggests that, for this intermittent operating cycle, the u-tube and coaxial overall performance would be similar.

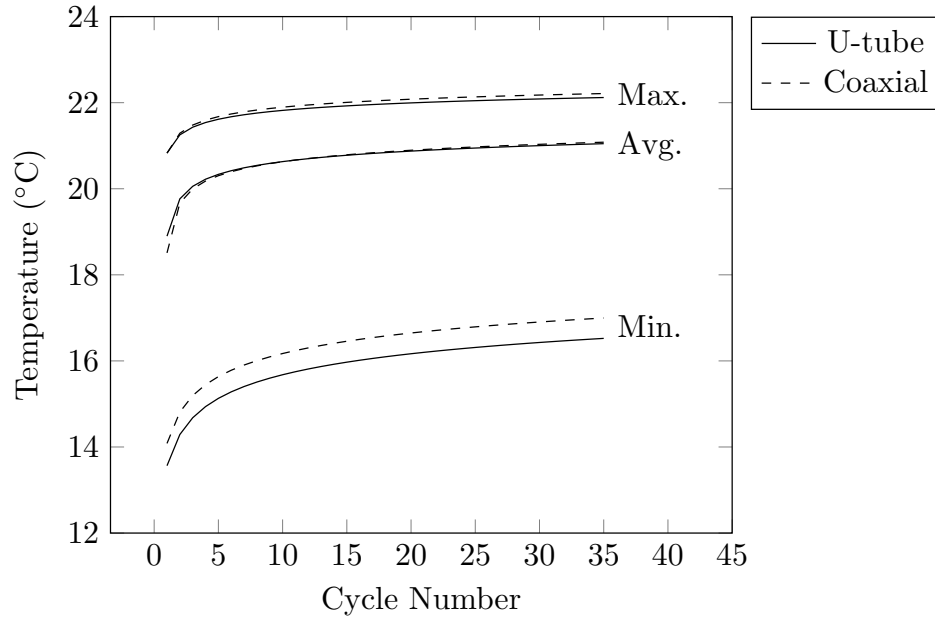


Figure 4.27: The minimum, average, and maximum operating outlet temperatures of the u-tube and coaxial heat exchangers over 35 cycles with a two-hour recovery period, where the u-tube operated for 1 hour and the coaxial operated for 1.17 hours, each with a constant inlet temperature of 25°C

Figure 4.28, which shows the average heat transfer rate per operating period, confirms that the two heat exchangers have very similar performance in this case. Initially, the coaxial design has a higher heat transfer rate, due to its high thermal mass lowering outlet temperatures in the first cycle. After the first cycle, however, there is negligible difference between the u-tube and coaxial heat transfer rates. Therefore, while the heat exchanger design did affect temperature recovery during the non-operational period, it did not have a significant impact on overall performance during this test.

Further testing was carried out to examine how the heat exchangers responded to a variety of recovery durations, the results of which are plotted in Figure 4.29. In each case, the u-tube and coaxial operating times were kept consistent at 1 hour

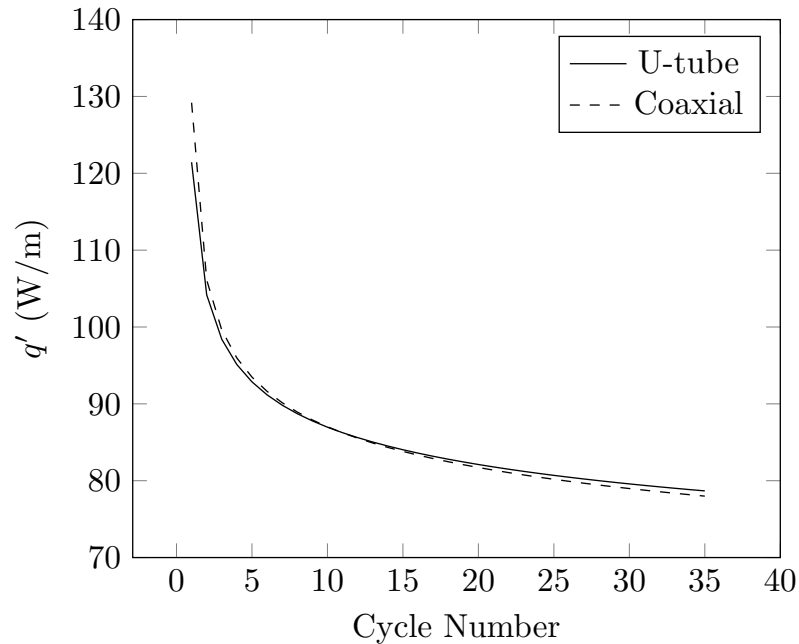


Figure 4.28: Heat transfer rate per unit length for u-tube and coaxial heat exchangers operating intermittently with a 2-hour recovery period, with heat transfer rates averaged over each operating period. The u-tube operated for 1 hour and the coaxial operated for 1.17 hours, each with a constant inlet temperature of 25°C

and 1.17 hours, respectively, while the length of the recovery time was varied. The results show that increasing recovery time improves the heat transfer rate. This finding, which agrees with existing findings in the literature [69, 70], demonstrates that allowing more time for the ground to cool results in better overall performance for both heat exchangers. The results also demonstrate that both heat exchanger designs respond similarly to a variety of recovery times. In fact, it can be seen that for times of 20 minutes to 2 hours, the difference between the average operating heat transfer rate was negligible. When the recovery time is increased to 4 and 8 hours, the coaxial heat exchanger performs slightly better than the u-tube. This difference occurs even though the coaxial temperature at the end of recovery is still higher than

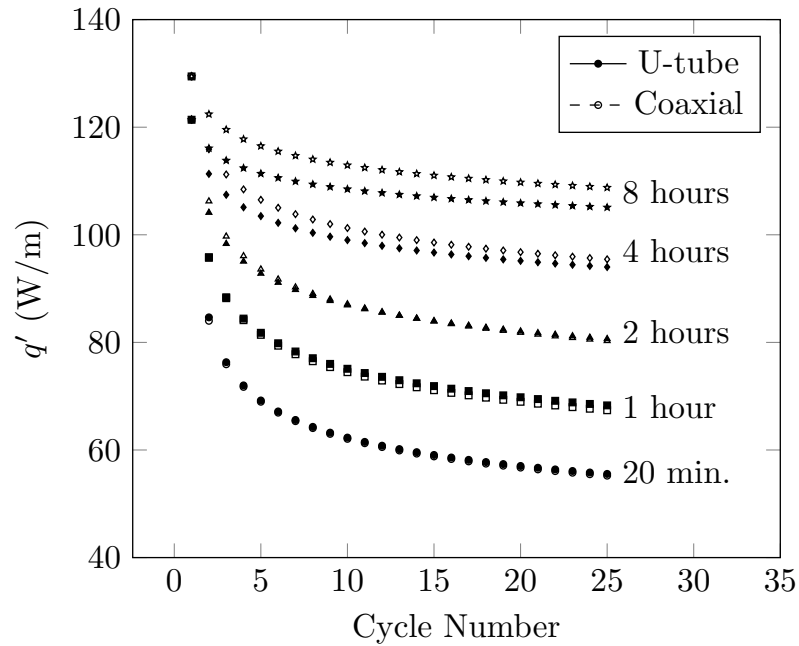


Figure 4.29: Average operating heat transfer rate per unit length for recovery times of 20 minutes, 1, 2, 4, and 8 hours, where the u-tube was operated for 1 hour and the coaxial was operated for 1.17 hours, each with a constant inlet temperature of 25°C

the u-tube value. When recovery time rises, the difference between the u-tube and the coaxial temperature at the end of the non-operational period becomes smaller. Additionally, while the peak in operating temperature is the same for both heat exchangers, the coaxial still has lower average temperatures during operation, due to its higher thermal mass. Therefore, when the u-tube recovery temperature becomes closer to the coaxial value, the coaxial heat exchanger will begin to perform better. This does not, however result in very significant differences in performance. In the 8 hour case, at the end of the simulation, the difference between the coaxial and u-tube heat transfer rates is 3.6 W/m, or 3.3%. As such, it can be concluded that recovery time has a marginal impact on differences in overall performance between designs.

Table 4.4: Operating, off, and total cycle times for 24-hour duty cycle tests

Duty cycle (%)	Operating duration (s)	Off time per cycle (s)	Total cycle duration (s)	Number of cycles in 24 hours
25		900	1200	72
50	300	300	600	144
75		100	400	216
25		1800	2400	36
50	600	600	1200	72
75		200	800	108
25		3600	4800	18
50	1200	1200	2400	36
75		400	1600	54
25		5400	7200	12
50	1800	1800	3600	24
75		600	2400	36
25		10800	14400	6
50	3600	3600	7200	12
75		1200	4800	18
25		21600	28800	3
50	7200	7200	14400	6
75		2400	9600	9

4.4.4 Duty cycle

The duty cycle parameter considers both operating and recovery times as a fixed ratio. It is expressed as the percentage of time during an intermittent cycle that the heat exchanger is operating. This study explored how varying the duty cycle could impact performance, considering duty cycles of 25%, 50%, and 75%, where the 25% cycle has the longest recovery time and the 75% has the shortest. A variety of operating times were considered for each duty cycle, resulting in a comprehensive study of how intermittent cycles impact heat exchanger performance. In each case, the inlet temperature was fixed at 25°C. Table 4.4 outlines all intermittent cycles explored in this section.

Figure 4.30 shows the results for each duty cycle over a variety of operating times. In this figure, the y-axis is the fluid outlet temperature after 24 hours of accumulated operating time; therefore, each case is compared for the same total duration of heat injection. The x-axis is the operating duration per cycle. These tests consider the duty cycles over a wide range of operating times. This plot demonstrates that shorter operating durations result in the lowest outlet temperatures when a smaller duty cycle is employed. While a 5 minute operating duration provided a considerably lower outlet temperature for the 25% duty cycle, the benefits diminish as the ratio of operation is raised to 50% and even further when raised to 75%. For instance, with a 5 minute operating duration in the u-tube, the outlet temperature was 2.5°C lower for the 25% duty cycle than it was for the 75% case. This indicates that adequate recovery is needed between operation to provide the full benefit of shorter operating durations.

When operating duration is increased, the outlet temperatures rise, as was seen in Section 4.4.2. Additionally, with an increase in operating duration, the difference between the duty cycles also decreases. When the operating time was 2 hours, there is a difference of only 0.58°C between the 25% and 75% duty cycle cases. These results suggest that the benefits of increasing the recovery time diminish when operating times are longer.

Overall, Figure 4.30 shows that, for most of the intermittent cycles, the coaxial heat exchanger had lower outlet temperatures and, therefore, better performance than the u-tube. This demonstrates that the coaxial design benefits more from intermittent operation, except when the u-tube performance is significantly improved by operating below the transit time.

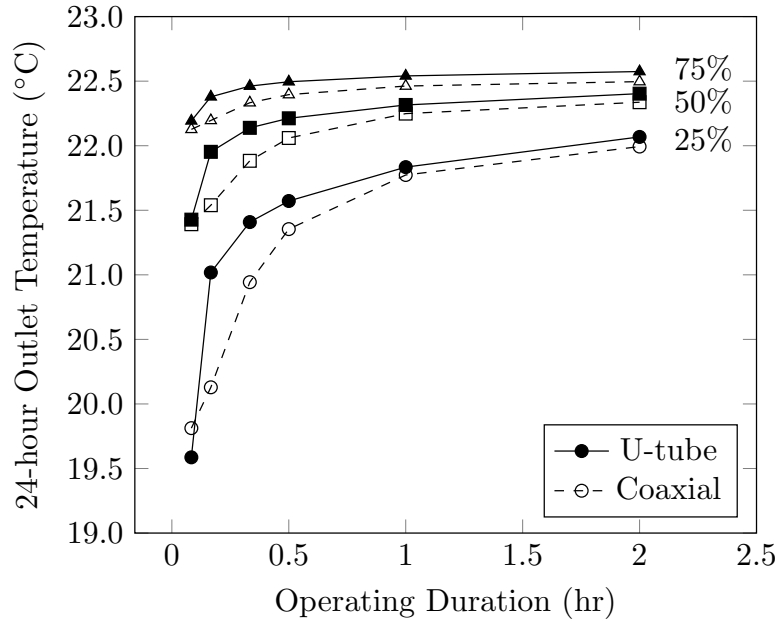


Figure 4.30: Outlet temperature after 24 hours of operation vs. operating durations for the u-tube and coaxial heat exchangers for duty cycles of 25%, 50%, and 75%. Heat exchangers are operated intermittently with an inlet temperature of 25°C

Figure 4.31 focusses on operating durations below 30 minutes, where the impacts of operating below the heat exchanger transit time can be seen more clearly. The findings in Section 4.4.2 established that when the u-tube is run for times shorter than its transit time of 381 s, it performs better than the coaxial. This is also seen here, but only for a duty cycle of 25%. When the duty cycle rises to 50% and 75%, the coaxial and u-tube outlet temperatures are very similar, with the coaxial temperature slightly lower. The effect of the coaxial transit time can also be seen when operating times exceed 883 s, with an increase in slope, most clearly shown in the 25% duty cycle curve. These results indicate that the benefits of operating the u-tube heat exchanger below the transit time are counteracted by shorter recovery times. This suggests that lateral heat transfer between the inlet and outlet flows is increased when

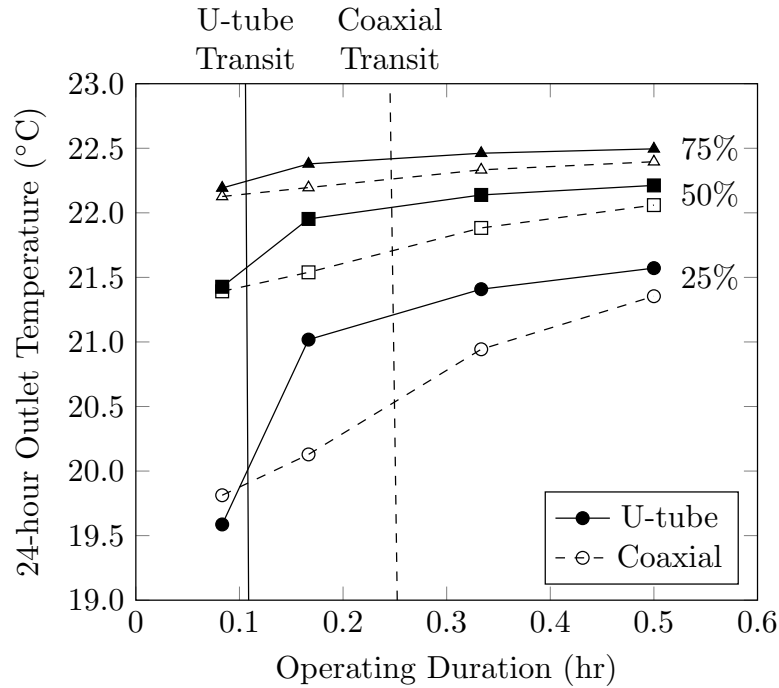


Figure 4.31: Outlet temperature after 24 hours of operation vs. operating durations for the u-tube and coaxial heat exchangers for duty cycles of 25%, 50%, and 75%, for durations below 0.5 hours. Heat exchangers are operated intermittently with an inlet temperature of 25°C

there is less time for heat to dissipate between operating periods.

The duty cycle summary plot can be non-dimensionalized, as shown in Figure 4.32. Here, the operating time is normalized according to the transit time, expressed as

$$\frac{ut_{dur}}{2H} = \frac{t_{dur}}{\tau_{transit}} \quad (4.4.3)$$

where u is the flow velocity (averaged for the coaxial case), t_{dur} is the operating duration, H is the borehole length, and $\tau_{transit}$ is the transit time. The non-dimensionalized

outlet temperature θ_{out} is defined as

$$\theta_{out} = \frac{T_{out} - T_{ground,\infty}}{T_{in} - T_{ground,\infty}} \quad (4.4.4)$$

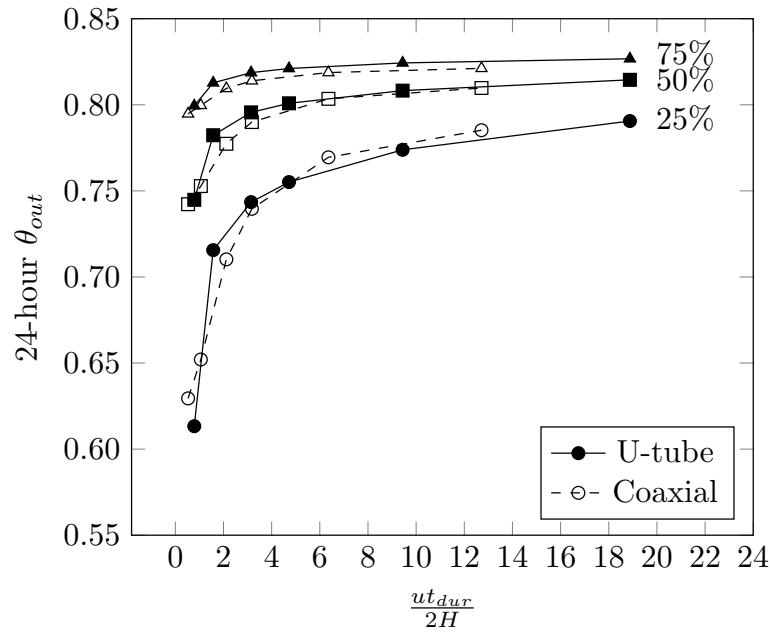


Figure 4.32: Non-dimensionalized outlet temperature after 24 hours of operation vs. operating duration for the u-tube and coaxial heat exchangers for duty cycles of 25%, 50%, and 75%. Heat exchangers are operated intermittently with an inlet temperature of 25°C

Figure 4.32 shows that the u-tube and coaxial results collapse when normalized with transit time. This strongly indicates that the differences in performance seen between the u-tube and coaxial heat exchangers under intermittent operation can be attributed to this factor. This agrees well with the findings in Section 4.4.3, which showed that the temperature recovery during non-operating times, which is dictated by the thermal mass of the system, had little bearing on differences in performance between the designs. The significance of this result is that if the u-tube and coaxial

heat exchangers shared the same flow conditions, their performance would be very similar. Since the coaxial design has a lower flow velocity in the outer annulus, and thus a higher transit time, it produces cooler outlet temperatures when operated at the same flow rate and for the same duration as the u-tube under most conditions.

The results can also be expressed in terms of heat exchanger effectiveness, as shown in Figure 4.33. The plot emphasizes that each heat exchanger is most effective when operating durations are low and recovery time is high. With reductions in the recovery time in the 50% and 75% cases, there is less variation in effectiveness over the range of operating times, indicating the benefits of lowering the operating time are counteracted when recovery is insufficient. Further, the significant drop in slope of each curve at a normalized time of 1 shows how operating below the transit time produces the greatest benefit to performance.

These findings demonstrate that the choice of heat exchanger design is more significant under intermittent operating conditions. This is relevant for applications of the heat exchangers that require short bursts of operation, such as ground source heat pumps used for building heating and cooling. In such applications, higher transit time heat exchangers with limited lateral heat exchange could result in improved performance.

4.5 Design Considerations for U-tube and Coaxial Heat Exchangers

The comparative study above consider a single u-tube and coaxial configuration for all tests. In this section, altering aspects of each heat exchanger design are explored.

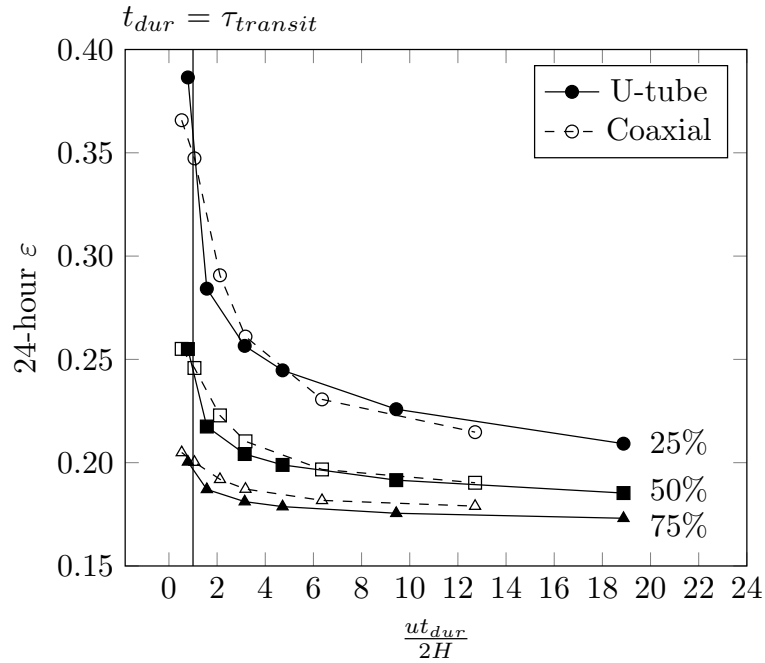


Figure 4.33: Effectiveness after 24 hours of operation vs. normalized operating duration for the u-tube and coaxial heat exchangers for duty cycles of 25%, 50%, and 75%. Heat exchangers are operated intermittently with an inlet temperature of 25°C

This includes enhancing the conductivity in the most thermally resistive components of the heat exchangers, and exploring the potential for borehole length reductions.

4.5.1 Thermal conductivity enhancement of high-resistance components

Numerical simulations were carried out to investigate the impacts of improving the u-tube and coaxial heat exchangers with higher conductivity materials. For each heat exchanger, the results from the continuous TRT simulations were used to identify the highest resistance components, the results of which are summarized in Table 4.5. Figure 4.34 shows the resistances in the borehole components. Thermal resistance was

Table 4.5: Resistance of each heat exchanger component from simulation results

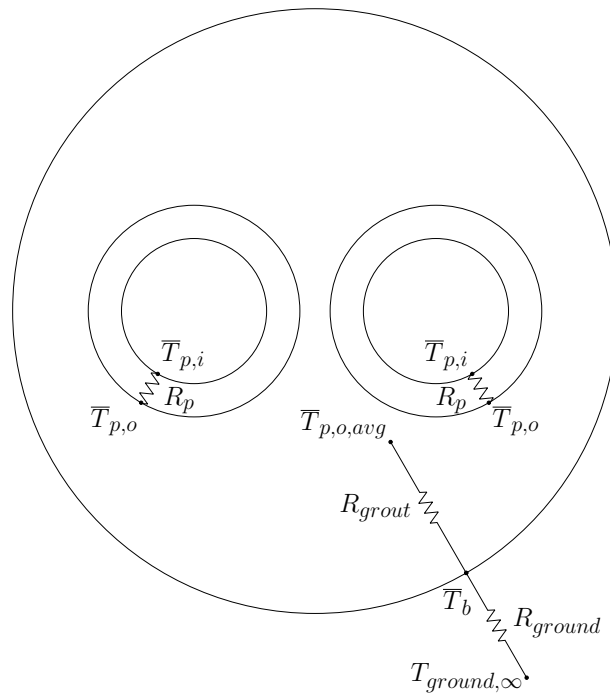
Component	U-tube [mK/W]	Coaxial [mK/W]
Inlet tube	4.39×10^{-2}	2.03×10^{-2}
Outlet tube	3.15×10^{-2}	4.92×10^{-2}
Grout	5.50×10^{-2}	2.13×10^{-2}
Ground	2.07×10^{-1}	2.08×10^{-1}

calculated from the simulation results by taking the average temperature at the inner and outer surface of each part. For instance, the tube resistances were calculated as

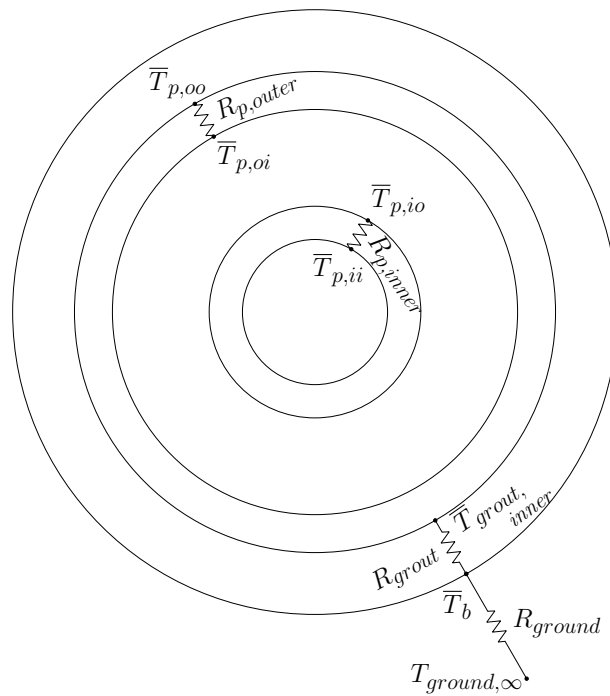
$$R_p = \frac{(\bar{T}_{p,i} - \bar{T}_{p,o})}{q'} \quad (4.5.1)$$

where $\bar{T}_{p,i}$ and $\bar{T}_{p,o}$ are the inner and outer average surface temperatures, respectively. For the u-tube grout, which has two inner surfaces, the average of both tube temperatures was taken as the inner temperature. The ground resistance was calculated by using the undisturbed ground resistance as the outer temperature, and results used to calculate the resistances were taken from the end of the 72-hour test.

From Table 4.5, it can be seen that the u-tube and coaxial designs each have different components that are responsible for the greatest thermal resistance in the borehole. In the u-tube heat exchanger, the greatest resistance is due to the grout, which occupies a large volume within the heat exchanger. Conversely, the component with the largest resistance in the coaxial heat exchanger is the outer tube. It should be noted that these findings are specific to the geometries selected for the heat exchangers in these tests. The table also shows that the ground resistance (taken at 72 hours) is an order of magnitude larger than the borehole component resistances. This emphasizes that borehole resistance often has less significant effect on performance when BHEs are operated continuously.



(a) U-tube



(b) Coaxial

Figure 4.34: Resistances for u-tube and coaxial heat exchangers (not to scale)

Table 4.6: Properties of steel coaxial outer pipe

Property	Symbol	Value
Density	ρ	7854 kg/m ³
Specific heat	c_p	434 J/kg K
Thermal conductivity	k	60.5 W/m K

As a consequence of these findings, the u-tube grout and coaxial outer tube were targeted to lower resistance in the heat exchangers. Higher conductivity alternatives were chosen for both components. In the coaxial design, the outer polyethylene tube was replaced with a steel pipe, a design choice that is sometimes discussed in the literature. The properties of steel used in this testing are detailed in Table 4.6. The bentonite grout in the u-tube was replaced with enhanced conductivity grout with a thermal conductivity of 3 W/mK, approximately three times the conductivity of standard bentonite grout [84].

Table 4.7: Performance of base and improved cases

Heat Exchanger Type	Steady Effectiveness [-]	Steady Borehole Resistance [mK/W]
Base u-tube	0.153	0.0966
Base coaxial	0.158	0.0847
Enhanced grout u-tube	0.165	0.0722
Steel outer pipe coaxial	0.187	0.0360

Each enhanced borehole design was simulated in a 72-hour test. The results of the simulation can be found in Table 4.7, compared alongside the base u-tube and coaxial configurations. The impact of design enhancements on effectiveness can also be seen in Figure 4.35. The findings show that the enhanced conductivity grout reduced the u-tube outlet temperature compared to the base case by 1.2°C to 23.5°C at the end of the test. This corresponds with an effectiveness of 0.165, 7.8% higher than the base u-tube configuration effectiveness. The higher conductivity grout reduced

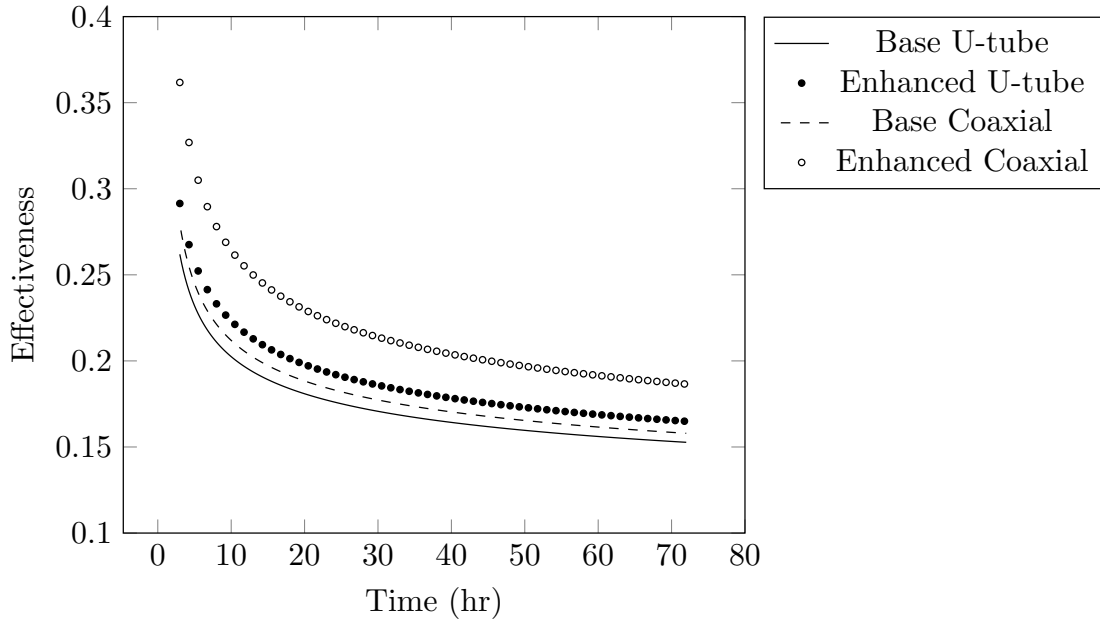


Figure 4.35: Effectiveness of u-tube heat exchanger with enhanced grout and coaxial heat exchanger with steel outer tube compared with base cases for each heat exchanger

the grout resistance by 46%, and lowered the u-tube borehole resistance by 25% to 0.0722 mK/W. The addition of the steel pipe to the coaxial design raised the effectiveness to 0.187, 18% greater than the coaxial base case. This can be attributed to the significantly improved borehole resistance of 0.036 mK/W, which is 57% lower than in the base coaxial case.

These findings indicate that borehole design choices can have an effect on performance, even when the heat exchangers are run continuously, but that there also is no definite favourable heat exchanger design when comparing the u-tube and coaxial. The results showed that enhancing the high resistance components can measurably improve performance during continuous operation, raising effectiveness in the u-tube

by 8% and by 22% in the coaxial, compared to their respective base cases. Additionally, the results showed that a u-tube with enhanced grout could have lower resistance and better effectiveness than the base coaxial design. Therefore, one cannot conclusively state that the coaxial heat exchangers always outperform the u-tube BHEs, but rather that the comparison in performance is heavily dependent upon the geometry and thermophysical properties of each heat exchanger.

4.5.2 Borehole length reductions

Borehole length reductions are often discussed in the literature as a potential benefit to using the coaxial BHE design. As such, 72-hour TRT simulations of the base and enhanced coaxial configurations were used to determine how much the borehole length could be reduced if a coaxial design was chosen. In these tests, the length of the coaxial heat exchanger was reduced until the outlet temperature matched that of the u-tube base configuration. In these simulations, the heat exchangers were subject to a constant heat injection rate of 9 kW.

The simulations showed that the coaxial base configuration could be shortened to 176 m, a 6.88 m or 3.8% reduction in length and perform as well as the u-tube at 72 hours of operation. This difference is quite small in comparison to some of the length reductions suggested in literature [21, 62], which range anywhere from 30 to 50%. It is important to note that the studies that predict such considerable length reductions, the simulations by Yavuzturk and Chiasson [21] and the experiments by Wang [62] use intermittent loading conditions. This likely contributed to the larger length reductions.

Testing the coaxial heat exchanger with the enhanced conductivity outer pipe, the

simulations showed that it was possible to reduce the length of the heat exchanger by 36.88 m, or 20%, while still maintaining similar performance to the u-tube at 72 hours. The coaxial heat exchanger modelled by Yavuzturk and Chiasson also contained a steel outer pipe, which may account for their larger predicted length reductions. These results lead to the conclusion that while some coaxial configurations can lead to larger length reductions, a coaxial heat exchanger with two polyethylene pipes will not be significantly shorter than a u-tube borehole.

It is important to predict length reduction using days-long tests, such as the 72-hour simulations used above. While it is clear from this study that the earlier performance of the u-tube and coaxial heat exchangers differs more, most systems that use BHEs, such as ground source heat pumps, must be sized according to their maximum load. For instance, GSHPs are designed to meet peak heating or cooling demand, when the heat pump may operate for many hours at a time. As such, the length reductions will be dictated by the performance on the scale of days, rather than minutes or hours. Thus, while the benefits of intermittent operation may not improve the borehole length, they can significantly enhance the efficiency of a geothermal system.

4.6 Assessment of Models for Multiple Thermally Interacting Boreholes

A significant advantage of the detailed numerical models developed for this study is their ability to predict heat exchanger performance over a vast range of time scales, from seconds to years. Grouping multiple boreholes together can have impacts on

the heat exchanger performance on the time scale of decades. While the comparative study of u-tube and coaxial heat exchangers relied upon early transient performance in particular, the modelling of multiple boreholes together requires long-term performance predictions.

Modelling multiple thermally interacting boreholes is of interest because many existing simplified models for borehole thermal response rely upon spatial superposition to account for the presence of more than one borehole in a field. This key assumption is difficult to test experimentally, since the bulk of the effects of the assumption are seen years into the operation of a typical heat exchanger. The numerical model developed in this study, however, is capable of testing multiple borehole heat exchangers over long periods of time without the use of the underlying superposition assumption. The objective of this study is to provide a comparison between the detailed OpenFOAM model, which simulates multiple boreholes simultaneously, with a superposition model. In this case, the Finite Line Source model was selected for comparison, since it accounts for end effects.

4.6.1 Multiple boreholes with a constant heat transfer boundary at the wall

This study considered a 2x2 borehole field with a constant heat transfer rate at the borehole wall equal to 50 W/m. The boreholes were spaced at a ratio of $B/H = 0.05$, which represents a close grouping of boreholes. Arranging the boreholes close together results in greater lateral heat transfer and, therefore, higher wall temperatures compared to more disperse borehole fields. The borehole radius to height ratio r_b/H was 0.0005. A constant temperature, equal to the initial temperature of the ground

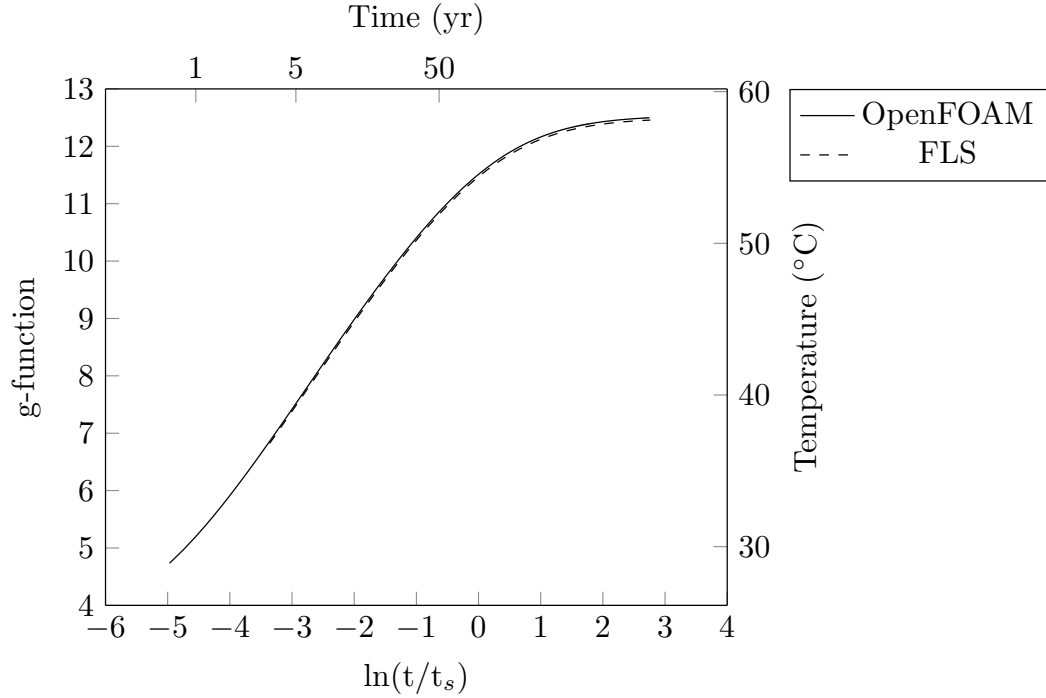


Figure 4.36: Constant heat transfer at the wall: comparison between a 2x2 borehole field modelled in OpenFOAM vs. FLS model of 2x2 boreholes using superposition for a case with a constant heat transfer rate at the borehole wall of 50 W/m

was selected for the surface boundary condition. This testing was compared to the FLS model, which applies the same boundary conditions. For this field geometry and boundary conditions, pygfunction [85] was used to generate the Finite Line Source prediction. The results of this comparison were presented as g-functions, shown in Figure 4.36. The g-function is defined as

$$g\left(\frac{t}{t_s}, \frac{r}{H}\right) = \frac{2\pi k}{q'} (T - T_{ground,\infty}) \quad (4.6.1)$$

where $r = r_b$ and $T = T_b$ for g-functions computed at the borehole wall. The borehole wall temperature T_b is determined by averaging the temperatures of all boreholes in

the field. The non-dimensional time t_s is defined as

$$t_s = \frac{H^2}{9\alpha_{ground}} \quad (4.6.2)$$

Figure 4.36 includes the non-dimensionalised g-function and time scales on the primary x - and y -axes. Additional dimensional values for time and temperature are included at the top and right of the figure. These dimensional values pertain to a particular borehole and ground conditions, specifically a ground diffusivity of $1.25 \times 10^{-6} \text{ m}^2 \text{ s}^{-1}$, a ground thermal conductivity of 2.1 W/mK , and a borehole depth of 183 m .

The plot shows near exact agreement between the FLS model and the borehole field simulated in OpenFOAM. This suggests that there is little difference between fully resolving the boreholes and using spatial superposition. This finding is specific to the borehole wall boundary condition selected for the test. The choice of a constant heat flux at the borehole wall means that the rate of heat transfer from the borehole will not change as a result of lateral heat transfer, resulting in a linear temperature response that can be accurately represented by superposition.

Figure 4.37 presents the OpenFOAM and FLS results for a 2×2 , 3×3 , and 4×4 borehole field arrangements as well as results for a single borehole. The additional borehole arrangements were modelled with boreholes of the same radius to height ratio, a spacing of $B/H=0.05$ where applicable, and with constant borehole heat fluxes. The findings show that the OpenFOAM models of the single borehole and 3×3 and 4×4 borehole fields also showed good agreement with the FLS model.

Figure 4.38 shows the radial g-functions for the single borehole and 2×2 borehole field cases modelled in OpenFOAM. The profiles are taken along a line that bisects

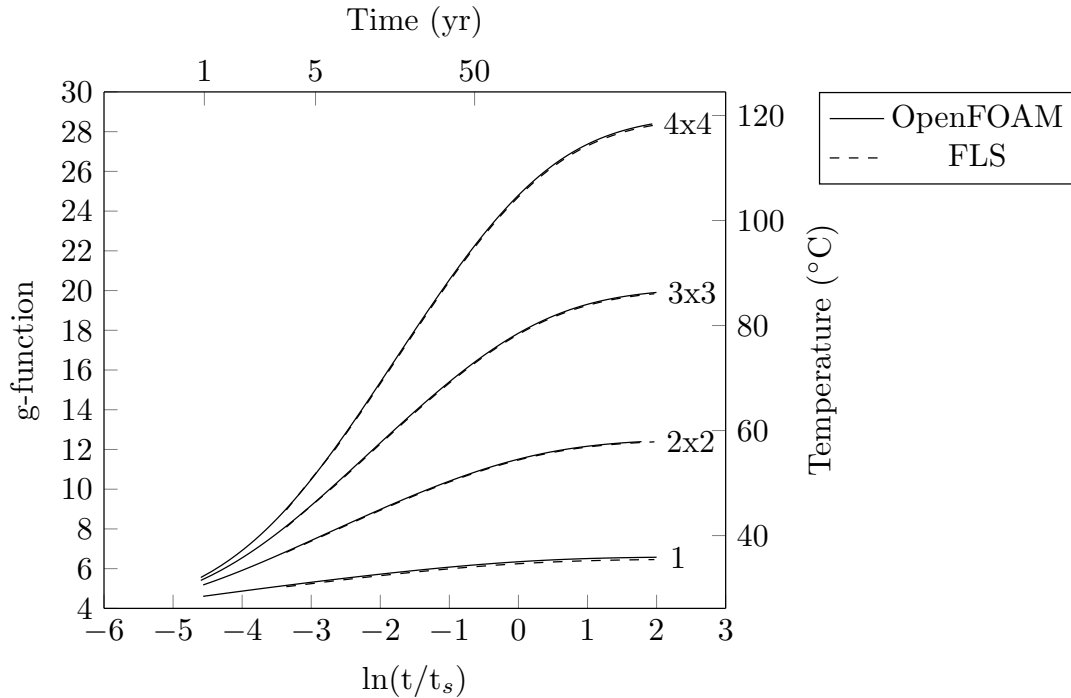


Figure 4.37: Constant heat transfer at the wall: comparison between boreholes modelled in OpenFOAM vs. FLS model for a single borehole, 2x2, 3x3, and 4x4 borehole fields, for cases with a constant heat transfer rate at the borehole wall of 50 W/m

all the boreholes in a single row of the field. The g-functions are taken at a variety of times, corresponding to $\ln(t/t_s) = -3, -2, -1, 0, 1,$ and 2 . The plots show how the ground temperature rises over time, as more thermal energy is added into the ground. There are clear differences between the single borehole and 2x2 case, with higher ground temperatures and a larger radius of temperature disturbance in the multiple borehole case. The axial variation in ground temperature is clearly demonstrated in both cases, with higher temperatures at the midpoint of the borehole and lower temperatures at the bottom. The results of the single borehole case indicate minimal temperature changes at a depth of $3H/2$, except for a small rise in temperature at

the longest time scale. Conversely, there is a more significant temperature rise in the ground below the multiple borehole field. The temperature disturbance at a height of $3H/2$ starts at $\ln(t/t_s) = 0$, which is equivalent to the characteristic time of the borehole.

4.6.2 Surface boundary condition

The choice of surface boundary condition is key in long-term simulations. In the days-long simulations described above, a zero heat flux condition was selected for the surface boundary condition, which matched well in the experimental validation cases. In analytical and simplified numerical models, the choice of surface boundary varies. In Eskilson's g-functions and FLS, a constant surface temperature boundary was chosen [9, 86]. Hellström employed a zero heat flux surface boundary in the DST model, since insulation is likely to be used at the surface in thermal storage fields [28].

Figure 4.39 shows a comparison between a case with a constant surface temperature and a surface with a zero heat flux condition for a 2x2 borehole field with a spacing of $B/H=0.05$, both modelled in OpenFOAM. In the constant temperature case, the surface temperature is set equal to the initial ground temperature. The figure clearly demonstrates the long-term differences between the surface boundary conditions. While the two cases exhibit similar behaviour early on in the test, they diverge starting at $\ln(t/t_s) \approx -3$. This corresponds to a time of 4.7 years for a 183 m deep borehole with the same ground thermal properties used throughout this study. As the test progresses beyond this point, the insulated surface g-function rises much faster than the constant surface case, resulting in higher temperatures at the borehole wall. For the same hypothetical borehole with a borehole wall heat transfer rate of

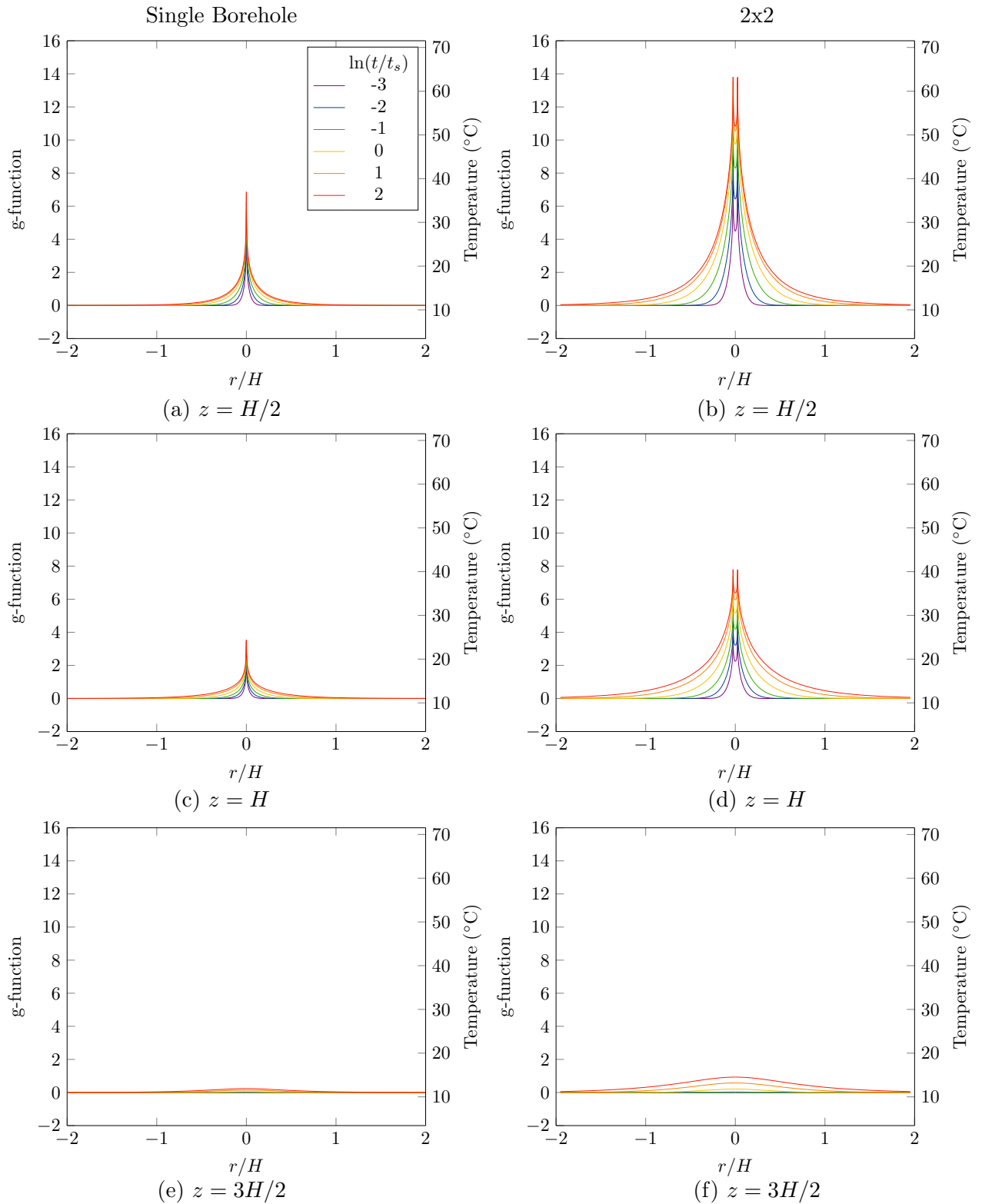


Figure 4.38: Radial g-functions of a single borehole and a 2x2 borehole field at depths of $z = H/2, H$, and $3H/2$ for a case with a constant heat transfer rate of 50 W/m, modelled in OpenFOAM

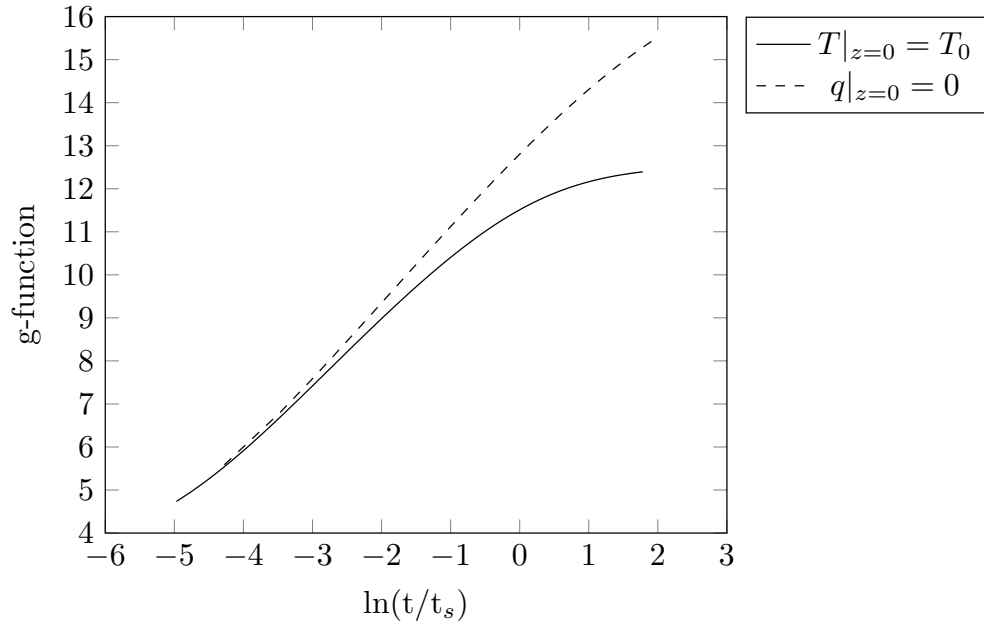


Figure 4.39: g -functions for constant surface temperature and zero surface heat flux boundaries, 2x2 borehole field, $r_b/H = 0.0005$, $B/H = 0.05$, each with a heat transfer rate at the borehole wall of 50 W/m

50 W/m, this represents a difference of 2.2°C in the borehole wall temperature at 25 years and 3.4°C at 50 years. This finding is significant because a time range of 5 to 50 years is within the expected lifetime of ground source heat pump and geothermal storage systems. This result is expected, since more thermal energy would be retained in an insulated case; however, it highlights the importance of selecting a simplified model with a boundary condition that accurately represents the surface conditions being considered.

Chapter 5

Summary and Conclusions

5.1 Summary

In this thesis, borehole heat exchanger performance for two prevalent heat exchanger designs was investigated. This was accomplished by developing numerical models for u-tube and coaxial heat exchangers, which enabled study of both the short- and long-term heat transfer performance of the BHEs. These high-fidelity multi-region conjugate heat transfer models developed in OpenFOAM used the finite volume method to solve the heat transfer equations for each component in the heat exchanger, including the conduction equation in the solid elements and 1D convection in the working fluid. The conjugate nature of the heat transfer was incorporated with a segregated solution algorithm, devised to iteratively solve the governing equations in each component domain while maintaining conservation. A custom multifaceted 1D mesh was developed to provide the correct surface and cross-sectional areas for circular pipes.

This study showed that the u-tube and coaxial heat exchangers exhibited marginal differences in performance when operated continuously for 72 hours. While previous

research had suggested a performance advantage for the coaxial design, the results of the numerical simulations indicated that the coaxial outlet temperature was 0.54°C lower than the u-tube after constant heat injection, corresponding to a difference in effectiveness of 3.3%. Analysis of the transient changes in the resistance of the borehole heat exchanger systems demonstrated that the resistance of the ground rises continually when subject to constant heat exchange while borehole resistance becomes steady within the first few hours of operation. Therefore, when a heat exchanger is operated continuously for long periods of time (greater than a few hours), the ground resistance is the dominant term influencing total BHE system resistance and is more significant than the difference in resistance between the u-tube and coaxial heat exchangers.

In contrast, there were greater differences observed between the two heat exchanger designs earlier on in the simulations, which indicated the potential for a larger dissimilarity in performance during intermittent operation. The intermittent study considered three key operating parameters: operating time, recovery time, and duty cycle. Testing of the u-tube and coaxial heat exchangers demonstrated a benefit to operating intermittently and pointed to further complexities in the performance differences between the two heat exchanger designs. In particular, the study showed that the differences in performance between the designs varied significantly with operating time. Intermittent performance benefits for the coaxial design ranged from 3.3% to 12.9%, unless the operating time was below the u-tube transit time, in which case the u-tube outperformed the coaxial heat exchanger by 9.6%. This led to the discovery that the heat exchanger transit time is critical to intermittent performance. Below the transit time, fluid that entered the heat exchanger at the beginning of an

intermittent cycle does not have enough time to reach the outlet, thus limiting the amount of heating of the solid components near the outlet. The results also showed that the heat exchanger design played a role in the magnitude of the transit time benefit, since heat exchangers with a higher level of internal interaction between inlet and outlet flows, such as the coaxial design, will experience more warming at the outlet during times below the transit time. The u-tube and coaxial models were validated using experimental data.

The intermittent study also involved an investigation of the duty cycle, the ratio between operating and recovery time. The findings showed that performance was improved when both the duty cycle and operating times were low, meaning that short operating periods were accompanied by relatively longer recovery times. The benefits of short operating times were significantly reduced when duty cycle was increased ($\epsilon_{24-hour} = 0.39$ for a duty cycle of 25% vs. $\epsilon_{24-hour} = 0.26$ for a 75% duty cycle, for a u-tube with a five-minute operating time), and the benefits of a lower duty cycle were mitigated by increasing the operating time ($\epsilon_{24-hour} = 0.21$ for a u-tube with an operating time of 2 hours and a 25% duty cycle). Critically, the duty cycle study included a non-dimensional analysis of the performance versus operating time curves. This analysis showed that when operating time is non-dimensionalized according to transit time, the performance of the u-tube and coaxial heat exchangers converge. This leads to the conclusion that the differences in performance for the heat exchangers during intermittent operation can be attributed specifically to differences in flow inside the heat exchangers.

The development of high-fidelity numerical models also enabled the investigation

of a variety of factors influencing both short- and long-term performance. In particular, the detailed models made it possible to identify the components that most limited heat exchange in each BHE design. This information was used to quantify the performance benefits associated with proposed design improvements discussed in Section 4.5. Further, the long term behaviour of borehole heat exchangers was explored in a study of thermally interacting boreholes and surface boundary conditions. The findings showed that superposition accurately captures the behaviour of thermally interacting boreholes when there is a fixed heat transfer rate at the wall. Additionally, it was shown that the choice of surface boundary condition can considerably impact long-term performance.

5.2 Conclusions

This thesis provides the first comparison of u-tube and coaxial heat exchangers that clearly describes the underlying physics behind the differences in performance between the two designs. This assessment involved the development of a detailed experimentally validated conjugate heat transfer numerical model, which was applied to test the heat exchangers under a broad range of continuous and intermittent loading conditions. The following are the major conclusions from this research.

5.2.1 Continuous Operation

- The u-tube and coaxial heat exchanger designs showed marginal differences in performance ($\Delta T = 0.54^\circ\text{C}$, $\Delta \varepsilon = 3.3\%$) when operated continuously with constant heat injection for 72 hours

- Differences between the two heat exchanger designs peaked very early in operation, at 15 minutes of operation in the continuous heat injection case considered ($\Delta\varepsilon = 17\%$)
- Effectiveness can be used in lieu of heat transfer rate to measure borehole heat exchanger performance, for instance when q is controlled and therefore cannot be compared using heat transfer rate as a metric
- The numerical model made steady borehole resistance predictions in line with the multipole method described by Hellström [28], with a maximum difference of 6.6% between the study simulations and the analytical model
- Borehole resistances became steady (reaching 95% of its resistance at 72 hours) after 4 hours for the u-tube and 4.5 hours for the coaxial, when operated with a constant inlet heat transfer rate, agreeing well with the criterion for borehole steadiness proposed by Eskilson [9]
- The time to steady state was shown to be dependent on inlet condition, with constant inlet temperature cases becoming steady sooner (1.5 hours for both heat exchanger designs)
- The most significant differences between u-tube and coaxial borehole resistances occurred at the beginning of the test due to both the transit time and thermal mass effects within the boreholes before they reached steady state
- Borehole resistances have the most significant impact on the overall system resistance early on in the test, before the ground resistance significantly exceeds

borehole resistances, and while the early transient changes in borehole heat transfer occur

- Ground resistance rises continually while subject to heat exchange, causing it to be the most important influence on performance when borehole heat exchangers are operated continuously and leading the borehole resistances to be less critical to long-term performance

5.2.2 Intermittent Operation

- Reducing the operating duration when operating heat exchangers intermittently improves the heat transfer rates of both u-tube and coaxial heat exchangers
- Operating a BHE below the transit time results in cooler temperatures at the outlet, because the warm fluid that entered the heat exchanger does not have the opportunity to reach the outlet and warm the surrounding components
- At times that are larger than both heat exchangers' transit times, reducing the operating duration increases the difference between the coaxial and u-tube heat transfer rates, with the coaxial performing better (a 3.7% difference in the continuously operated case compared with a 12.9% difference in the 1/2 hour case)
- Operating the u-tube below its transit time results in a significant performance benefit for the u-tube due to its limited internal thermal interaction, with a heat transfer rate 9.6% greater than the coaxial design for a 5 minute operating duration

- At an operating time below the coaxial transit time but above the u-tube transit time, there is no significant advantage to the coaxial heat exchanger over the u-tube design (with only 3.3% greater heat exchange in the coaxial design) because the coaxial heat exchanger experiences more significant internal thermal interaction across its inner pipe
- Increasing the intermittent recovery time improves the heat transfer rates of both the u-tube and coaxial heat exchangers
- When operating durations are equivalent, the largest difference in temperature between the heat exchangers occurs at the end of the recovery period, with very little difference between the average and maximum cycle temperatures, indicating that recovery time had a similar effect on both designs' performances
- The heat exchangers' performance was better with the shortest operating durations combined with the lowest duty cycle of 25%
- Raising the duty cycle (reducing relative recovery time) raises the outlet temperature and reduces performance
- Increasing the operating duration reduces borehole heat exchanger performance
- With the exception of the operating duration below the the u-tube transit time, the coaxial heat exchanger significantly outperforms the u-tube when operated for shorter operating times (less than 1/2 hour in these tests) at the lowest duty cycle
- Raising the duty cycle reduces the difference between the u-tube and coaxial performance

- Increasing the operating time also reduces the difference between the u-tube and coaxial performance
- Non-dimensionalizing the operating time by the transit time causes the u-tube and coaxial outlet temperature vs. operating time curves to collapse, proving that the differences in performance between the the designs are due to the flow effects and not due to differences in thermal mass

5.2.3 Design considerations

- Enhancing the conductivity of the highest resistance components can significantly improve heat exchanger performance. Specifically, adding a steel outer pipe in the coaxial improved effectiveness by 18%, while using enhanced conductivity grout in the u-tube increased effectiveness by 8%.
- Employing enhanced conductivity grout in the u-tube resulted in an resistance lower than the coaxial base case, indicating that the coaxial resistance is not guaranteed to be lower than the u-tube
- The base coaxial design did not lead to significant length reductions, with results indicating that the coaxial length could be 3.8% shorter than u-tube to maintain the same performance as the u-tube at 72 hours
- More significant length reductions are possible with the steel outer pipe coaxial design, where length can be shortened by 20% compared to the base u-tube design while maintaining the same performance at 72 hours

5.2.4 Multiple thermally interacting boreholes

- Modelling multiple boreholes simultaneously with a fixed heat flux at the borehole predicts a g-function curve that closely matches the FLS model using superposition for several borehole field configurations
- Employing a zero heat flux surface boundary results in significantly higher long term temperatures compared a fixed surface temperature

5.3 Original Contributions

5.3.1 Systematic comparison of u-tube and coaxial borehole heat exchangers under continuous loading

- This study represents the first conclusive assessment of the differences in u-tube and coaxial heat exchanger performance
- A novel resistance-based analysis methodology that enables the comparison of heat exchangers is introduced
- It is established that the greatest differences in heat exchanger performance between u-tube and coaxial heat exchangers occur early in operation, within the first 15 minutes for the case considered in this study

5.3.2 Framework for assessing borehole heat exchanger performance during intermittent operation

- Established that operating and recovery time are key parameters that govern performance of BHEs and that the fixed ratio of both terms, duty cycle, is an important predictor of heat exchanger performance
- Identified that borehole heat exchanger transit time is a key time scale that determines intermittent performance, below which heating of the outlet is greatly reduced
- Further, identified that the design-specific thermal interaction between inlet and outlet flows is a mitigating factor for sub-transit-time performance benefits
- Conclusively demonstrated that the differences in performance between the u-tube and coaxial heat exchangers collapse when operating time is non-dimensionalized according to transit time

5.4 Future Work

While this thesis has answered many key questions about borehole heat exchanger design and performance, other unknowns remain. The following are suggestions for future work that builds upon this body of research:

1. This research could be extended to several other heat exchanger designs, such as double u-tube and helical borehole heat exchangers. The modelling strategy described in this thesis would make it possible to establish short- and long-time scale heat transfer performance in a wide variety of heat exchanger designs.

This approach could be used to investigate the borehole heat exchangers' performance under continuous and intermittent loading conditions.

2. Building upon the use of effectiveness as a measure of heat exchanger performance in this study, further work is needed to demonstrate the relationship between flow rate and effectiveness in borehole heat exchangers. A study of borehole heat exchangers under a variety of flow rates would help clarify when effectiveness is useful as a measure of performance.
3. The findings from the intermittent portion of this study should be expanded upon to consider the effect on the coefficient performance of heat pumps. An understanding of the impact on COP could be used to inform a cost/benefit analysis for intermittently operating GSHPs.
4. Further work is needed to understand the implications of intermittent operation in borehole strings. Connecting borehole heat exchangers in series would serve to extend the transit time. Additionally, each individual borehole in the string is separate from the others, which may reduce the mitigating effects of internal thermal interaction for sufficiently small operating periods. As such, a study of borehole strings under intermittent operation could uncover greater performance benefits.
5. Based on the findings of this thesis pertaining to intermittent operation, further work is needed to develop application-specific control strategies for geothermal systems such as ground source heat pumps and geothermal storage. This work could include additional modelling to account for the effects of the application on inlet conditions, such as the introduction of a heat pump model.

Bibliography

- [1] Natural Resources Canada. Energy efficiency trends in Canada 1990 to 2013. <https://www.nrcan.gc.ca/energy/publications/19030>, 2016.
- [2] Statistics Canada. Household and the environment: Energy use. <http://www.statcan.gc.ca/pub/11-526-s/11-526-s2013002-eng.pdf>, 2013.
- [3] Natural Resources Canada. Heating and cooling with a heat pump. <https://natural-resources.canada.ca/energy-efficiency/energy-star-canada/about/energy-star-announcements/publications/heating-and-cooling-heat-pump/6817#b>, 2022.
- [4] U.S. Department of Energy. Heat pump systems. <https://www.energy.gov/energysaver/heat-pump-systems>.
- [5] S. Nadel and C. Kallakuri. Opportunities for energy and economic savings by replacing electric resistance heat with higher-efficiency heat pumps. Technical report, American Council for an Energy-Efficient Economy (ACEEE), 2016.
- [6] Manitoba Hydro. Geothermal system components. https://www.hydro.mb.ca/your_home/geothermal_heat_pumps/components/.

- [7] B. Asgari, M. Habibi, and A. Hakkaki-Fard. Assessment and comparison of different arrangements of horizontal ground heat exchangers for high energy required applications. *Applied Thermal Engineering*, 167, 2020.
- [8] K. S. Lee. Borehole thermal energy storage. In *Underground Thermal Energy Storage*, pages 95–123. Springer, 2013.
- [9] P. Eskilson. *Thermal Analysis of Heat Extraction Boreholes*. PhD thesis, University of Lund, 1987.
- [10] A. Walch, N. Mohajeri, A. Gudmundsson, and Jean-L. Scartezzini. Quantifying the technical geothermal potential from shallow borehole heat exchangers at regional scale. *Renewable Energy*, 165:369–380, 2021.
- [11] Aalborg CSP. Pit thermal energy storage (PTES). <https://www.aalborgcsp.com/business-areas/thermal-energy-storage-tes/pit-thermal-energy-storage-ptes>.
- [12] Wikimedia Commons, KVDP. HeatAndColdStorageWithHeatPump. <https://commons.wikimedia.org/wiki/File:HeatAndColdStorageWithHeatPump.svg>.
- [13] A. Kallesøe, T. Vangkilde-Pedersen, J. Nielsen, G. Bakema, P. Egermann, C. Maragna, F. Hahn, L. Guglielmetti, and Koornneef J. HEATSTORE - Underground Thermal Energy Storage (UTES) - State of the Art, Example Cases and Lessons Learned. In *World Geothermal Congress*, 2021.
- [14] Natural Resources Canada. Borehole thermal energy storage (BTES). <http://www.dlsc.ca/borehole.htm>.

- [15] P. Kandiah and M. F. Lightstone. Modelling of the thermal performance of a borehole field containing a large buried tank. *Geothermics*, 60:94–104, 2016.
- [16] H. S. Carslaw and J. C. Jaeger. *Conduction of Heat in Solids*. Oxford University Press, 2nd edition, 1959.
- [17] L. R. Ingersoll, O. J. Zobel, and A. C. Ingersoll. *Heat Conduction With Engineering and Geological Applications*. McGraw-Hill, New York, 2nd edition, 1954.
- [18] H. Y. Zeng, N. R. Diao, and Z. H. Fang. A finite line-source model for boreholes in geothermal heat exchangers. *Heat Transfer - Asian Research*, 31(7):558–567, 2002.
- [19] L. Lamarche and B. Beauchamp. A new contribution to the finite line-source model for geothermal boreholes. *Energy and Buildings*, 39:188–198, 2007.
- [20] J. Claesson and S. Javed. An analytical method to calculate borehole fluid temperatures for time-scales from minutes to decades. *ASHRAE Transactions*, 117:279–288, 2011.
- [21] C. Yavuzturk and J. D. Spitler. A short time step response factor model for vertical ground loop heat exchangers. *ASHRAE Transactions*, 105(2):475–485, 1999.
- [22] M. Cimmino and M. Bernier. A semi-analytical method to generate g-functions for geothermal bore fields. *International Journal of Heat and Mass Transfer*, 70:641–650, 2014.

- [23] P. Bayer, M. de Paly, and M. Beck. Strategic optimization of borehole heat exchanger field for seasonal geothermal heating and cooling. *Applied Energy*, 136:445–453, Dec. 2014.
- [24] B. Dusseault, P. Pasquier, and D. Marcotte. A block matrix formulation for efficient g-function construction. *Renewable Energy*, 121:249–260, 2018.
- [25] T. Blomber, J. Claesson, P. Eskilson, G. Hellström, and B Sanner. EED - Earth Energy Designer. <http://www.buildingphysics.com/index-filer/Page1099.htm>.
- [26] J. D. Spitler. GLHEPro. <https://hvac.okstate.edu/glhepro/overview>, 2014.
- [27] Thermal Dynamics Inc. Gld: Ground loop design. <https://www.groundloopdesign.com/>.
- [28] G. Hellström. *Ground heat storage: Thermal analyses of duct storage systems*. PhD thesis, Lund University, 1991.
- [29] TRNSYS: Transient Simulation Tool. <https://www.trnsys.com>.
- [30] D. Pahud, A. Fromentin, and J. C. Hadorn. The duct ground heat storage model (DST) for TRNSYS used for the simulation of heat exchanger piles. Technical Report December, DGC-LASEN, École Polytechnique Fédérale de Lausanne, 1996.
- [31] B. Sibbitt, D. McClenahan, R. Djebbar, J. Thornton, B. Wong, J. Carriere, and J. Kokko. The performance of a high solar fraction seasonal storage district heating system - Five years of operation. *Energy Procedia*, 30:856–865, 2012.

- [32] N. D. Paul. *The effect of grout thermal conductivity on vertical geothermal heat exchanger design and performance*. PhD thesis, Mechanical Engineering Department, South Dakota State University, 1996.
- [33] J. Bennet, J. Claesson, and G. Hellström. *Multipole method to compute the conductive heat flows to and between pipes in a composite cylinder*. Husbyggnadsteknik, Tekniska högsk., 1987.
- [34] Y. Gu and D. L. O’Neal. Development of an equivalent diameter expression for vertical u-tubes used in ground-coupled heat pumps. *ASHRAE Transactions*, 104(2):347–355, 1998.
- [35] S. P. Kavanaugh. *Simulation and Experimental Verification of Vertical Ground-Coupled Heat Pump Systems (Closed Loop)*. PhD thesis, Oklahoma State University, 1985.
- [36] L. Lamarche, S. Kajl, and B. Beauchamp. A review of methods to evaluate borehole thermal resistances in geothermal heat-pump systems. *Geothermics*, 39(2):187–200, 2010.
- [37] M. He. *Numerical modelling of geothermal borehole heat exchanger systems*. PhD thesis, De Montfort University, 2012.
- [38] Y. Çengel and A. J. Ghajar. *Heat and Mass Transfer: Fundamentals and Applications*. New York: McGraw-Hill Higher Education, 4th edition, 2011.
- [39] D. Bauer, W. Heidemann, H. Müller-Steinhagen, and H.-J. G. Diersch. Modelling and simulation of groundwater influence on borehole thermal energy stores. In *EFFSTOCK*, 2009.

- [40] S. Javed and J. Claesson. New analytical and numerical solutions for the short-term analysis of vertical ground heat exchangers. *ASHRAE Transactions*, 117(1):3–12, 2011.
- [41] M. Philippe, M. Bernier, and D. Marchio. Validity ranges of three analytical solutions to heat transfer in the vicinity of single boreholes. *Geothermics*, 38:407–413, 2009.
- [42] L. Lamarche and B. Beauchamp. New solutions for the short-time analysis of geothermal vertical boreholes. *International Journal of Heat and Mass Transfer*, 50(7-8):1408–1419, 2007.
- [43] C. Yavuzturk and A. Chiasson. Performance analysis of u-tube, concentric tube, and standing column well ground heat exchangers using a system simulation approach. In *ASHRAE Transactions*, pages 925–938, 2002.
- [44] S. Li, W. Yang, and X. Zhang. Soil temperature distribution around a U-tube heat exchanger in a multi-function ground source heat pump system. *Applied Thermal Engineering*, 29(17):3679–3686, 2009.
- [45] S. Koochi-Fayegh and M. A. Rosen. An analytical approach to evaluating the effect of thermal interaction of geothermal heat exchangers on ground heat pump efficiency. *Energy Conversion and Management*, 78:184–192, 2014.
- [46] T. Başer, N. Lu, and J. S. McCartney. Operational response of a soil-borehole thermal energy storage system. *Journal of Geotechnical and Geoenvironmental Engineering*, 142(4):1–12, 2016.

- [47] B. Bouhacina, R. Saim, and H. F. Oztop. Numerical investigation of a novel tube design for the geothermal borehole heat exchanger. *Applied Thermal Engineering*, 79:153–162, 2015.
- [48] S. Chen, J. Mao, and X. Han. Heat transfer analysis of a vertical ground heat exchanger using numerical simulation and multiple regression model. *Energy and Buildings*, 129, 2016.
- [49] J. Chen, L. Xia, B. Li, and D. Mmereki. Simulation and experimental analysis of optimal buried depth of the vertical u-tube ground heat exchanger for a ground-coupled heat pump system. *Renewable Energy*, 73:46–54, 2015.
- [50] A. Moradi, K. M. Smits, N. Lu, and J. S. McCartney. Heat transfer in unsaturated soil with application to borehole thermal energy storage. *Vadose Zone Journal*, 15(10):1–17, 2016.
- [51] R. Zhang, N. Lu, and Y. Wu. Efficiency of a community-scale borehole thermal energy storage technique for solar thermal energy. In *GeoCongress 2012*, pages 4386–4395, 2012.
- [52] N. Catolico, S. Ge, and J. S. McCartney. Numerical modeling of a soil-borehole thermal energy storage system. *Vadose Zone Journal*, 15(1):1–17, 2016.
- [53] TOUGH2 Software. <http://eesatough.lbl.gov/software/tough2.html>.
- [54] R. Al-Khoury, P. G. Bonnier, and R. B. J. Brinkgreve. Efficient finite element formulation for geothermal heating systems. Part I: Steady state. *International Journal for Numerical Methods in Engineering*, 63(7):988–1013, 2005.

- [55] R. Al-Khoury and P. G. Bonnier. Efficient finite element formulation for geothermal heating systems. Part II: Transient. *International Journal for Numerical Methods in Engineering*, 67(5):725–745, 2006.
- [56] J. Wołoszyn and A. Gołaś. Modelling of a borehole heat exchanger using a finite element with multiple degrees of freedom. *Geothermics*, 47:13–26, 2013.
- [57] J. Wołoszyn. Global sensitivity analysis of borehole thermal energy storage efficiency on the heat exchanger arrangement. *Energy Conversion and Management*, 166:106–119, 2018.
- [58] S. J. Rees and M. He. A three-dimensional numerical model of borehole heat exchanger heat transfer and fluid flow. *Geothermics*, 46:1–13, 2013.
- [59] A. Zarrella, A. Capozza, and M. De Carli. Performance analysis of short helical borehole heat exchangers via integrated modelling of a borefield and a heat pump: A case study. *Applied Thermal Engineering*, 61(2):36–47, 2013.
- [60] J. Acuña and B. Palm. First Experiences with Coaxial Borehole Heat Exchangers. *IIR Conference on Sources/Sinks*, 2:59–66, 2011.
- [61] R. A. Beier, J. Acuña, P. Mogensen, and B. Palm. Transient heat transfer in a coaxial borehole heat exchanger. *Geothermics*, 51:470–482, 2014.
- [62] J. Wang. Comparative heat transfer efficiency study of coaxial and u-loop boreholes. *GSTF International Journal of Engineering Technology*, 2(3):14–20, 2014.
- [63] C. J. Wood, H. Liu, and S. B. Riffat. Comparative performance of ‘u-tube’ and ‘coaxial’ loop designs for use with a ground source heat pump. *Applied Thermal Engineering*, 37:190–195, May 2012.

- [64] T. Sliwa and M. A. Rosen. Efficiency analysis of borehole heat exchangers as grout varies via thermal response test simulations. *Geothermics*, 69:132–138, 2017.
- [65] J. Desmedt, J. Van Bael, H. Hoes, and N. Robeyn. Experimental performance of borehole heat exchangers and grouting materials for ground source heat pumps. *International Journal of Energy Research*, 36(13):1238–1246, Oct 2012.
- [66] D. Quaggiotto, A. Zarrella, G. Emmi, M. De Carli, L. Pockel, J. Vercruysse, M. Psyk, D. Righini, A. Galgaro, D. Mendrinis, and A. Bernardi. Behavior of coaxial and double u-tube borehole heat exchangers. *Energies*, 12, 2019.
- [67] J. Jalaluddin and A. Miyara. Thermal performance investigation of several types of vertical ground heat exchangers with different operation mode. *Applied Thermal Engineering*, 33-34:167–174, 2012.
- [68] C. Li, J. Mao, Z. Xing, J. Zhou, and Y. Li. Analysis of geo-temperature restoration performance under intermittent operation of borehole heat exchanger fields. *Sustainability (Switzerland)*, 8(1):1–14, 2016.
- [69] X. Cao, Y. Yuan, L. Sun, B. Lei, N. Yu, and X. Yang. Restoration performance of vertical ground heat exchanger with various intermittent ratios. *Geothermics*, 54:115–121, 2015.
- [70] S. H. Baek, M. S. Yeo, and K. W. Kim. Effects of the geothermal load on the ground temperature recovery in a ground heat exchanger. *Energy & Buildings*, 136:63–72, 2017.
- [71] The OpenFOAM Foundation. OpenFOAM v.4.1. openfoam.org.

- [72] OpenCFD. Mesh description. <https://www.openfoam.com/documentation/user-guide/4-mesh-generation-and-conversion/4.1-mesh-description>.
- [73] Marco Fossa. The temperature penalty approach to the design of borehole heat exchangers for heat pump applications. *Energy & Buildings*, 43(6):1473–1479, 2011.
- [74] S. Lanini, F. Delaleux, X. Py, R. Olivès, and D. Nguyen. Improvement of borehole thermal energy storage design based on experimental and modelling results. *Energy and Buildings*, 77:393–400, 2014.
- [75] P. J. Pritchard and J. W. Mitchell. *Fox and McDonald’s Introduction to Fluid Mechanics*, chapter 6. Wiley, 9 edition, 2016.
- [76] V. Gnielinski. New equations for heat and mass transfer in turbulent pipe and channel flow. *International Chem. Eng.*, 16(2):359–368, 1976.
- [77] G. K. Filonenko. Hydraulic drag in pipes. *Teploenergetika*, 1(4):40–44, 1954.
- [78] Y. A. Cengel and A. Ghajar. *Heat and Mass Transfer (Fundamentals and Applications)*. McGraw-Hill Education, 4th edition, 2011.
- [79] V. Gnielinski. G2 Heat transfer in concentric annular and parallel plate ducts. In *VDI Heat Atlas*. Springer, 2010.
- [80] A. S. Foust and G. A. Christian. Non-boiling heat transfer coefficients in annuli. *Am. Inst. Chem. Eng*, 36:54, 1940.
- [81] W. M. Kays and H. C. Perkins. In W. M. Rohsenow and J. P. Hartnett, editors, *Handbook of Heat Transfer*, chapter 7. McGraw-Hill Publisher, New York, 1972.

- [82] S. Javed and P. Fahle. Thermal response testing of a multiple borehole ground heat exchanger. *International Journal of Low-Carbon Technologies*, 6(2):141–148, 2011.
- [83] A. Zarrella, M. Scarpa, and M. De Carli. Short time-step performances of coaxial and double u-tube borehole heat exchangers: Modeling and measurements. *HVAC and R Research*, 17(6):959–976, 2011.
- [84] D. Kim and S. Oh. Optimizing the design of a vertical ground heat exchanger: Measurement of the thermal properties of bentonite-based grout and numerical analysis. *Sustainability*, 10(8), 2018.
- [85] M. Cimmino, D. Thorne, C. D. Langevin, and M. C. Sukop. Pygfunction: an open-source toolbox for the evaluation of thermal response factors for geothermal borehole fields. In *Proceedings of eSim 2018*, 2018.
- [86] M. Cimmino, M. Bernier, and F. Adams. A contribution towards the determination of g-functions using the finite line source. *Applied Thermal Engineering*, 51(1-2):401–412, 2013.

Appendix A

Input data file used for test case set up

A.1 Input file for a u-tube type heat exchanger

```
%%%%%%%%%%%%%%%%%%%%%%%%%%%%%%%%%%%%%%%%%%%%%%%%%%%%%%%%%%%%%%%%%%%%%%%% INPUT FILE %%%%%%%%%%%%%%%%%%%%%%%%%%%%%%%%%%%%%%%%%%%%%%%%%%%%%%%%%%%%%%%%%%%%%%%%%  
  
Borehole Type (utube)  
  
# Runtime [s]  
time = 259200  
  
%%%%%%%%%%%%%%%%%%%%%%%%%%%%%%%%%%%%%%%%%%%%%%%%%%%%%%%%%%%%%%%%%%%%%%%% GEOMETRY %%%%%%%%%%%%%%%%%%%%%%%%%%%%%%%%%%%%%%%%%%%%%%%%%%%%%%%%%%%%%%%%%%%%%%%%%  
  
# Borehole diameter [m]  
bh_d = 0.10795  
# Borehole length [m]  
bh_l = 182.88  
# Domain size (single borehole) [m]  
soil_d = 6  
  
# U TUBE
```

```
# Tube outer diameter [m]
tube_od = 0.042164
# Tube thickness [m]
tube_thk = 0.004064
# Tube centre to centre spacing [m]
tube_cl2cl = 0.046863

%%%%%%%%%%%%%%%%%%%%%%%%%%%%%%%%%%%%%%%%%%%%%%%%%%%%%%%%%%%%%%%%%%%%%%%% MESH %%%%%%%%%%%%%%%%%%%%%%%%%%%%%%%%%%%%%%%%%%%%%%%%%%%%%%%%%%%%%%%%%%%%%%%%%

# Number of axial cells
z_cells = 128
# Number of soil radial cells
soil_r_cells = 63

# U TUBE
# Number of faces on fluid (must be divisible by 3)
fluid_theta_cells = 24
# Number of faces on soil
soil_theta_cells = 24
# Number of tube radial cells
tube_r_cells = 3
# Number of cells on grout symmetry faces (3 faces)
grout_symm_cells = 3

%%%%%%%%%%%%%%%%%%%%%%%%%%%%%%%%%%%%%%%%%%%%%%%%%%%%%%%%%%%%%%%%%%%%%%%% THERMOPHYSICAL %%%%%%%%%%%%%%%%%%%%%%%%%%%%%%%%%%%%%%%%%%%%%%%%%%%%%%%%%%%%%%%%%%%%%%%%%

# TUBE
# Thermal conductivity [W/m/K]
tube_k = 0.45
# Density [kg/m^3]
tube_rho = 950
# Specific heat [J/kg/K]
tube_cp = 1900

# GROUT
# Thermal conductivity [W/m/K]
grout_k = 1.5
# Density [kg/m^3]
grout_rho = 1300
# Specific heat [J/kg/K]
```

```

grout_cp = 3100

# SOIL
# Thermal conductivity [W/m/K]
soil_k = 2.1
# Density [kg/m^3]
soil_rho = 2115
# Specific heat [J/kg/K]
soil_cp = 795

# FLUID
# Thermal conductivity [W/m/K]
fluid_k = 0.607
# Density [kg/m^3]
fluid_rho = 997
# Specific heat [J/kg/K]
fluid_cp = 4184
# Prandtl number
fluid_pr = 6.14
# Viscosity [kg/m/s]
fluid_mu = 0.000891

%%%%%%%%%%%%%%%%%%%%%%%%%%%%%%%%%%%%%%%%%%%%%%%%%%%%%%%%%%%%%%%%%%%%%%%% FLOW/INLET CONDITIONS %%%%%%%%%%%%%%%%%%%%%%%%%%%%%%%%%%%%%%%%%%%%%%%%%%%%%%%%%%%%%%%%%%%%%%%%%

# Ground initial temperature [K]
T_init = 284.15
# Fluid flow rate [kg/s]
mdot = 0.87
# Fluid inlet temperature [K]
T_in = 284.15
# Injection type (prescribed temp.=T, prescribed q=Q,
# specify file=file)
input_type = Q
# Inlet q (if prescribed q. Zero if prescribed temp.) [W]
input_q = 9000
# Is the heat input intermittent? (if yes, give period in
# seconds, if no 0) [s]
interOn = 0
# If intermittent, how long is the total on/off cycle?
interTot = 0

```

A.2 Input file for a coaxial type heat exchanger

```
%%%%%%%%%%%%%%%%%%%%%%%%%%%%%%%%%%%%%%%%%%%%%%%%%%%%%%%%%%%%%%%%%%%%%%%% INPUT FILE %%%%%%%%%%%%%%%%%%%%%%%%%%%%%%%%%%%%%%%%%%%%%%%%%%%%%%%%%%%%%%%%%%%%%%%%%
Borehole Type (coaxial)

# Runtime [s]
time = 259200

%%%%%%%%%%%%%%%%%%%%%%%%%%%%%%%%%%%%%%%%%%%%%%%%%%%%%%%%%%%%%%%%%%%%%%%% GEOMETRY %%%%%%%%%%%%%%%%%%%%%%%%%%%%%%%%%%%%%%%%%%%%%%%%%%%%%%%%%%%%%%%%%%%%%%%%%

# Borehole diameter [m]
bh_d = 0.10795
# Borehole length [m]
bh_l = 182.88
# Domain size (single borehole) [m]
soil_d = 6

# COAXIAL
# Inner tube outer diameter [m]
tube_inner_od = 0.04
# Inner tube thickness [m]
tube_inner_thk = 0.0036
# Outer tube outer diameter [m]
tube_outer_od = 0.0882142
# Outer tube thickness [m]
tube_outer_thk = 0.0057404

%%%%%%%%%%%%%%%%%%%%%%%%%%%%%%%%%%%%%%%%%%%%%%%%%%%%%%%%%%%%%%%%%%%%%%%% MESH %%%%%%%%%%%%%%%%%%%%%%%%%%%%%%%%%%%%%%%%%%%%%%%%%%%%%%%%%%%%%%%%%%%%%%%%%

# Number of axial cells
z_cells = 128
# Number of soil radial cells
soil_r_cells = 63

# COAXIAL
# Number of inner tube radial cells
tube_inner_r_cells = 3
# Number of outer tube radial cells
```

```
tube_outer_r_cells = 3
# Number of grout radial cells
grout_r_cells = 5
```

```
%%%%%%%%%%%%%%%%%%%%%%%%%%%%%%%%%%%%%%%%%%%%%%%%%%%%%%%%%%%%%%%%%%%%%%%% THERMOPHYSICAL %%%%%%%%%%%%%%%%%%%%%%%%%%%%%%%%%%%%%%%%%%%%%%%%%%%%%%%%%%%%%%%%%%%%%%%%%
```

```
# TUBE
# Thermal conductivity [W/m/K]
tube_k = 0.45
# Density [kg/m^3]
tube_rho = 950
# Specific heat [J/kg/K]
tube_cp = 1900
```

```
# GROUT
# Thermal conductivity [W/m/K]
grout_k = 1.5
# Density [kg/m^3]
grout_rho = 1300
# Specific heat [J/kg/K]
grout_cp = 3100
```

```
# SOIL
# Thermal conductivity [W/m/K]
soil_k = 2.1
# Density [kg/m^3]
soil_rho = 2115
# Specific heat [J/kg/K]
soil_cp = 795
```

```
# FLUID
# Thermal conductivity [W/m/K]
fluid_k = 0.607
# Density [kg/m^3]
fluid_rho = 997
# Specific heat [J/kg/K]
fluid_cp = 4184
# Prandtl number
fluid_pr = 6.14
# Viscosity [kg/m/s]
```

```
fluid_mu = 0.000891
```

```
%%%%%%%%%%%%%%%%%%%%%%%%%%%%%%%%%%%%%%%%%%%%%%%%%%%%%%%%%%%%%%%%%%%%%%%% FLOW/INLET CONDITIONS %%%%%%%%%%%%%%%%%%%%%%%%%%%%%%%%%%%%%%%%%%%%%%%%%%%%%%%%%%%%%%%%%%%%%%%%%
```

```
# Ground initial temperature (constant for now) [K]
T_init = 284.15
# Fluid flow rate [kg/s]
mdot = 0.87
# Fluid inlet temperature [K]
T_in = 284.15
# Injection type (prescribed temp.=T, prescribed q=Q,
# specify file=file)
input_type = Q
# Inlet q [W] (if prescribed q. Zero if prescribed temp.)
input_q = 9000
# Is the heat input intermittent? (if yes, give period in
# seconds, if no 0) [s]
interOn = 0
# If intermittent, how long is the total on/off cycle?
interTot = 0
# Flow direction (inner or outer)
inlet_loc = inner
```